Developing Novel Culture Substrates for *In Vitro* Construction of Corneal Endothelium



A thesis submitted for the Degree of Doctor of Philosophy

Siqi Dai
Linacre College
University of Oxford

Michaelmas 2023

Developing Novel Culture Substrates for *In Vitro* Construction of Corneal Endothelium

A thesis submitted for the Degree of Doctor of Philosophy
Michaelmas 2023

Siqi Dai, Linacre College, University of Oxford

Abstract

The corneal endothelium plays a pivotal role in maintaining ocular clarity. However, its limited regenerative capacity in humans necessitates innovative therapeutic strategies. This thesis delves into the development of effective and sustainable methods for the in vitro culture and application of the immortalised human corneal endothelial cell line, HCEC-12, aiming to revolutionise corneal endothelial tissue engineering.

The initial focus was on the foundational role of collagen type IV (COL4) in HCEC-12 culture. COL4, abundant in endothelial basement membranes, facilitates rapid cell attachment to culture surfaces. By optimising the coating procedure, the research established that a concentration of 100μg/mL COL4 was ideal for HCEC-12 culture. This concentration not only enhanced cell adherence and proliferation but also maintained the desired "cobblestone-like" morphology, reminiscent of a healthy human corneal endothelium. The expression levels of key proteins, such as ZO-1 and ATP1A1, further validated the biological relevance of the chosen coating concentration.

Building on the foundational work, the study explored the potential of dECM derived from HCEC-12 cells. The dECM, especially when derived from cells cultured on COL4 (dECM-

COL4), emerged as a superior substrate, closely mimicking the natural cellular microenvironment. Notably, cells cultured on dECM-COL4 exhibited enhanced proliferation, resilience against endothelial-to-mesenchymal transition (EMT), and retained their typical corneal endothelial phenotype. The findings highlighted the potential of dECM-COL4 in maintaining cellular integrity, even under challenging conditions.

Venturing further, the research delved into developing a Descemet's Membrane (DM)-derived substrates – posterior porcine cornea (PPC). The findings illuminated the conducive environment offered by PPC, enriched with essential ECM components reminiscent of DM. This environment was found to be instrumental in promoting cell adherence, proliferation, and phenotype maintenance. Notably, seeding HCEC-12 cells cultured with PPC coating on a cell carrier successfully reconstructed a transplantable model of the corneal endothelium in vitro, positioning PPC as a promising avenue for corneal endothelial tissue engineering.

In summary, this thesis offers a holistic exploration into the substrates for HCEC-12 culture, from the foundational work with COL4 to the innovative strides with dECM and PPC. The collective findings not only chart a promising trajectory for corneal endothelial tissue engineering but also underscore the potential for developing affordable and effective treatments for corneal endothelial dysfunctions.

List of Publications

Lim B., Ratcliff J., Nawrot D. A., Yu Y., Sanghani H. R., Hsu C. C., Peto L., Evans S., Hodgson S. H., Skeva A., Adam M., Panopoulou M., Zois C. E., Poncin K., Vasudevan S. R., **Dai S.**, Ren S., Chang H., Cui Z., Simmonds P., Huang W. E., Andersson M. I. Clinical validation of optimised RT-LAMP for the diagnosis of SARS-CoV-2 infection. Sci Rep 11, 16193 (2021). https://doi.org/10.1038/s41598-021-95607-1.

Yu Y., **Dai S.**, Zhou X., Huang W. E., Cui Z. Thermostabilising Functional Proteins with Matrix Assisted Room Temperature Drying (Manuscript Submitted)

Dai S., Cui Z. Cell-Derived Decellularised Extracellular Matrix Protects Human Corneal Endothelial Cultures from Endothelial-to-Mesenchymal Transition (Manuscript Prepared)

Dai S., Cui Z. Extracellular Matrix of Posterior Porcine Cornea Supports In Vitro Culture of Human Corneal Endothelial Cells (Manuscript Prepared)

List of Awards

Team member, Winner of Innovative Product Award, 2023 IChemE Global Awards

Team member, Winner of Business Start-up Award, 2023 IChemE Global Awards

Team member, Winner of Outstanding Achievement Award, 2023 IChemE Global Awards

Acknowledgements

As I stand at the culmination of this journey, my heart is filled with gratitude for all those who have provided me with the strength, guidance, and companionship necessary to navigate this challenging yet rewarding path.

First and foremost, my deepest appreciation goes to my mum, dad, and brothers. Your unconditional love, sacrifices, and unwavering belief in me have been the foundation of my strength and determination. It is your support that has fuelled my perseverance and made my accomplishments more meaningful.

I am profoundly grateful to my supervisor, Prof. Zhanfeng Cui, for his invaluable mentorship, patience, and guidance. His wisdom and support were instrumental in navigating the complexities of this research. My sincere thanks also go to Prof. Hua Ye, whose insights and advice have significantly shaped my academic journey. I am also thankful to Prof. Nicholas Hankins and Prof. Wei Huang for their careful assessment and constructive feedback on my study. I extend my gratitude to Dr. Julian George, Dr. Chia-Chen Hsu, Dr. Eleanor Scott, and Dr. Arthur Dyer for their invaluable assistance with experimental techniques and methodologies. Their teachings have been foundational to my research.

I wish to thank my fellow researchers Dr. Boon Lim, Dr. Ching Lam, Dr. Viorica Patrulea, Dr. Rui Lei, Flurin Caviezel, Haoyu Wu, Simge Bahcevanci, Yutong Yin, Li Liu, Carla Fuenteslópez, and Johnny Zhou, for their collaborative spirit and enriching academic exchanges. Special thanks go to Dr. Yejiong Yu, Dr. Liyiwen Yuan, Dr. Shuai Ren, and Dr.

Yun Chen for their camaraderie. Our shared experiences and enriching discussions have made this journey unforgettable.

Lastly, I express my deepest gratitude to my fiancé, Dr. Meng Qi. Your unwavering love and support have been my guiding light, and this achievement is as much yours as it is mine.

I am reminded that no endeavour is a solo act, but rather a symphony of collective effort and encouragement. To all of you, I am eternally grateful.

Table of Contents

Abstract **1**

List of Publications **3**

List of Awards **4**

Acknowledgements **5**

Table of Contents **7**

List of Abbreviations **10**

List of Figures **14**

Chapter 1 Introduction **20**

1.1 Background 20

1.2 Research Justification 21

1.3 Aims and Objectives 23

Chapter 2 Literature Review – Research Advances in Corneal Endothelial Tissue Engineering 25

2.1 Overview of the Corneal Endothelium 26

2.2 In vivo Proliferation of Corneal Endothelial Cells 29

2.3 Corneal Endothelial Transplantation 30

2.4 Cell-based Therapy 32

2.5 Tissue-engineered Graft 39

2.6 Summary 49

Chapter 3 HCEC-12 Cell Culture and Functional Assays **51**

3.1 HCEC-12 Culture 51
3.2 Collagen Type IV Coating for Cell Culture 53
3.3 Assessment of Cell Adherence and Proliferation 54
3.4 Immunofluorescence Microscopy 55
3.5 Cellular Protein Extraction 56
3.6 SDS-PAGE and Irreversible Visualisation of Protein Bands 56
3.7 Reversible Visualisation of Protein Bands and Western Blot 57
3.8 Flow Cytometry 58
3.9 Statistical Analysis 59

Chapter 4 Optimisation of Collagen IV Coating Procedure for HCEC-12 Culture 60

4.1 Introduction 60
4.2 Materials and Methods 62
4.3 Results and Discussions 64
4.4 Summary 78

Chapter 5 Cell-Derived Decellularised Extracellular Matrix Supports HCEC-12 Culture 80

5.1 Introduction 80
5.2 Materials and Methods 81
5.3 Results 84
5.4 Summary 98

Chapter 6 Development of a Novel Biomimetic Culture Substrate from Posterior Porcine Corneal Tissue 100

6.1 Introduction 100
6.2 Materials and Methods 101
6.3 Results 109

6.4 Summary 113

Chapter 7 Effective Maintenance of HCEC-12 Culture Using PPC Coating 115

7.1 Introduction 115

7.2 Materials and Methods 117

7.3 Results and Discussion 121

7.4 Summary 136

Chapter 8 General Discussion and Concluding Remarks 138

References 143

Appendices 162

Appendix 1 162

Appendix 2 164

Appendix 3 165

List of Abbreviations

AM	Amniotic membrane
APCS	Acellular porcine corneal stroma
α-SMA	Alpha smooth muscle actin
ATP1A1	Na+/K+ ATPase α1 subunit
BCA	Bicinchoninic acid assay
BSA	Bovine serum albumin
CCK-8	Cell counting kit-8
CD	Cluster of differentiation
CEC	Corneal endothelial cell
CIL	Contact inhibition of locomotion
COL1	Collagen type IV
COL4	Collagen type IV
COL8	Collagen type VIII
COL8A2	Collagen type VIII α2 chain
CV	Coefficient of variation
dECM	Cell-derived decellularised extracellular matrix
dECM-COL4	dECM prepared with HCEC-12 grown on 100µg/mL COL4 coating
dECM-TCPS	dECM prepared with HCEC-12 grown on TCPS
DEGMA	Diethyleneglycol methacrylate

DM	Descemet's membrane
DMEK	Descemet's membrane endothelial keratoplasty
DMSO	Dimethyl sulfoxide
DSAEK	Descemet's stripping automated endothelial keratoplasty
DSEK	Descemet's stripping endothelial keratoplasty
ECM	Extracellular matrix
EDC	1-Ethyl-3-(3-dimethylaminopropyl) carbodiimide
EDTA	Ethylenediaminetetraacetic acid
EK	Endothelial keratoplasty
EMT	Endothelial-to-mesenchymal transition
ESC	Embryonic stem cell
FBS	Fetal bovine serum
FECD	Fuch’s endothelial corneal dystrophy
GTA	Glutaraldehyde
HA	Hyaluronic acid
HALC	Human anterior lens capsule
HCEC	Human corneal endothelial cells
HCEC-12	An immortalised HCEC cell line, named HCEC-12
HRP	Horseradish peroxidase
iPSC	Induced pluripotent stem cell
LCST	Lower critical solution temperature
LDS	Lithium dodecyl sulfate

NC	Neural crest
NGMA	N-glycidylmethacrylate
NHS	N-hydroxysuccinimide
OCT	Ocular coherence tomography
OD	Optical density
PAGE	Polyacrylamide gel electrophoresis
PBS	Phosphate buffered saline
PC	Plastic compression
PCL	Polycaprolactone
PDMS	Polydimethylsiloxane
PEG	Polyethylene glycol
PFA	Paraformaldehyde
PGA	Polyglycolic acid
PHB	Poly 3-hydroxybutyrate
PKP	Penetrating keratoplasty
PLGA	Poly lactic-co-glycolic acid
PMMA	Polymethylmethacrylate
pNIPAAm	Poly N-isopropylacrylamide
PPC	Posterior porcine cornea
PVA	Polyvinyl alcohol
PVDF	Polyvinylidene fluoride
RIPA	Radio immunoprecipitation assay

SD	Standard deviation
SDS	Sodium dodecyl sulphate
SEM	Standard error of the mean
SF	Silk fibroin
TBST	Tris-buffered saline containing 0.1% Tween-20
TCPS	Tissue culture polystyrene
TEER	trans-endothelial electrical resistance
TGF-β1	Transforming growth factor β1
ZO-1	Tight junction protein zonula occludens-1

List of Figures

Figure 1. An illustrative representation of the human eye with emphasis on the cornea. The eye can be divided into the anterior segment, which encompasses the lens and all tissues anterior to it, and the posterior segment, which houses the remaining eye tissues. Positioned at the forefront of the eye, the cornea comprises five layers: the epithelium, Bowman's layer, the corneal stroma, Descemet's membrane, and the corneal endothelium. Hydration level in the corneal stroma is maintained by a pump-leak mechanism. 27

Figure 2. An illustration of endothelial-mesenchymal transition (EMT), a process where the tightly packed corneal endothelial cells take a phenotypic drift and become irregularly shaped and lose the cell-cell contact. 34

Figure 3. Comparative calibration curves for collagen type IV using traditional and modified Bradford assays. (A) Calibration curve obtained from the traditional Bradford assay. (B) Calibration curve derived from the modified Bradford assay. Data points represent the mean optical density values at 595nm wavelength for each collagen type IV concentration, with error bars indicating the standard error of the mean (SEM). Experiments were conducted in triplicate (n=3). 65

Figure 4. Analysis of collagen type IV coating efficiency across different concentrations. (A) Plot illustrating the relationship between the amount of coated collagen type IV and the coating concentration for each specific condition. (B) Bar chart comparing the coating efficiencies across the tested concentrations. Data points and bars represent the mean values for each concentration, with error bars indicating the standard error of the mean (SEM). Experiments were conducted in triplicate (n=3). 66

Figure 5. Evaluation of HCEC-12 P12 proliferation on culture surfaces coated with varying concentrations of collagen type IV using the CCK-8 assay. (A) Calibration curve depicting the relationship between optical density at 450nm (OD_{450}) and the number of cells in standard HCEC-12 suspensions. (B) Bar chart illustrating the OD_{450} values from day 1 to day 9, representing cell proliferation across different collagen type IV coating concentrations. (C) Bar chart showcasing the doubling levels of HCEC-12 on days 7 and 9 since day 1, providing insights into the growth rate of the cells on the coated surfaces. Data points and bars represent the mean values for each concentration, with error bars indicating the standard error of the mean (SEM). Experiments were conducted in triplicate (n=3). * denotes statistical significance with $P<0.05$. 69

Figure 6. Immunofluorescence micrographs of HCEC-12 P12 cells cultured on surfaces coated with varying concentrations of collagen type IV (0-100µg/mL). (A-D) Visualisation of tight junction protein ZO-1 (yellow), adherens junction ATP1A1 (red), and cell nuclei (blue). (E-H) Depiction of cytoskeletal F-actin (yellow), fibroblast marker α-SMA (red), and cell nuclei (blue). (I-L) Imaging of extracellular matrix protein collagen type I (yellow), collagen type IV (red), and cell nuclei (blue). (M-P) Representation of collagen type VIII (red) in relation to cell nuclei (blue). All images are accompanied by scale bars representing 100µm, providing a reference for cell and protein structure sizes. 72

Figure 7. Comprehensive analysis of protein expressions in HCEC-12 P12 cells cultured on varying concentrations of collagen type IV. (A) BCA calibration curve showcasing the relationship between optical density at 562nm and a series of bovine serum albumin (BSA) concentrations ranging from 0 to 2mg/mL. Data points represent the mean optical density values for each BSA concentration, with error bars indicating standard deviation (SD), n=3. (B) Immunoblot analysis of total proteins extracted from the cultured HCEC-12 P12. Following electrophoresis, proteins with different molecular weights were transferred to a nitrocellulose membrane and subsequently probed with specific antibodies to visualise the expressions of ZO-1, ATP1A1, COL8A2, β-actin, and α-SMA. The bands provide insights into the relative protein expressions across the different collagen type IV coating concentrations. 74

Figure 8. Flow cytometry histograms representing the protein expression intensities in HCEC-12 P12 cells cultured on surfaces with varying concentrations of collagen type IV. Cells were fixed and stained with specific antibodies targeting ZO-1 (blue), ATP1A1 (orange), and α-SMA (green). Additionally, cells not stained with any antibody served as a blank control (red). The combined histograms provide a comparative view of protein expression across the different coating concentrations: (A) Uncoated or 0µg/mL, (B) 20µg/mL, (C) 50µg/mL, (D) 100µg/mL, and (E) 150µg/mL. The x-axis represents the fluorescence intensity of the labelled proteins, while the y-axis indicates the frequency of HCEC-12 cells emitting the respective fluorescence, providing insights into the relative protein expressions for each coating concentration. 77

Figure 9. Fluorescence Micrographs and Photos of dECM Preparation. (A-C) HCEC-12 P4 cells cultured on TCPS and (D-F) on COL4 coating. (A, D) Fluorescence micrographs reveal HCEC-12 cells (brightfield) and their nuclei stained with DAPI (blue) prior to decellularisation. (B, E) Post-decellularisation images show minimal DAPI staining, confirming effective removal of cells and nuclear debris. Scale bars are 100µm. Adjacent photos depict the gelatinous matrices of (C) dECM-TCPS and (F) dECM-COL4 retained in the culture-wares following decellularisation. 85

Figure 10. SDS-PAGE and western blot analysis of reconstituted dECM-COL4 and dECM-TCPS. Protein profiles of reconstituted dECM-COL4 and dECM-TCPS were

compared against collagen types I and IV controls. (A) Post-electrophoresis, proteins were transferred to a nitrocellulose membrane and stained with Ponceau S, revealing the protein bands differentiated by molecular weight. Visible protein bands of the dECM-COL4 sample are denoted by arrows. (B) For western blot analysis, the membrane was incubated with antibodies to probe COL1, COL4, and COL8A2. The resultant blot is superimposed on the Ponceau S-stained membrane, providing a comparative view alongside the protein ladders. 87

Figure 11. CCK-8 Proliferation Assay of HCEC-12 P4 on Various Culture Surfaces. HCEC-12 P4 cells were cultured on TCPS, COL4 coating, dECM-TCPS, and dECM-COL4. (A) Bar chart comparisons depict the optical density at 450nm (OD_{450}) from day 1 to day 9. (B) Doubling levels are illustrated for days 7 and 9, relative to day 1. Data are presented as means ± SEM, with n=4. Significance levels are indicated as * P<0.05, ** P<0.01, and *** P<0.001. 89

Figure 12. Immunofluorescence analysis of HCEC-12 P4 on various culture surfaces. Micrographs depict HCEC-12 P4 cells cultured on TCPS, COL4 coating, dECM-TCPS, and dECM-COL4. Specific antibody stainings visualise (A-D) ZO-1 (yellow), (E-H) α-SMA (red), and (I-L) COL8A2 (red). Each image is equipped with a scale bar of 100µm for size reference. Comprehensive immunofluorescence images, which combine staining of ZO-1, ATP1A1, α-SMA, F-actin, COL1, COL4, COL8, and DAPI-labelled nuclei, can be found in the supplementary material (Figure 28 in Appendix 2). 91

Figure 13. Western blot analysis of proteins from HCEC-12 P4 cultured on various surfaces. Protein extracts from HCEC-12 P4 cells cultured on TCPS, COL4 coating, dECM-TCPS, and dECM-COL4 were subjected to SDS-PAGE and subsequently transferred to a nitrocellulose membrane. The membrane was probed with antibodies to visualise the proteins ZO-1, ATP1A1, COL8A2, β-actin, and α-SMA. The corresponding molecular weight of each protein is indicated on the right side of the blot.....93

Figure 14. Immunofluorescence analysis of HCEC-12 P4, stimulated to undergo EMT, on various culture surfaces. Micrographs depict EMT-induced HCEC-12 P4 cells cultured on TCPS, COL4 coating, dECM-TCPS, and dECM-COL4. Specific antibody stainings visualise (A-D) ZO-1 (yellow), (E-H) α-SMA (red), and (I-L) COL8A2 (red). Each image is equipped with a scale bar of 100µm for size reference. Comprehensive immunofluorescence images, which combine staining of ZO-1, ATP1A1, α-SMA, F-actin, COL1, COL4, COL8, and DAPI-labelled nuclei, can be found in the supplementary material (Figure 29 in Appendix 3). 95

Figure 15. Western blot analysis of proteins from EMT-induced HCEC-12 P4 cultured on various surfaces. Total proteins were extracted from EMT-induced HCEC-12 P4 cells, cultured on TCPS, COL4 coating, dECM-TCPS, and dECM-COL4, with TGF-β1 supplementation in the culture medium. Following SDS-PAGE separation, the proteins were

transferred to a nitrocellulose membrane. The membrane was probed with antibodies to visualise the proteins ZO-1, ATP1A1, COL8A2, β-actin, and α-SMA. The corresponding molecular weight of each protein is indicated on the right side of the blot. 97

Figure 16. Decellularisation Apparatus and Process for PPCs. This figure illustrates the sequence and components of the decellularisation process for PPC tissues. (A) Shows the initial step where vacuum-sealed PPC tissues are prepared for decellularisation. (B) Depicts these tissues being transferred to the tank of a custom-built decellularisation setup. (C) Demonstrates the flow of decellularisation reagents, facilitated by a peristaltic pump, which moves the reagents from a conical flask through the tank (where the tissues are agitated on a rocking bed, as indicated by the arrows), and finally to a waste beaker for collection. (D) Displays the decellularised PPCs post-process, laid out in a glass petri dish for visual inspection. 103

Figure 17. Design and illustration of a working prototype of the PPC decellularisation bioreactor. (A) Showcases the design of the rotating cylinder of the bioreactor. (B) Displays the assembly of the bioreactor. (C) Presents a flowchart detailing the operational setup of the decellularisation process. This includes solenoid valve-controlled introduction of four reagents - SDS, Triton X-100, Benzonase, and PBS - into the rotating cylinder, following the decellularisation protocol. Another solenoid valve at the outlet end regulates the outflow of reagents to a waste container. 105

Figure 18. Visual representation of the thickness measurements of PPC tissues from porcine corneas. Optical coherence tomography (OCT) was utilised to determine the thickness, with images (A) showcasing the operating software's interface and (B) presenting the average thicknesses derived from six individual PPC samples, with measurements taken across varied regions. (C) A photograph depicting a whole porcine cornea along with the adjacent sclera, excised from the eyeball, showcasing its natural appearance. (D) The same cornea but inverted to display its posterior side. 110

Figure 19. Histological analysis of PPC tissues. This figure presents representative histological images of native and decellularised PPC tissues. (A) and (C) show native PPC tissues prior to decellularisation using the rudimentary setup and the bioreactor, respectively, highlighting intact cells (indicated by white arrows). (B) and (D) depict PPC tissues post-decellularisation, treated using the rudimentary setup and the bioreactor, respectively, illustrating the absence of cells. All images were stained with haematoxylin and eosin to highlight cellular and matrix structures. Scale bars in each image represent 50μm. 111

Figure 20. Protein component analysis of PPC. (A) Representative SDS-PAGE gel image showcasing protein separation, stained with Coomassie Brilliant Blue. (B-D) Western blot results for the identification of specific collagen types in PPC. The blots were probed with antibodies against (B) COL1, (C) COL4, and (D) COL8A2. For clarity, images of the stained nitrocellulose membrane are superimposed on the gel, providing a visual reference for

molecular weight determination. In all panels, the lanes are designated as follows: lane 1 - protein ladder, serving as a molecular weight reference; lane 2 - recombinant COL4, used as a positive control for collagen type IV; lane 3 - reconstituted PPC, representing the protein profile of the treated porcine cornea; lane 4 - control sample, consisting of the PPC dissolvent (pepsin/HCl solution).....112

Figure 21. Characterisation of HCEC-12 cell adhesion on different substrates. (A-F) Representative brightfield microscopic images depicting HCEC-12 cells on TCPS (A, D), COL4 coating (B, E), and PPC coating (C, F) at two time points: 5 minutes (A-C) and 60 minutes (D-F) post-seeding. The images highlight the differences in cell attachment across the three surfaces. Scale bars represent 100µm. (G) A column chart illustrating the comparative analysis of the number of HCEC-12 cells that stably adhered to the culture surfaces in the TCPS, COL4, and PPC groups at four distinct time intervals: t=5, 30, 60, and 120 minutes. Each group consisted of four samples (N=4). Statistical significance was determined using two-way ANOVA, denoted by ** $p < 0.01$ and *** $p < 0.001$.....122

Figure 22. Comparative analysis of HCEC-12 cell proliferation on different substrates. The chart displays the growth rates of HCEC-12 cells cultured on TCPS, COL4 coating, and PPC coating over a period of 9 days. Cell counts were determined using CCK-8 assays, conducted every other day starting 12 hours post-seeding. Each experimental group consisted of four replicates (N=4). Statistical differences between groups were determined through two-way ANOVA, with significance denoted by *$p < 0.05$, **$p < 0.01$, and ****$p < 0.0001$.....124

Figure 23. Morphological assessment of HCEC-12 cells across multiple passages. Representative brightfield microscopic images depict the cellular morphology of HCEC-12 cells at passages P1, P2, and P5 when cultured on different substrates: TCPS (A), COL4 coating (B), and PPC coating (C). All images were taken 5 days post-seeding for each respective passage. Scale bars represent 100µm for all images.....126

Figure 24. Evaluation of ZO-1 protein expression in HCEC-12 cells. (A) Western blot analysis showcasing ZO-1 expression in cells cultured for five passages on TCPS (left lane), COL4 coating (middle lane), and PPC coating (right lane). B-actin, stained as a reference protein, is used for normalisation. The column chart illustrates the ratios of ZO-1 to β-actin expression, with significance determined using a t-test in comparison to the TCPS group (* $p<0.05$). (b-d) Immunofluorescence images of HCEC-12 cells after 5 days of culture at the fifth passage on TCPS (B), COL4 coating (C), and PPC coating (D). The images highlight ZO-1 expression (yellow) on the cellular membrane and the cellular nuclei (blue). Scale bars represent 50µm. 128

Figure 25. Evaluation of HCEC-12 cell proliferation and migration in an in vitro scratch assay. (A-C) Representative timelapse images depict the progression of HCEC-12 cells on (A) TCPS, (B) COL4 coating, and (C) PPC coating, at intervals of 0, 12, 24, and 36

hours post-scratching. The boundaries of the created gaps are highlighted for clarity. Scale bars represent 100µm. (D) A chart illustrating the quantified cell-free areas at the start (t=0hr) and end (t=36hr) of the observation period, determined using ImageJ software. (E) A subsequent chart displays the percentage of the gap area that was recolonised by cells at t=36hr. Statistical significance was ascertained using two-way ANOVA, with * indicating $p < 0.05$. 130

Figure 26. Evaluation of contact inhibition of locomotion in HCEC-12 cultures. (A-C) Representative timelapse images showcasing HCEC-12 cells on (A) TCPS, (B) COL4 coating, and (C) PPC coating, at intervals of 32, 48, and 64 hours after seeding. Cells observed clumping, and traversing over other cells are highlighted with red circles. Each scale bar corresponds to 20µm. (D) A column chart presenting the frequency at which the absence of contact inhibition of locomotion was observed in HCEC-12 cells across the different substrates. The data were derived from three separate experiments (N=3), with each experiment comprising 4 distinct wells for every condition. Each well contained 6 designated observation regions, culminating in a total of 24 observations (n=24). Statistical significance was ascertained using one-way ANOVA, with significance denoted by * $p<0.05$ and ** $p<0.01$. 132

Figure 27. Morphology and protein expression assessment of HCEC-12 cells seeded on RAFT™. Representative images of HCEC-12 cells derived from cultures on (A-C) TCPS, (D-F) COL4 coating, and (G-I) PPC coating, and subsequently expanded on RAFT™. (A, D, G) Brightfield images captured one day and (B, E, H) three days post-seeding showcase the cellular morphology and proliferation. (C, F, I) Immunofluorescence images taken on the third day highlight the expression of the tight junction protein ZO-1 (yellow) and the cellular nuclei (blue). Scale bars represent 100µm. 134

Figure 28. Supplementary Figure: Comprehensive immunofluorescence staining of HCEC-12 P4 on various substrates. Representative micrographs depicting HCEC-12 cells at passage 4 (P4) cultured on TCPS, 100µg/mL COL4 coating, dECM-TCPS, and dECM-COL4. Images display cells stained for (A-D) for ZO-1 (yellow), ATP1A1 (red), and nuclei (blue); (E-H) F-actin (yellow), α-SMA (red), and nuclei (blue); (I-L) collagen type I (yellow), collagen type IV (red), and nuclei (blue); (M-P) collagen type VIII (red) and nuclei (blue). All images are scaled with bars representing 100µm. 164

Figure 29. Supplementary Figure: Comprehensive immunofluorescence staining of HCEC-12 P4 on various substrates, with TGF-β1 treatment. Representative micrographs depicting HCEC-12 cells at passage 4 (P4) cultured on TCPS, 100µg/mL COL4 coating, dECM-TCPS, and dECM-COL4, with TGF-β1 treatment to induce EMT. Images display cells stained for (A-D) for ZO-1 (yellow), ATP1A1 (red), and nuclei (blue); (E-H) F-actin (yellow), α-SMA (red), and nuclei (blue); (I-L) collagen type I (yellow), collagen type IV (red), and nuclei (blue); (M-P) collagen type VIII (red) and nuclei (blue). All images are scaled with bars representing 100µm. 165

Chapter 1

Introduction

1.1 Background

"The eyes are the windows to the soul," a phrase often attributed to William Shakespeare, metaphorically underscores the vital role of vision in human experience. Diverging from poetic musings, this thesis embarks on a scientific exploration of the cornea, the eye's 'outer glass pane' in this metaphor.

As the primary interface for light entering the eye, the cornea is crucial for clear vision. Despite its significance, corneal opacity remains a leading cause of blindness globally, as reported by the World Health Organization in 2019 [1]. The demand in the UK alone underscores the issue, with approximately 5,000 corneal transplants needed yearly [2]. The cornea's complex structure comprises five distinct layers: the epithelium with its basement membrane – the Bowman's layer, the stroma, the Descemet's membrane (DM), and the endothelium which produces the DM [3]. The stroma forms the bulk of this structure, while the epithelium and endothelium regulate hydration and nutrients [4,5]. Notably, a diseased corneal endothelium presents a unique challenge due to human corneal endothelial cells' (HCECs) limited regenerative capacity. Instead of proliferating, HCECs enlarge to cover damaged areas. A significant loss of these cells can result in oedema, leading to a clouded cornea [6].

Patients with corneal endothelial dysfunction typically undergo tissue transplantation via the traditional penetrative keratoplasty (PK) or the more recent approach of endothelial

keratoplasty (EK) [7]. However, these surgical procedures depend on the availability of donated corneas, which are in limited supply worldwide. To circumvent the reliance on donor tissues, alternative treatments, such as cell injection and tissue engineered grafts have been explored.

The field of corneal endothelial tissue engineering has seen significant advancements over the years. However, there remain persistent challenges in maintaining the phenotype and function of HCECs during in vitro culture, and one of the primary concerns is endothelial-to-mesenchymal transition (EMT). It occurs over time and successive passages, where the cells undergo a phenotypic drift, shifting from the endothelial phenotype to a mesenchymal phenotype. This cellular transformation compromises the purity and functionality of the cultured cells, thereby impacting their therapeutic potential.

1.2 Research Justification

When HCECs are passaged, the cells are detached from the culture surface and dissociated with each other, and the repeated breaking and forming of cell-cell contacts are believed to cause EMT [8-10]. While some conventional culture substrates may inadvertently promote EMT, there is a growing body of evidence suggesting that extracellular matrix (ECM) proteins derived from the DM can potentially maintain HCEC culture and suppress EMT. Coating the culture surface with these proteins has shown potential in maintaining HCECs' phenotype [11,12]. Composed of a complex range of ECM proteins, including collagen type IV (COL4), collagen type VIII (COL8), and laminin, the DM provides a microenvironment that guides cell adhesion, proliferation, and differentiation during development [13-15]. Collagen type IV (COL4), in particular, is an abundantly found protein in endothelial basement membranes. Its significance

is underscored by its ability to facilitate rapid attachment of primary HCECs and HCEC-12, when coated to culture plates [16,17].

Meanwhile, collagen type VIII, has also garnered significant attention due to its unique presence in the DM. This nonfibrillar collagen exists as a heterodimer and forms a hexagonal lattice structure, and it is postulated to not only provide structural integrity to the DM but also maintain a healthy endothelial function in vivo. For instance, mutations in the protein's α2 chain (COL8A2) encoding gene were identified in cases of corneal endothelial dystrophies [18]. Furthermore, the suppression of COL8A2 expression led to changes in cell morphology, reduced cell proliferation, and impaired barrier functions, underscoring its importance [19]. Unfortunately, at the time of writing this thesis, there have not been any studies that involved using COL8 as a coating substrate for HCEC cultures, and this may be attributed to this protein's rarity.

The exploration of protein coatings derived from the DM presents a promising avenue for advancing HCEC culture techniques. Given the limitations of current methods and the potential benefits, there is a compelling justification for delving deeper into understanding the intricacies of ECM protein interactions with HCECs. Therefore, this study aims to create culture substrates that mimic the in vivo environment to further uncover the support that the DM may bring to HCEC cultures.

Primary HCECs are challenging to source and can exhibit variations among donors. The immortalised cell line HCEC-12 provides an alternative, as they are more readily available and display a morphology and protein expression profile akin to primary HCECs [20]. Similar to their primary counterparts, healthy HCEC-12 cells adhere to the culture surface and form a monolayer, with cells efficiently arranged in a hexagonal pattern [20,21]. This arrangement reflects

the in vivo structure of the corneal endothelium, allowing the cells to collectively serve as a selective barrier at the cornea's posterior [4,5]. Therefore, this study employs HCEC-12 as a substitute for primary HCECs in cellular experiments.

1.3 Aims and Objectives

The overarching goal of this study is to develop an effective substrate for culturing HCEC-12 cells, aimed at advancing corneal endothelial tissue engineering. The objectives are designed to address the challenges of maintaining the phenotype and function of corneal endothelial cells in vitro:

1) Establish a Control Culture Condition using Collagen Type IV (COL4) Coating:
    a) Evaluate the effectiveness of different volumes, concentrations, and durations of COL4 coating in achieving optimal cell adhesion and proliferation, while preserving cell phenotype.
    b) Develop a standard protocol for COL4 coating as a benchmark for subsequent experiments.
2) Investigate the Effects of HCEC-12-Derived ECM (dECM) on HCEC-12 Culture:
    a) Prepare and characterise dECM substrates.
    b) Assess the proliferation and phenotype maintenance of HCEC-12 cells cultured on dECM substrates.
    c) Compare HCEC-12 cell performance on dECM substrates against the established COL4 control condition.
3) Evaluate DM-Derived Substrates for HCEC-12 Culture In Vitro:
    a) Prepare reconstituted solutions from posterior corneal tissues and analyse their composition.
    b) Examine the adhesion, proliferation, and phenotype maintenance of HCEC-12 cells on surfaces coated with these reconstituted solutions.
    c) Contrast the performance of HCEC-12 cells on DM-derived substrates with the optimised COL4 control condition.

d) Scale up substrate production for broader application.
e) Develop a transplantable model using cultured HCEC-12 cells on a suitable carrier.

These objectives are structured to provide a comprehensive understanding of the optimal culture conditions for HCEC-12. By exploring traditional and innovative substrates, the research aims to pave the way for improved methods of human corneal endothelial cell culture, which can have significant implications for therapeutic applications in corneal endothelial diseases.

Chapter 2

Literature Review – Research Advances in Corneal Endothelial Tissue Engineering

Covering the front of the eye, the cornea plays a pivotal role in focusing light onto the retina. In fact, the cornea contributes approximately two-thirds of the eye's total refractive power [22,23]. Critical to its clarity is the innermost layer, the corneal endothelium [3]. This is a monolayer of tightly packed polygonal cells attached to the Descemet's membrane. The primary function of these corneal endothelial cells (CECs) is to maintain the correct fluid balance in the cornea, ensuring its transparency. In adults, CECs have a limited capacity for regeneration; they do not readily divide and multiply in vivo. If the cell density in the endothelium diminishes below approximately 400-500 cells/mm^2 due to injuries, diseases, or age-related degeneration, the cornea loses its ability to maintain transparency [24]. As a result, corneal oedema, cloudiness, and even blindness can occur, and the treatment of choice for corneal endothelial dysfunction is usually endothelial keratoplasty [7]. This surgical procedure involves transplanting the posterior segment of the cornea from a donor. However, with a growing number of patients requiring such surgeries and a significant shortage of donor tissues globally, alternative solutions have become imperative [25]. One promising avenue is tissue engineering, which involves cultivating CECs in vitro and then constructing an artificial corneal endothelium for transplantation. The idea of growing corneal cells in a controlled environment and using them for therapeutic applications offers hope to many patients [26-28]. This article delves into the

advancements in CEC culture techniques and explores the potential of tissue-engineered corneas constructed using these cultured cells.

2.1 Overview of the Corneal Endothelium

As illustrated in Figure 1, the cornea is comprised of five layers, listed anteriorly to posteriorly: the epithelium, Bowman's layer, stroma, Descemet's membrane, and endothelium [3]. This intricate structure keeps the refractive medium transparent. Being avascular, the cornea relies on the tear film and the aqueous humour for the transfer of necessary nutrients and oxygen. The epithelial cells, attached to its basement membrane, the Bowman's layer, act as a watertight barrier to maintain the appropriate level of hydration in the cornea [29]. In addition, they protect the stroma against the invasion of foreign particles and pathogens [30]. The stroma, constituting ~90% of the thickness of the cornea, gives the latter its mechanical strength and optical properties [31]. To prevent swelling in the stroma, another barrier exists on the posterior side of the tissue. The endothelium accomplishes this job thanks to the junctional complexes between the cells. It also actively manipulates fluid movement between the stroma and the aqueous humour [4,5].

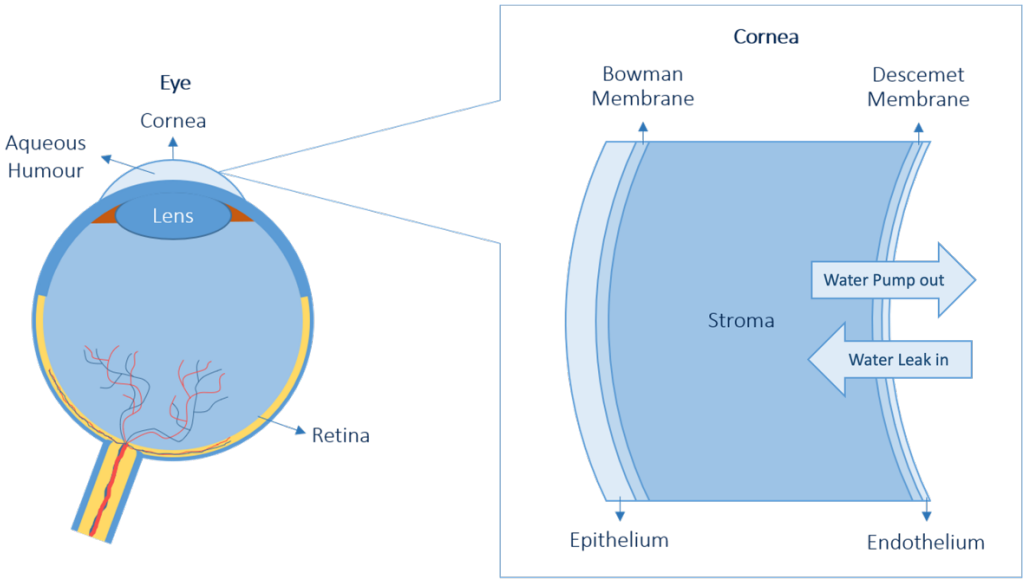

Figure 1. An illustrative representation of the human eye with emphasis on the cornea. The eye can be divided into the anterior segment, which encompasses the lens and all tissues anterior to it, and the posterior segment, which houses the remaining eye tissues. Positioned at the forefront of the eye, the cornea comprises five layers: the epithelium, Bowman's layer, the corneal stroma, Descemet's membrane, and the corneal endothelium. Hydration level in the corneal stroma is maintained by a pump-leak mechanism.

The function of the corneal endothelium is largely dependent on the morphology and density of its cells. These cells establish their shape during gestation, becoming polarised and flattened [32]. They are separated from the corneal stroma by the Descemet's membrane, which is formed from the extracellular matrix components that the cells secrete. As many as 500,000 endothelial cells cover the posterior side of the cornea at birth, predominantly adopting a hexagonal shape [33,34]. Bound together by tight junctions, they arrange into a dense, honeycomb-patterned monolayer. Postnatally, the number of cells reduces at an estimated rate of 0.52% each year [35]. The morphology also shifts as a person ages. In their 80s, only approximately 61% of the cells retain a hexagonal shape, while the remainder adopt four to nine-sided configurations [36]. With a declined cell density and hexagonality, the endothelium's ability to regulate water and nutrient transfer becomes impaired. Clinically, this characteristic shift can be detected using specular microscopy.

Electron microscopy offers a more nuanced view of the corneal endothelium. It reveals a profusion of interdigitations between adjacent cells, which fortify intercellular adhesions [37]. Where junctional complexes, such as tight junctions, gap junctions and adherens junctions, are present, the space between human corneal endothelial cells (HCECs) is constricted from 25-40nm to only ~3nm [38,39]. Notably, these connections are discontinuous, allowing aqueous humour to percolate into the corneal stroma. Accumulation of aqueous humour in the cornea can lead to oedema and, consequently, opacity from excess scattering of light [40]. To counter this, an osmotic gradient is created by the transmembrane Na^+/K^+ ATPase to actively extrude fluid from the stroma to the anterior chamber of the eye. The water content of the cornea is sustained at ~78% through this pump-leak equilibrium, ensuring the clarity of the tissue [41,42].

A major loss of HCECs can significantly hamper the layer's barrier function. Such a loss can occur due to diseases such as bullous keratopathy, glaucoma, and diabetes, or it can be a complication of intraocular procedures, laser cornea surgeries or drug treatments [6]. One of the most prevalent causes of corneal endothelial cell loss is Fuch's endothelial corneal dystrophy (FECD), which affects more than 7% of the global population [43]. FECD typically manifests in patients in their 40s. It is characterised by a drastic decrease in the number of HCECs and a build-up of abnormal collagenous extracellular matrix, or "guttae", in the Descemet's membrane over a period of more than ten years. The cornea becomes swollen as the condition progresses, and in severe cases, when the cell density drops below 400-500 cells/mm^2, the patients may lose their vision [24,44].

2.2 In vivo Proliferation of Corneal Endothelial Cells

Human corneal endothelial cell density at birth is approximately 6000 cells/mm². This number decreases to around 3500 cells/mm² during infancy due to the expansion of the corneal surface. Over the subsequent eight decades, the cell density further declines to around 2500 cells/mm². As the number of cells reduces, the cell area enlarges, and the characteristic hexagonal cell shape becomes less prevalent [35,45]. This trend is also observed in various other species, including monkeys, cats, rats, dogs, and rabbits [46-48]. In rats, especially, the reduction in endothelial cell density mirrors that of humans but over a shorter lifespan [49]. Interestingly, despite the gradual decrease in cell count with age, the density of Na^+/K^+ ATPase pumps on the corneal endothelium remains relatively stable throughout life. This indicates that the existing endothelial cells increase their pump site expressions to compensate for the loss of cells, thereby maintaining corneal transparency [50].

Due to cell cycle arrest in the G1 phase, HCECs exhibit limited in vivo proliferation [51]. Several factors contribute to this limitation, including contact inhibition between cells, a deficiency of growth factors, and inhibition of cell entry into the S phase. The inhibition may be attributed to elevated levels of TGF-β2 in the aqueous humour [15]. During development, periocular neural crest (NC) cells proliferate and migrate to form the endothelial monolayer [52]. Once cell-cell contacts are established, this proliferation ceases, a pattern also observed in adult corneal endothelial cells. Research on rat CEC differentiation post-birth has shown a relationship between the establishment of these cell-cell contacts and the end of cell division. This correlation is accompanied by an increased expression of p27kip1 protein, which mediates the TGF-β2 signalling [53,54].

The contact between HCECs is broken when a cell dies or detaches due to injuries, but instead of undergoing mitosis, neighbouring cells migrate and enlarge to cover the defect [6,55].

This is likely due to a lack of stimulation from growth factors. Although mitogenic growth factors are detectable in the aqueous humour, the levels might be inadequate, or the factors might be inactive, resulting in inefficient signalling for proliferation [51,56]. TGF-β2, primarily latent in the aqueous humour, can be activated by HCEC-expressed proteins, such as thrombospondin-1 [57]. Endothelial cells express mRNA and proteins of TGF-β receptors I, II, and III, which are essential for TGF-β signalling [58]. Studies on animal models suggest that both exogenous and self-secreted TGF-β2 can inhibit cell transition into the S phase, thus limiting cell proliferation [59,60].

2.3 Corneal Endothelial Transplantation

For cases of irreversible corneal endothelial decompensation, the traditional remedy has been corneal transplantation. Developed in the 19th century, penetrating keratoplasty (PKP) was the primary method to restore vision from corneal endothelial dysfunction, in which the entire thickness of the cornea was replaced with a donor substitute [61]. However, in recent decades, endothelial keratoplasty (EK) has emerged as the preferred surgical intervention. EK provides a more targeted approach, replacing only the damaged corneal endothelial layer. This method is less invasive, preserves the structural integrity of the eye, and reduces the potential for corneal suture-related issues and infections. When compared to PKP, EK offers patients a faster and more effective recovery. Moreover, with a reduced or even absent stroma in the graft, the number of antigen-presenting cells is lower, which in turn reduces the likelihood of graft rejection [62].

Two specific types of EK, namely Descemet's stripping endothelial keratoplasty (DSEK) and Descemet's membrane endothelial keratoplasty (DMEK), have demonstrated considerable

success [63]. DSEK was first pioneered by Melles et al. and Price et al. in the early 2000s [64,65]. During the operation, the surgeon creates a small incision in the cornea, then uses a specialised instrument to access the anterior chamber and remove the corneal endothelium, Descemet's membrane, and a thin portion of the stroma. A healthy donor counterpart is then positioned and sutured into place before the wound is closed. Over time, the procedure was refined, leading to the variant termed Descemet stripping automated endothelial keratoplasty (DSAEK) [66]. DMEK, on the other hand, is a more recent procedure where only the endothelium and the Descemet's membrane are replaced. This technique leaves the host's corneal stroma intact, facilitating a faster recovery. DMEK offers superior surgical outcomes and is highly disease-specific. However, it requires a higher level of surgical expertise, making it more challenging to execute [67,68].

Despite significant technical advancements, the widespread application of EK is hindered by a shortage of corneal grafts. The promising results of EK, along with the impact of an aging population experiencing a surge in late-onset ocular conditions (e.g., cataracts or glaucoma) that cause corneal endothelial damage, have encouraged both ophthalmologists and patients to consider EK during earlier stages of endothelial dysfunction [69]. The graft for EK requires a donor cornea with high-quality endothelial cells. However, the natural reduction in HCEC density with age, coupled with strict donor selection criteria, makes finding suitable donors increasingly difficult. In regions where tissue and organ donation are discouraged due to cultural beliefs, the challenge is exacerbated. In essence, the escalating demand for corneal transplants is met with a concerning decline in the availability of suitable donors [70]. As a result, there is a growing interest in regenerative medicine. Key areas of exploration in this field encompass cell injection and the development of tissue-engineered corneal endothelial grafts employing seed cells and carrier scaffolds.

2.4 Cell-based Therapy

Cell-based therapy presents as a viable alternative to relieve the shortage in donor corneas. Relative to endothelial keratoplasty, it offers the benefit of a less invasive delivery approach. Cultured HCECs are suspended and then injected into the anterior chamber, ideally near the site of endothelial loss or injury [71]. A well-preserved Descemet's membrane is generally a prerequisite for optimal postoperative results. However, modulating the quantity and behaviour of the injected cells is rather challenging. Insufficient cells can result in an inadequate final cell density, compromising the efficacy against conditions like corneal oedema. Conversely, cells in excess cannot all adhere to the Descemet's membrane and might obstruct the trabecular meshwork around the cornea, hampering aqueous humour outflow from the anterior chamber, hence elevating intraocular pressure. Another concern is an uneven deposition of the cells, which may lead to tumours if they attach to unintended places of the eye [72].

Various strategies are employed to enhance the success rate of cell delivery and ensure even distribution of the injected cells. For instance, after the operation, patients are advised to lie in a prone position, which helps the cells fall to the posterior surface of the cornea. Controlled eye movements further aid in achieving a uniform distribution [73]. The cell-settling process may be assisted by labelling the corneal endothelial cells with magnetic particles. Results from animal studies have been promising, demonstrating that these magnetically labelled cells can be guided to specific regions [74-76]. Additionally, reports suggest ROCK-inhibitor Y-27632 added to the cell suspension enhances cell adhesion, promotes expression of functional markers and maintains the hexagonal cell shape in animal models [77,78]. In a clinical trial involving 11 human individuals with bullous keratopathy, the addition of Y-27632 in the injected cell suspension facilitated recovery of HCEC density within 24 weeks [79]. Their five-year follow-up study revealed that 10 out of the 11 treated eyes successfully restored endothelial function,

boasting an average of 1257 cells/mm^2 HCEC density, thus verifying the safety and efficacy of this approach. However, the authors also found that FECD patients still had some guttae in their Descemet's membranes, and the abnormal microenvironment of the FECD eyes was considered a major factor for the less optimal results [80]. Therefore, the scope of application and longer-term effects of primary HCEC transplantation still need further exploration.

A significant amount of HCECs is required for cell-based therapies. They are either expanded from primary HCECs or differentiated from various types of stem cells, such as pluripotent stem cells and corneal endothelial progenitor cells:

2.4.1 Primary HCECs

Primary HCECs are typically sourced from donor corneas that do not meet transplantation standards or from the residual limbal areas of donor corneas post-transplantation. During in vitro cultivation, the breakdown of cell-cell connections combined with the influence of suitable growth factors allows these cells to exit the G1 phase, thereby completing the cell cycle and proliferating [81]. This means that HCECs harvested from just one donor cornea can, after expansion, potentially treat multiple patients with corneal endothelial decompensations – a significant advantage over direct graft transplantation.

However, this cultivation process is not without its challenges. A key concern is promoting the growth of these naturally low-proliferative HCECs while preventing endothelial-mesenchymal transition (EMT), a process that sees endothelial cells morph into fibroblast-like cells (Figure 2), losing their natural function [82]. It is crucial to avert EMT to maintain the cells' inherent functionality, which is vital for successful corneal transplantation. Over the past few decades, numerous culture media additives have been trialled on HCECs, including ascorbic

acid [83], insulin-like growth factor [84], nerve growth factor [85], epidermal growth factor [86] and fibroblast growth factor [87]. Among these, ROCK-inhibitor Y-27632 emerged as particularly effective [88]. Complementing this, Li et al. revealed that nicotinamide not only amplifies HCEC proliferation and suppresses EMT in vitro but also showcases promising effects when applied topically in rabbit models in vivo [89].

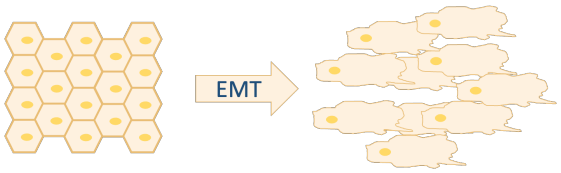

Figure 2. An illustration of endothelial-mesenchymal transition (EMT), a process where the tightly packed corneal endothelial cells take a phenotypic drift and become irregularly shaped and lose the cell-cell contact.

Despite significant advancements in media formulation, achieving a consistent yield of cultured HCECs remains elusive, unable to address the deficit of donor corneas fully. While some researchers have explored the realms of gene regulation and attempted to immortalise HCECs, the risk of tumorigenesis and chromosomal abnormality renders these cells unsuitable for clinical purposes [20,90]. Intriguingly, peripheral corneal endothelial cells display heightened in vitro proliferation, potentially owing to the presence of corneal endothelial progenitors in this zone [91]. This discovery might hint at a novel source of robust HCECs for transplantation. Moreover, biomimetic substrates, emulating the stiffness and specific extracellular matrix components of the Descemet's membrane, have proven to be instrumental in enhancing the in vitro proliferation of HCECs and in curbing EMT [17]. Adding another layer of complexity, donor-related factors such as age, medication use, cellular metabolic activity, and oxidative stress from excessive UV exposure can all influence cell proliferation and phenotype preservation [92-94]. Selecting donors based on criteria like cause of death, age, medication history,

and other relevant variables may help control variance and increase consistency in HCEC cultivation success.

2.4.2 Pluripotent Stem Cells

Stem cells are uniquely characterised by their capability for self-renewal and directed differentiation into specific cell lineages given appropriate conditions. In light of the inherently limited regenerative potential of HCECs, pluripotent stem cells present a compelling alternative for the regeneration or replacement of compromised corneal endothelium. Induced pluripotent stem cells (iPSCs) and embryonic stem cells (ESCs) represent the primary categories of pluripotent stem cells. Both of these cells possess the proficiency to differentiate into a spectrum of epithelial and endothelial lineages [95,96]. In contrast to primary HCECs, pluripotent stem cells manifest an augmented in vitro expansion rate and are not constrained by corneal donor availability. While ESCs are a prospective reservoir for HCEC generation, their application is encumbered by ethical issues. Conversely, iPSCs, derived via cellular reprogramming, offer a novel therapeutic strategy. Typically sourced from autologous patient cells, they mitigate graft rejection risks and can proliferate in vitro, unburdened by the ethical concerns associated with ESCs [97].

Most research approaches direct iPSCs towards a neural crest (NC) lineage in line with the origins of HCECs. Once these cells take on an NC character, a variety of techniques are used to further differentiate them into corneal endothelial-like cells. Exposing the intermediate neural crest-like cells to platelet-derived growth factor-B, WNT signalling inhibitor DKK-2, and basic fibroblast growth factor results in the formation of hexagonal cells exhibiting endothelial traits [98]. Similarly, a combined application of SB431542 and ROCK-inhibitor H-1125 induces analogous outcomes [99]. Moreover, pilot research by Bosch et al. demonstrated

the possibility of guiding NC cells towards an endothelial fate with conditioned media from existing HCEC cultures [100]. Some researchers bypass the intermediate stage, directing pluripotent stem cells directly to a corneal endothelial fate [101,102]. One of the studies, for example, found that a mix of cholera toxin, epidermal growth factor, and ROCK inhibitor Y-27632 in the culture medium can directly differentiate iPSCs into corneal endothelial-like cells [102].

One of the main challenges in using pluripotent stem cells therapeutically is ensuring the purity of the differentiated cells. Due to their vast potential and complex differentiation mechanisms, unwanted cell types might be produced, causing inconsistencies. Therefore, it is crucial to closely monitor each stage of differentiation using specific cellular markers. Early NC cells can be identified using markers such as p75NTR and HNK-1 [99]. Furthermore, markers for corneal endothelial cells, like CD166 and CD340, may help in isolating the desired cells [103]. In addition, using recombinant proteins instead of animal-sourced extracellular matrix components for cell cultures minimises inconsistencies and eliminates risks of contamination [104]. Before these cells can be used clinically, their safety, particularly concerning tumour formation, and their functionality must be thoroughly verified.

2.4.3 Corneal Endothelial Progenitor Cells

Progenitor cells are a subset of cells capable of differentiating into a limited range of specialised cells. Research suggests that cells in the corneal endothelium's periphery, notably the trabecular meshwork, may possess the ability to differentiate into CECs [105,106]. These cells exhibit markers linked with the neural crest and form spheroids when cultured in vitro – a characteristic behaviour of stem cells from the neural crest [107]. Post-injury, the cornea has been found to express additional stem cell markers, including Oct-3/4 and Wnt-1, as well as

differentiation markers Pax-6 and Sox-2. Notably, Pax-6 and Sox-2 are also expressed in the corneal endothelium's periphery [108]. Research by Yam et al. identified niches in the posterior limbus surrounding the endothelium, housing progenitor-like cells with the capacity to differentiate into CECs [107]. Complementary to this, animal studies have produced promising results. Corneal endothelial-like cells generated from progenitor cells were successfully transplanted to rabbit models, highlighting the clinical potential of corneal endothelial progenitor cells [109,110]. These findings suggest that corneal endothelial progenitor cells may be present in the posterior peripheral regions of the cornea and play a role in the repair of endothelial cell damage.

2.4.4 Adult Stem Cells

In comparison to pluripotent stem cells, adult stem cells offer certain advantages: they are more straightforward to isolate and culture, and they present fewer challenges related to epigenetic anomalies and ethical controversies. An array of adult stem cells has been investigated for their potential to differentiate into CECs. This includes neural crest (NC) cells [52], skin-derived precursor cells [111], umbilical cord mesenchymal stem cells [112], and various other cell types. NC cells, which play a crucial role in numerous embryonic developmental processes, can be found in adult skin and hair follicles, or alternatively derived from pluripotent stem cells. Employing conditioned media from cultured rat CECs, researchers generated endothelial-like cells from differentiated NC cells. However, only approximately half of the initial cells underwent differentiation, and the proliferative capacity of the resultant cells was somewhat restricted [113]. Meanwhile, dermal progenitor cells, like HCECs, have their origins in the neural crest. They are found in various regions of the human dermis, can be extensively propagated in vitro, and are amenable to long-term cryopreservation. Their ability to suppress

T-cell immune responses underscores their potential therapeutic utility, particularly in countering graft rejection [111]. In a similar vein, umbilical cord mesenchymal stem cells, derived from the umbilical cord tissue obtained during labour, exhibit subdued immunogenicity [114]. Yamashita et al. documented the successful restoration of transparency and thickness in rabbit corneas following transplantation of corneal endothelial-like cells differentiated from allogeneic umbilical cord mesenchymal stem cells [112].

2.4.5 Quality Assessment for Seed Cells

Regardless of the seed cells' origin or the cultivation method employed, a rigorous quality assessment is paramount to ensure the harvest of a healthy, homogenous culture of HCECs. The hexagonal structure of the cells is closely monitored during in vitro cultivation and especially upon reaching confluence. This monitoring helps identify and exclude the presence of spindle-shaped fibroblast-like cells, which are hallmarks of EMT [82]. Two metrics are particularly useful in this assessment: circularity and the coefficient of variation (CV) [14,115]. The former, determined using the formula $\mathbf{Circularity = Parameter^2/4\pi \cdot Area}$, gauges the similarity of a cell's shape to that of a circle; and the latter reveals cell size variation by dividing the standard deviation of cell area by the mean cell area. For instance, in an ideal hexagonal pattern of an HCEC monolayer, the average circularity would be 1.1, with a CV of 0. If a culture undergoes EMT, these values will noticeably increase, indicating potential issues in the cell culture.

Additional assessments involve the identification of molecular hallmarks and functional analysis. Typical positive markers include Na^+/K^+ ATPase and ZO-1 expressions on the cell membrane, as well as collagen type VIII secretion in the extracellular matrix [116,117]. However, it is important to note that these indicators are not exclusive to corneal endothelial cells; they

also appear in other cell types like lung and intestinal epithelium and even corneal epithelial cells. Conversely, in cases where the cell culture undergoes EMT, increased levels of mesenchymal markers, most notably α-smooth muscle actin, are often observed [15,118]. Studies have characterised various other genes and proteins, including cluster-of-differentiation (CD) markers, showing either positive or negative expression as indicative of HCEC phenotypes [103,119]. However, a consensus has yet to be reached for exclusive signs of HCECs. When monitoring for EMT in HCECs, it is advisable to test a combination of markers, as relying on the presence or absence of a single one might not definitively confirm or rule out the undesired transition [120]. Moreover, the mere presence of the Na^+/K^+ ion channels does not vouch for their operational capability. In vitro tests like the trans-endothelial electrical resistance (TEER) and Ussing chamber studies serve to evaluate the ion transport mechanism of the seed cell monolayer [117,121].

2.5 Tissue-engineered Graft

In addressing the challenges and risks associated with anterior chamber HCEC injections, tissue-engineered corneal endothelial grafts have gained prominence. The grafts are designed to have an optimal cell density that surpasses the standard requirement for endothelial keratoplasty (EK), enhancing the potential for graft survival and integration [122]. Nevertheless, these grafts necessitate a considerably smaller number of cells in comparison to the cell injection approach. The typical figure is around 2×10^5 HCECs per graft, allowing treatment for up to 50 patients from a single donor cornea [123]. Employing a deliverable cell carrier, a tissue-engineered graft ensures a monolayer of HCECs is adhered to the cornea's posterior surface. An optimal cell carrier mirrors the basement membrane's role for HCECs in vivo. Essential criteria for these carriers encompass non-cytotoxicity, biocompatibility, and facilitating a

favourable microenvironment for key cellular activities, such as adhesion, migration, proliferation, and differentiation [124]. Moreover, they must possess robust structural integrity to endure surgical manipulations and ideally maintain transparency with a refractive index approximating 1.373, akin to the posterior surface of the cornea [125].

The materials used in the fabrication of cell carriers can be broadly classified into two primary categories: biological derivatives and polymers. Biological derivatives include materials such as decellularised corneal stroma [126], Descemet's membrane [127], amniotic membrane [128], anterior lens capsule [129], and fish scale [130]. Among these, the decellularised corneal stroma has gained significant attention and has been predominantly preferred in preclinical studies [126,131-134]. Polymers, on the other hand, encompass a broad spectrum ranging from natural molecules like silk fibroin [135] and collagen [136] to synthetic counterparts such as polyglycolic acid (PGA) [137] and polycaprolactone (PCL) [138]. They present an opportunity to reduce the dependency on donor tissues and mitigate risks of xenogeneic immune reactions. Intriguingly, thermosensitive matrices introduce the potential to formulate a transplantable monolayer of HCECs without the need for cell carriers, although the cell sheet's innate delicacy poses surgical challenges [139].

2.5.1 Decellularised Biological Derivatives

2.5.1.1 Corneal Stroma

Decellularised corneal stroma derived from various species, such as humans [134], pigs [133], and ostriches [140], have been explored as substrates for the in vitro culture of CECs. The objective of decellularisation is to eliminate cellular components, pathogens, and immunogenic substances from the stroma whilst preserving the integrity of the extracellular matrix. However,

there have been concerns that α-gal, a prevalent xenoantigen, is retained in xenogeneic tissues following decellularisation processes. This residual substance might provoke an immune response upon grafting, leading to possible rejection [141].

Among the range of species, human derivatives are perceived as the prime choice since they are free of xenogeneic immunogens. Proulx et al. highlighted the potential of using human corneas for corneal endothelial regeneration. When feline CECs were cultured on decellularised human corneal stroma, they exhibited polygonal morphology and typical corneal endothelial protein expressions [134]. Trials in monkey models demonstrated a recovery of roughly 75% and 60% of endothelial pump function after grafting HCECs with human and porcine decellularised corneal stroma, respectively [126]. Yet, the employment of human tissues faces restrictions due to the persisting challenge of donor scarcity. To address this, a more economical approach was exploited by preparing six stroma slices from each human donor cornea using femtosecond laser dissection. Notably, these structures retained their efficacy after being stored at reduced temperatures for up to two years [132].

Acellular porcine corneal stroma (APCS) presents as a potential alternative, independent of human donors. It parallels its human equivalent in dimensions and optical characteristics and demonstrates biocompatibility. Originally devised for lamellar keratoplasty, where the anterior portion of the cornea is transplanted, various clinical studies have affirmed the feasibility of APCS as a substitute for donor corneas [142-144]. Progress in decellularisation, complemented by gene editing techniques, aspires to eliminate xenoantigens and lessen the threat of immune rejection [145]. An innovative approach involves crosslinking the decellularised tissue with chondroitin sulphate has shown a marked reduction in α-gal presence in APCS, thus diminishing immune response post-operation [146].

2.5.1.2 Descemet's Membrane

Situated directly posterior to the corneal stroma, the Descemet's membrane (DM) functions as the basement membrane for HCECs. Its intricate molecular composition, featuring fibronectin [147], laminin [148], and types IV [149] and VIII collagen [150], is fundamental for ensuring the stability of HCECs. The significance of laminin in this context was underscored in a study, where HCECs cultured on substrates coated with laminin-511 or laminin-521 displayed augmented adhesion and proliferation [151]. Moreover, efforts to replicate the DM's natural stiffness have yielded encouraging outcomes. Notably, coating type IV collagen on polydimethylsiloxane (PDMS) moulds with 50kPa elastic modulus has proven efficacious in establishing an optimal microenvironment for the proliferation of bovine CECs [17].

The DM presents an unparalleled potential as a cell carrier in the crafting of tissue-engineered corneal endothelial grafts. However, the pressing scarcity of human donor corneas has necessitated the exploration of xenogeneic DM alternatives. Lange et al. successfully cultured a confluent rabbit CEC monolayer on a bovine DM substrate with a density approximating 3,000 cells/mm^2 within a week [127]. These bioengineered tissues remained clear post-grafting in rabbits with induced corneal oedema. In another investigation, HCECs, which had undergone extensive prior sub-culturing, formed a monolayer with characteristic hexagonal patterns on decellularised porcine DM within five days. These cells also manifested crucial molecular markers like ZO-1 and Na+/K+-ATPase. Subsequent transplantation of the recellularised DM restored the corneal clarity and thickness in feline models [152]. Nonetheless, potential xenoantigen concerns might pose challenges for clinical applications.

2.5.1.3 Human Anterior Lens Capsule

The human anterior lens capsule (HALC), a transparent basement membrane frequently discarded during cataract surgeries, presents as an intriguing alternative substrate for corneal endothelial tissue engineering. This resilient and minimally immunogenic membrane parallels the DM in its key molecular components, notably collagen type IV and laminin [153]. When cultured on HALC, HCECs not only reached a density of 3000 cells/mm^2 but also aptly replicated the characteristic morphology and protein expressions inherent to native HCECs [129]. Likewise, Spinozzi et al. also achieved promising outcomes seeding HCECs on HALC. Interestingly, through simulated surgeries, the authors compared HALC with DM and a collagen-based substrate, assessing their efficacy as HCEC carriers. The results were illuminating: HALC exhibited comparable HCEC adherence and post-operative cell viability to DM, and its surgical manipulability rivalled that of DMEK donor grafts [154]. The field currently awaits clinical validation to highlight HALC's potential as a viable HCEC carrier.

2.5.1.4 Human Amniotic Membrane

The amniotic membrane (AM), an integral part of the placenta, possesses the thickest basement membrane in the human body. Its inherent properties, such as sufficient transparency, reduced immunogenicity, and a rich composition of desired ECM proteins, have already put the AM in use for ocular surface reconstruction [155-157]. While its translation to clinical settings for corneal endothelial regeneration is yet to be realised, in vitro and animal studies have shown promising results. Notably, the AM has demonstrated its ability in maintaining the native morphology and functionality of HCECs [128,158,159]. In an animal study involving primate models, HCECs cultured on the AM demonstrated impressive results post-transplantation: the bioengineered graft remained clear for the duration of the experiment, exhibited cell

morphology comparable to native corneal endothelial cells, and displayed no signs of inflammation or graft rejection [160]. However, while the AM holds promise, certain limitations, such as its inconsistent stiffness, absence of cornea-like curvature, variable thickness, and potential for disease transmission, mandate a cautious approach and further refinement before deeming it an optimal HCEC carrier [161,162].

2.5.1.5 Fish Scales

Fish scales, with their multi-layered type I collagen arrangement, resemble the structural organisation of the human corneal stroma, making them an economical candidate for the construction of tissue-engineered corneal endothelium [130]. Previous research indicated that corneal epithelial cells, when co-cultured with corneal stromal cells on decellularised fish scales, adopted favourable phenotypes [163]. However, when HCECs were cultured on decellularised fish scales, only approximately two-thirds took on the desired polygonal shape, and both cell adhesion and proliferation proved to be suboptimal [164].

2.5.2 Natural Polymers

2.5.2.1 Collagen

The cornea is primarily composed of collagen, which constitutes approximately 71% of its dry weight, with type I collagen being the predominant form, complemented by collagen types III, IV, V, and VIII [165,166]. Given its exceptional biocompatibility, biodegradability, and minimal immunogenicity, type I collagen is regarded as an attractive scaffold material for tissue-engineered corneas. Minami et al. pioneered this approach by seeding primary bovine corneal epithelial, stromal, and endothelial cells in a co-culture system within three

dimensional type I collagen gels, resulting in tissue-engineered constructs remarkably reminiscent of native corneas [167]. Subsequent investigations also replicated this success using human corneal cells [168]. Moreover, monkey CECs, after being cultured on type I collagen scaffolds for a month, exhibited a hexagonal shape and typical corneal endothelial protein expressions. When these engineered tissues were grafted onto monkey corneas, they maintained clarity throughout the study, and the CEC density consistently exceeded 1600 cells/mm^2 in vivo over a span of 2 years [169].

However, employing type I collagen hydrogels as cell carriers presents certain challenges. An obvious drawback is its inadequate mechanical resilience, which hinders suturing or precise manipulation, coupled with suboptimal transparency. Expelling water from the hydrogel causes the collagen fibrils to align in the direction of flow and pack more densely together, thereby enhancing the transparency and mechanical strength [170]. Such a process, known as plastic compression (PC), involves either exerting downward pressure to expel fluid from the hydrogel with a load [170], or using an upward absorption method with a commercially available kit, namely Lonza RAFT™ [171]. Research has shown that both immortalised HCEC lines and primary HCECs can form a tightly packed monolayer on these compressed collagen scaffolds [172].

2.5.2.2 Gelatine

Gelatine, a partially hydrolysed derivative of collagen, is viewed as a promising material for corneal tissue engineering because of its biocompatibility, biodegradability, and ability to support cell adhesion and proliferation [173,174]. However, its mechanical strength is insufficient for surgical procedures [175]. This challenge can be addressed with chemical crosslinking. Schwartz and McCulley were early to adopt this method using glutaraldehyde (GTA). As they

reported, rabbit CECs grown on GTA-crosslinked gelatine films showed traits and functions similar to natural corneal endothelium, and initially opaque rabbit corneas progressively regained transparency following transplantation [176]. Crosslinking with 1-Ethyl-3-(3-dimethylaminopropyl) carbodiimide (EDC) and N-hydroxysuccinimide (NHS) proves less harmful to cells than glutaraldehyde [177]. Through EDC/NHS crosslinking, researchers crafted sturdy, thin gelatine grafts that can be folded and inserted into a rabbit's anterior chamber through a small opening [178]. Moreover, shaping the gelatine films to match the curvature of the cornea can prevent wrinkles in the graft, which helps it integrate with the host after transplantation. In monkey experiments, those receiving gelatine films carrying monkey CECs showed reduced oedema and gained clearer vision [179].

2.5.2.3 Hyaluronic Acid

As a natural compound present in the eye's aqueous and vitreous humour, hyaluronic acid (HA) offers great potential for corneal endothelial tissue engineering. This viscoelastic glycosaminoglycan binds to HCECs [180], facilitates cell adhesion and proliferation, and aids in integration with the host cornea upon transplantation [181]. However, its rapid degradation in aqueous environments, such as the anterior chamber, and limited mechanical strength might limit its use as a scaffold for tissue-engineered corneas [182]. To enhance HA's suitability as a cell carrier, scientists have adjusted its structure through crosslinking. For example, an HA hydrogel disc crosslinked with EDC has shown strength, flexibility, and transparency while supporting rabbit CEC culture [183].

2.5.2.4 Silk Fibroin

Silk fibroin (SF) is renowned for its tuneable biodegradability and mechanical properties [184]. With FDA approval, this biomaterial has been widely adopted in tissue engineering [185] and drug delivery [186]. In constructing tissue-engineered corneal endothelium, the primary advantage of SF lies in its micropatterns, which guide cell growth and the orientation of ECM fibrils [187]. However, due to its modest support for cell adhesion, researchers typically pre-coat SF films with ECM proteins, such as collagen, prior to seeding CECs [188,189]. Research has shown that when primary HCECs are cultured on SF films coated with type IV collagen, they form a continuous monolayer, adopt a polygonal shape, and express characteristic markers. [135]. Similarly, rabbit CECs grown on SF films coated with FNC displayed attributes akin to in vivo CECs. When grafted onto rabbit corneas, these constructs successfully restored corneal transparency and thickness within six weeks [190].

2.5.2.5 Chitosan

Chitosan, a naturally derived polysaccharide, offers biocompatibility and biodegradability, with versatility for chemical modifications [191]. Its inherent fragility can be addressed by blending with other materials. For instance, chitosan-PCL hybrid scaffolds have shown enhanced mechanical robustness while promoting bovine CEC attachment and proliferation and maintaining the morphology and phenotype of the cells [192,193]. Similar benefits were observed when chitosan was combined with gelatine and chondroitin sulphate for rabbit CEC cultures, though in vivo evaluations indicated mild inflammatory responses [194]. Additionally, crosslinking chitosan with polyvinyl alcohol (PVA) and coupling its amine groups have been shown to amplify the material's fluid uptake and mechanical strength [195].

2.5.3 Synthetic Polymers

Synthetic materials provide uniform compositions, which can be tailored to meet specific requirements such as optical clarity, mechanical property, and controlled degradation. This, combined with their cost-effectiveness and scalability, underscores their appeal in tissue engineering research as alternatives to natural scaffolds [196]. However, synthetic polymers may lack biocompatibility, leading to suboptimal cell adhesion and proliferation. This was evident when HCEC-12, an immortalised HCEC line, cultured on a composite scaffold of polymethylmethacrylate (PMMA), poly lactic-co-glycolic acid (PLGA), and PCL failed to form a consistent monolayer [185]. Surface modification enhancing biocompatibility can address such challenges. For example, collagen type I-coated PLGA films not only improved surface roughness, transparency, and hydrophilicity, but also supported rabbit CEC growth and phenotypic maintenance [197]. Similarly, polyvinylidene fluoride (PVDF) films coated with type IV collagen fostered the growth of bovine CECs, leading to a consistent monolayer formation and typical cell markers expression [198]. In addition, Ozcelik et al. developed ultrathin chitosan-polyethylene glycol (PEG) hydrogels that mirrors the mechanical profile of human corneas. Their experiments confirmed the scaffold's biocompatibility, showcasing hexagonal cell monolayer formation by ovine CECs within a week and minimal inflammation in vivo [199,200].

2.5.4 Cell Sheets

Cell sheets offer control over graft size, shape, and positioning during transplantation without relying on cell carriers [201]. Typically, CEC sheets are derived by seeding cells on thermo-responsive substrates, notably poly N-isopropylacrylamide (pNIPAAm). After reaching a confluent monolayer at 37°C, reducing the temperature below the substrate's lower critical solution temperature (LCST) enables the CECs to detach as an intact sheet, with cells

remaining interconnected [202]. Crucially, these cell sheets maintain the ECM complex secreted by the cells, facilitating rapid adherence to the posterior corneal surface upon transplantation [203]. Several pNIPAAm derivatives, including pNIPAAM-co-diethyleneglycol methacrylate (DEGMA) [204], pNIPAAm-co-glycidylmethacrylate (NGMA) [205], and pNIPAAM-poly 3-hydroxybutyrate (PHB)-pNIPAAM [206], have also proven effective for CEC sheet cultivation and detachment. Besides the thermo-responsive approach, photo-responsive [207], pH-responsive [208], electro-responsive [209], and mechanical scraping [210] methods have also been explored for cell sheet preparation. While mechanical detachment offers simplicity without the risk of inducing cytotoxicity, it also presents challenges, including potential sheet rupture during extraction and transfer. Nevertheless, using this method, Hitani et al. created rabbit CEC sheets, and the cells mostly retained on the corneal surface a week after transplantation [211].

2.6 Summary

Corneal endothelial tissue engineering aims to craft a substitute that parallels the intricate structure, cellular morphology, functionality, and mechanical attributes of native donor grafts. Ideally, the surgical manipulation of this engineered tissue should echo the handling of DMEK or DSAEK donor grafts. While significant efforts have been made in the realms of seed cell cultivation and carrier scaffold preparation, several challenges persist.

Seed cells need to be produced on a large scale and should closely match the phenotype and function of native HCECs. It is pivotal to mitigate endothelial-to-mesenchymal transition (EMT), a phenomenon that pushes cells towards a fibroblast-like state. A wealth of studies has documented both the in vitro cultivation of primary CECs and the differentiation of corneal endothelial progenitor cells and various types of stem cells. Some investigations have hinged

on immortalised HCEC lines. While these cells capture certain characteristics of their native counterparts, their potential carcinogenicity exclude them from clinical application [90,212].

An ideal HCEC carrier scaffold should exhibit optimal transparency, superior biocompatibility, robust mechanical properties, and a lack of immunogenicity. Despite extensive research into biological derivatives as well as both natural and synthetic polymers, few have comprehensively met the criteria for corneal endothelial reconstruction. Biological derivatives present concerns regarding disease transmission, potential immunogenic responses, and can vary in composition. On the other hand, while natural and synthetic polymers offer compositional consistency, they may fall short in mechanical properties or biocompatibility. Cell sheets, which bypass the need for cell carriers, are delicate and can be easily damaged during transplant.

Chapter 3

HCEC-12 Cell Culture and Functional Assays

This chapter presents the methodology for culturing and assaying the human corneal endothelial cell line, HCEC-12, focusing on optimising cell adhesion and proliferation. The cells were cultured in flasks pre-coated with laminin and chondroitin sulphate, with protocols for seeding, medium formulation, and cryopreservation. The efficacy of collagen type IV (COL4) as a coating substrate was evaluated. Quantitative assessments of cell adherence and proliferation were conducted using the cell counting kit-8 (CCK-8) assay. Immunofluorescence microscopy provided insights into the cells' morphological responses to various coatings. Protein expressions crucial for maintaining the corneal endothelial cell phenotype were analysed through Western Blot and flow cytometry.

3.1 HCEC-12 Culture

The human corneal endothelial cell line, HCEC-12 (DMSZ, ACC-646), was employed for cellular experiments in this study. Adhering to the supplier's guidelines, the procured frozen vial of HCEC-12 cells was inoculated at a density of 6000 cells/cm^2 in tissue culture treated flasks. These flasks were pre-coated with a combination of laminin and chondroitin sulphate to enhance cell attachment and growth. For the coating process, a stock solution of chondroitin sulphate was prepared by dissolving lyophilised chondroitin sulphate (Sigma-Aldrich, C9819) in PBS (ThermoFisher, 10010-023) to achieve a concentration of 100mg/mL. This stock

solution was then combined with a stock laminin solution (Sigma-Aldrich, 11243217001) to produce a working solution containing 10µL/mL laminin and 10mg/mL chondroitin sulphate. T-75 and T-175 flasks were coated with 9mL and 21mL of this filter-sterilised working solution, respectively. The flasks were incubated for 5 hours at 37°C to allow for effective coating. Post-incubation, the coating solution was discarded, and the flasks were rinsed with PBS to prepare them for cell inoculation.

The culture medium for HCEC-12 cells was formulated by blending 47% F-12 nutrients (ThermoFisher, 21765029) and 47% Medium 199 (ThermoFisher, 31150022). This mixture was supplemented with 5% fetal bovine serum (ThermoFisher, 10082147) and 1% penicillin/streptomycin (ThermoFisher, 15070063). The medium was refreshed every 2-3 days, as per the supplier's recommendations. For cryopreservation, cells harvested from initial subcultures were combined with a cryoprotective solution containing 10% dimethyl sulfoxide (DMSO, Fisher Scientific, BP231-100), 20% FBS, and 70% culture medium. These cells were stored either at -80°C or in liquid nitrogen. Upon requirement, a vial of these cryopreserved cells was thawed and cultured until they reached 80% confluency before being harvested for further experiments. For cell harvesting, a trypsinisation method was employed. The adherent HCEC-12 cells were first rinsed twice with PBS (ThermoFisher, 10010-023). Subsequently, they were treated with 0.05% trypsin/EDTA (ThermoFisher, 25300054) for a duration of 5 minutes at 37°C. This enzymatic treatment facilitated the detachment of cells from the culture surface. The detached cells were collected, centrifuged at 600x g to form a pellet, and then resuspended in fresh culture medium. These resuspended cells were then seeded in new culture-wares for subsequent experiments.

3.2 Collagen Type IV Coating for Cell Culture

Collagen type IV (COL4) derived from the human placenta (Sigma-Aldrich, C5533-5MG) was chosen as a substrate for coating culture surfaces to facilitate the comparison study with the reconstituted PPC solution. Initially, a stock solution was prepared by dissolving the collagen in 0.5M acetic acid (Sigma-Aldrich, 695092) to achieve a concentration of 1mg/mL. This stock solution was subsequently diluted using 0.5M acetic acid to formulate a working solution with a concentration of 150µg/mL. For the coating process, specific volumes of the working COL4 solution were added to the desired culture-ware based on its surface area. For instance, a 96-well plate received 50µL of the solution per well, which is equivalent to 155.5µL/cm^2. Similarly, a T-75 flask was coated using 11.66mL of the solution. The culture-ware, now laden with the COL4 solution, was then incubated for 5 hours at 37°C. This ensured optimal adsorption of the collagen onto the culture surface, providing a conducive environment for HCEC-12 cell attachment and growth.

Following the overnight incubation, any residual COL4 solution was carefully discarded. The coated surfaces were then subjected to two rinses with phosphate-buffered saline (PBS, ThermoFisher, 10010-023) to eliminate any lingering acetic acid or unattached collagen. To ensure sterility, the culture-ware underwent UV radiation exposure within a biosafety cabinet for an hour. With these steps, the culture surfaces were adequately prepared and sterilised, making them ready for the seeding of HCEC-12 cells.

3.3 Assessment of Cell Adherence and Proliferation

The influence of various coatings, specifically TCPS, COL4, and PPC, on the adherence and proliferation of HCEC-12 cells was meticulously evaluated using the Cell Counting Kit 8 (CCK-8, NBS Biologicals, CK04). This kit operates on a colorimetric principle, wherein viable cells reduce a tetrazolium salt, WST-8, producing a yellow-coloured formazan dye. The quantity of the resultant formazan dye is a direct reflection of the number of living cells present. For the preparation, in accordance with the manufacturer's guidelines, 10μL of the CCK-8 reagent was combined with 100μL of the culture medium in each well of a 96-well plate. This was followed by an incubation period at 37°C for 2 hours. During this time, metabolically active cells facilitated the reduction of WST-8, leading to the emergence of the yellow formazan dye. Post-incubation, the optical density (OD) of each well was ascertained at a wavelength of 450nm using a plate reader (Molecular Devices, SpectraMax i3x). The intensity of the resultant colour serves as a direct indicator of the number of viable cells in the well.

These assays collectively provided a comprehensive understanding of the adherence and proliferation behaviours of HCEC-12 cells on the different coatings, facilitating a comparative analysis of the cellular responses to each substrate. For the proliferation study, HCEC-12 cells were cultured over a period of 9 days, spread across five distinct 96-well plates. Each plate was representative of a specific day, namely days 1, 3, 5, 7, and 9 post-seeding. To ensure optimal growth conditions, the culture medium was replenished every two days. In the context of the adherence study, HCEC-12 cells were seeded onto 96-well plates and allowed specific durations for adherence: 5, 30, 60, and 120 minutes. Each time duration was allocated its own plate. After the designated adherence time, non-adherent cells were gently removed with two PBS (ThermoFisher, 10010-023) washes. The CCK-8 assay was then executed to quantify the number of adhered cells.

3.4 Immunofluorescence Microscopy

HCEC-12 cells were cultured on glass slides situated within 24-well plates. After a period of 7 days, the cells reached confluency and were subsequently fixed using 3.6% paraformaldehyde (PFA, Sigma-Aldrich, 47608) to preserve their cellular structures and maintain their morphology. For the analysis of membrane and extracellular matrix (ECM) proteins, the fixed cells underwent staining with specific primary antibodies. These antibodies targeted ZO-1 (Cell Signaling Technology, 13663S), ATP1A1 (ThermoFisher, MA3-928), COL1 (SCBT, sc-59772), COL4 (Abcam, ab6586), and COL8A2 (ThermoFisher, PA5-35077). In order to assess the intracellular protein α-SMA, cells were first permeabilised using 0.2% Triton X-100 (Sigma-Aldrich, T8787) to allow the antibody to penetrate the cell membrane. Following permeabilisation, the cells were stained with the α-SMA primary antibody (ThermoFisher, MA5-11547). Subsequent to primary antibody incubation, cells were treated with secondary antibodies to amplify the signal and provide fluorescence. The secondary antibodies employed were goat-anti-mouse AlexaFluor 568 (ThermoFisher, A11004), goat-anti-mouse AlexaFluor 647 (ThermoFisher, A21236), goat-anti-rabbit AlexaFluor 568 (ThermoFisher, A11011), and goat-anti-rabbit AlexaFluor 647 (ThermoFisher, A21245). These antibodies bind to the primary antibodies and emit fluorescence when exposed to specific wavelengths of light. For the visualisation of cell nuclei, cells were counterstained with DAPI (ThermoFisher, R37606). AlexaFluor™ 647 phalloidin (ThermoFisher, A22287) was applied to illuminate F-actin, highlighting the cytoskeletal structure of the cells. The stained cells were examined under a Nikon Eclipse Ti widefield fluorescent microscope. The captured images were processed and analysed using the NIS Elements AR software, allowing for a detailed observation of protein expression and cellular structures.

3.5 Cellular Protein Extraction

Cells that reached approximately 80% confluency were detached using rubber cell scrapers (Corning, 353086). The collected cells were transferred to 1.5mL tubes and lysed using radio immunoprecipitation assay (RIPA) buffer (ThermoFisher, 89900) supplemented with 1% protease inhibitor (ThermoFisher, 78430). Following lysis, the cell lysates underwent centrifugation at 12,000rpm for 15 minutes at 4°C. The clear supernatants were carefully pipetted into new 0.5mL tubes. The protein concentration in each lysate was determined using the bicinchoninic acid assay (BCA, ThermoFisher, 1859078). The protein samples were adjusted to the same concentration using a combination of RIPA/protease inhibitor, 4x lithium dodecyl sulfate (LDS) sample buffer (ThermoFisher, NP0007), and 10x dithiothreitol sample reducing agent (ThermoFisher, NP0009). The protein samples were then heated at 90°C for 5 minutes and stored at -20°C until further analysis.

3.6 SDS-PAGE and Irreversible Visualisation of Protein Bands

Sodium dodecyl sulphate-polyacrylamide gel electrophoresis (SDS-PAGE) was performed to separate proteins by size and characterise the composition of protein samples. Samples alongside a protein ladder (Bio-Rad, 1610375) were loaded onto 4-20% precast polyacrylamide gels (Bio-Rad, 4561093). Gel electrophoresis was performed in a Mini-PROTEAN® Tetra Vertical Electrophoresis Cell (Bio-Rad, 1658004) filled with Tris-glycine SDS buffer (ThermoFisher, 28362) at 100V for 1.5 hours. The proteins were separated in this process by their molecular weights. The protein bands can be irreversibly visualised by applying Coomassie Brilliant Blue (Bio-Rad, 1610436) on the gel for two hours at room temperature.

Sodium dodecyl sulphate-polyacrylamide gel electrophoresis (SDS-PAGE) was utilised to separate and characterise protein samples based on their molecular sizes. Protein samples, along with a protein ladder (Bio-Rad, 1610375), were loaded onto 4-20% precast polyacrylamide gels (Bio-Rad, 4561093). Gel electrophoresis was conducted in a Mini-PROTEAN® Tetra Vertical Electrophoresis Cell (Bio-Rad, 1658004), filled with Tris-glycine SDS running buffer (ThermoFisher, 28362), and run at 100V for 1.5 hours. Post-electrophoresis, the protein bands can be irreversibly visualised by staining the gel with Coomassie Brilliant Blue (Bio-Rad, 1610436) for two hours at room temperature.

3.7 Reversible Visualisation of Protein Bands and Western Blot

Proteins separated on polyacrylamide gel through electrophoresis were transferred from the gel to nitrocellulose membranes (Bio-Rad, 1620145) using a wet-transfer method at 300mA for 1.5 hours. Staining the membrane with 0.1% Ponceau S (ThermoFisher, 161470250) allowed reversible visualisation of the protein bands. The membrane was rinsed five times with tris-buffered saline (Bio-Rad, 1706435) containing 0.1% Tween-20 (Bio-Rad, 1610781) (TBST) to remove the Ponceau S stain, thereby preparing the membrane for antibody probing.

To prevent non-specific binding, membranes were blocked with 5% non-fat milk (Bio-Rad, 1706404). Depending on the molecular weights of interest, membranes were cut and incubated with primary antibodies overnight at 4°C. The primary antibodies used were anti-ZO-1 (Cell Signaling Technology, 13663S), ATP1A1 (ThermoFisher, MA3-928), COL8A2 (ThermoFisher, PA5-35077), α-SMA (ThermoFisher, MA5-11547), and β-actin (ThermoFisher, MA5-15739). Following primary antibody incubation, membranes were treated with either anti-rabbit-HRP secondary antibody (SCBT, sc-2357) or HRP conjugated

mouse antibody binding protein (SCBT, sc-516102). The Clarity Western ECL substrate (Bio-Rad, 1705061) was applied to the membranes to visualise the bound proteins through chemiluminescence. Protein bands were then captured on X-ray films (GE Healthcare, 28906837) for analysis.

3.8 Flow Cytometry

Upon reaching an approximate confluency of 80%, cell were detached using a non-enzymatic dissociation solution (Sigma-Aldrich, C5914). Post-detachment, these cells were promptly fixed in a solution containing 3.6% paraformaldehyde (PFA) combined with 1% FBS (ThermoFisher, 10082147) in PBS (ThermoFisher, 10010-023). For the purpose of analysing membrane proteins, the fixed cells were subjected to incubation with specific primary antibodies. These antibodies were targeted against ZO-1 (Cell Signaling Technology, 13663S) and ATP1A1 (ThermoFisher, MA3-928). To detect the intracellular protein α-SMA, cells were permeabilised using a solution of 0.2% Triton X-100 (Sigma-Aldrich, T8787). Once permeabilised, the cells were stained with the primary antibody specific for α-SMA (ThermoFisher, MA5-11547). Following the primary antibody incubation, cells were treated with secondary antibodies to detect the bound primary antibodies. The secondary antibodies used were goat-anti-mouse AlexaFluor 488 (ThermoFisher, A11004) and goat-anti-rabbit AlexaFluor 488 (ThermoFisher, A21236). The analysis of the stained cell samples was achieved using a FACSCalibur flow cytometer (BD Biosciences). The data acquired from the flow cytometer were further processed and comprehensively analysed with the assistance of the FlowJo™ software.

3.9 Statistical Analysis

A one-way ANOVA with Post-Hoc Tukey analysis was utilised to explore significant variations in protein expression and events of contact inhibition of locomotion (CIL) across various culture conditions, while a two-way ANOVA with Post-Hoc Tukey analysis was employed to assess the impact of different culture conditions on cell number changes over time. All statistical analyses were conducted using GraphPad Prism 8 (GraphPad Software. Inc, USA). For all tests, a p-value of less than 0.05 was considered significant.

Chapter 4

Optimisation of Collagen IV Coating Procedure for HCEC-12 Culture

The human corneal endothelium is pivotal for maintaining corneal clarity, but its limited regenerative capacity poses challenges for therapeutic interventions. This chapter focuses on optimising the process to coat collagen type IV (COL4), a commonly used substrate for human corneal endothelial cell (HCEC) culture. Given the challenges associated with primary HCECs, we employed the immortalised HCEC-12 cell line, which retains many native HCEC characteristics. Through systematic experimentation, varying the volume, concentration, and incubation time of COL4 solutions, an optimal coating condition was identified. The results revealed that coating each well of a 96-well plate with 50µL of 100µg/mL COL4 solution for 5 hours at 37°C provides an effective substrate for HCEC-12 culture. This optimised protocol ensures consistent cell adhesion and proliferation, setting a benchmark for subsequent corneal endothelial tissue engineering studies.

4.1 Introduction

The human corneal endothelium plays a crucial role in maintaining the cornea's transparency and visual acuity. However, the limited regenerative capacity of HCECs poses significant challenges in treating corneal endothelial diseases. Tissue engineering offers a promising avenue to address these challenges, with the potential to culture HCECs in vitro and utilise

them for therapeutic applications. A pivotal aspect of successful HCEC culture is the substrate on which these cells are grown. Extracellular matrix (ECM) proteins, particularly COL4, have been identified as key components that influence HCEC adhesion, proliferation, and phenotype maintenance.

While primary HCECs offer a direct representation of the native corneal endothelium, their limited proliferative capacity and the challenges associated with sourcing and isolating them make their use in experimental setups somewhat restrictive. In addition, the potential risks of disease transmission and ethical issues with human samples can hamper the research. To circumvent these challenges and ensure consistency across experiments, we opted to use an immortalised cell line of HCEC, namely HCEC-12. This cell line retains many of the characteristic features of primary HCECs, making it a suitable model for our investigations.

Although COL4 has been employed in various studies as a coating substrate for cell culture, there exists a wide variability in the methodologies adopted. Factors such as the volume, concentration, and incubation time of the COL4 solution can significantly influence the efficacy of the coating process. An optimised and standardised protocol for COL4 coating is essential to ensure reproducibility and consistency across experiments, thereby providing a reliable foundation for subsequent studies.

This chapter embarked on a systematic investigation to establish a control culture condition for HCEC-12 cells by optimising the COL4 coating process. By exploring a range of volumes, concentrations, and incubation durations, we aimed to identify the optimal parameters that would provide an effective and consistent COL4 coating for HCEC-12 culture. The culmination of this rigorous exploration led to the identification of a specific set of conditions that maximised HCEC-12 adhesion and proliferation without compromising their native

phenotype. This optimised protocol not only serves as a benchmark for our subsequent experiments but also offers valuable insights for the broader scientific community engaged in corneal endothelial tissue engineering.

4.2 Materials and Methods

4.2.1 COL4 Coating Efficiency Investigation

Stock solutions of 1mg/mL collagen type IV (COL4) were prepared by dissolving COL4 (Sigma-Aldrich, C5533) in 0.5M acetic acid (Sigma-Aldrich, 695092). Subsequently, six different concentrations for coating were prepared by diluting the stock solution in acetic acid: 5, 10, 20, 40, 80, and 160µg/mL. This range provided a broad spectrum of concentrations, allowing for a detailed understanding of how varying concentrations might influence the coating efficiency. Three incremental volumes, 50, 100, and 150µL were used for a pre-determined 100µg/mL concentration. These volumes were carefully pipetted into individual wells of a 96-well plate (Corning Costar, 3997). Once the collagen solutions were added to the wells, the plates were incubated at 37°C. Four distinct incubation durations were tested: 1, 2, 3, and 5 hours. Post-incubation, the residual unbound collagen solutions were carefully aspirated from each well and transferred to pre-weighed 0.5mL tubes (Fisher Scientific, 10025720). This step was crucial to determine the amount of collagen that remained unbound. This step was crucial to determine the amount of collagen that remained unbound and, by extension, the amount that had successfully coated the well.

4.2.2 Modified Bradford Assay

A series of standard protein solutions were prepared with COL4 (Sigma-Aldrich, C5533) and 0.5M acetic acid (Sigma-Aldrich, 695092) at 0-160μg/mL concentrations. These standards serve as a reference in Bradford assays to generate a calibration curve, which is used to determine the concentration of COL4 sample solutions. The traditional Bradford reagent (Sigma-Aldrich, B6916) was modified by adding 0.0035% sodium dodecyl sulphate (SDS, ThermorFisher, 28312). To each 5μL protein standard and sample in a 96-well plate, 250μL of the modified Bradford reagent was added. The mixture was then vortexed briefly to ensure thorough mixing. The absorbance of the samples and standards was measured at a wavelength of 595nm (OD_{595}) using a plate reader (Molecular Devices, SpectraMax i3x).

4.2.3 COL4 Coating Efficiency in Cellular Experiments

Stock solutions of 1mg/mL collagen type IV (COL4) were prepared by dissolving COL4 (Sigma-Aldrich, C5533) in 0.5M acetic acid (Sigma-Aldrich, 695092). Subsequently, five different concentrations for coating were prepared by diluting the stock solution in acetic acid: 10, 20, 50, 100, and 150μg/mL. Prior to cell seeding, culture plates were incubated with each COL4 concentration for 5 hours at 37°C. The volume of the coating solutions depended on the area of the culture surface. Specifically, volumes equivalent to 155.5μL/cm^2 were used, translating to 50μL for a microplate well or 11.66mL for a T-75 flask. After incubation, residual COL4 solutions were carefully discarded from the culture-wares. The coated surfaces were then rinsed gently twice with phosphate buffered saline (PBS, ThermoFisher, 10010-023). The coated culture-wares were exposed to UV radiation within a sterile biosafety cabinet for a duration of one hour. The coated surfaces were covered with 1% penicillin/streptomycin

(ThermoFisher, 15070063) in PBS and stored at 4°C before being used for cellular experiments. The maximum storage duration was two weeks.

4.3 Results and Discussions

4.3.1 Optimised COL4 Coating Efficiency

To accurately assess the effects of varying COL4 coating conditions, it was imperative to calibrate the measurement of the coating solution's concentration. The Bradford assay, a widely used method for protein quantification, was employed for this purpose. The objective was to determine if the concentration, volume of the initial coating solutions, and the duration of coating influenced the amount of COL4 coated on the culture-ware. Using the Bradford assay, a calibration curve was plotted, correlating COL4 concentration with optical density at 595nm. However, the assay encountered challenges in accurately plotting the curve at the lower COL4 concentrations. To address this limitation, the assay was modified by incorporating 0.0035% SDS, as described in a previous research article [213]. The modified assay yielded a calibration curve that demonstrated significantly enhanced reliability for collagen type IV, as depicted in Figure 3.

The Bradford assay is a colorimetric protein assay based on the binding of Coomassie Brilliant Blue dye to proteins, resulting in a shift in the dye's absorbance maximum from 465nm to 595nm [214]. While the assay is rapid and simple, it has its limitations, especially when quantifying proteins at lower concentrations. In addition, collagen proteins have a unique amino acid composition, with a high content of proline, hydroxyproline, and glycine. Traditional protein assays, including the Bradford assay, might not bind as efficiently to these

amino acids, leading to underestimation of collagen content. The addition of SDS in the modified Bradford assay, as described by Lopez et al., likely enhances the binding of the Coomassie dye to collagen proteins. SDS, being an anionic detergent, can unfold proteins and expose more binding sites for the dye, leading to a more robust and reliable detection [213].

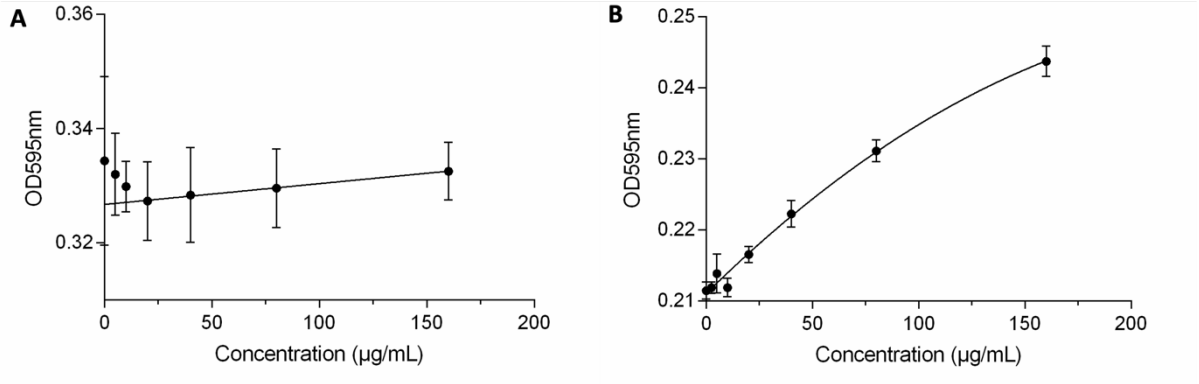

Figure 3. Comparative calibration curves for collagen type IV using traditional and modified Bradford assays. (A) Calibration curve obtained from the traditional Bradford assay. (B) Calibration curve derived from the modified Bradford assay. Data points represent the mean optical density values at 595nm wavelength for each collagen type IV concentration, with error bars indicating the standard error of the mean (SEM). Experiments were conducted in triplicate (n=3).

To determine the optimal conditions for coating COL4 on culture-wares, a series of experiments were conducted using a range of concentrations (0-160 µg/mL) of COL4. These solutions were incubated in the 96-well plates using different volumes (50, 100, or 150µL) and were left for varying durations (1, 2, 3, or 5 hours) at 37°C. Post-coating, the residual solutions were collected, weighed, and their concentrations were determined. The amount of coated COL4 can then be calculated by:

$$M_{coated} = C_{initial} \times V_{initial} - C_{residual} \times V_{residual}$$

With the amount of COL4 coated in the process, the efficiency can be determined:

$$Coating\ Efficiency = \frac{M_{coated}}{C_{initial} \times V_{initial}} \times 100\%$$

Where M_{coated} is the mass of coated COL4; $C_{initial}$ and $V_{initial}$ are the concentration and volume of the initial coating solution; $C_{residual}$ and $V_{residual}$ are the concentration and volume of the residual solution removed from the 96-well plate post-coating.

The results, as depicted in Figure 4, revealed a direct proportionality between the amount of COL4 coated and the coating concentration across all conditions. Increases in the amount of coated COL4 were observed with higher coating volumes and longer coating durations. However, the coating efficiency, while positively correlated with coating duration, showed diminishing returns. The highest efficiency was observed at 5 hours, but 3 hours of coating yielded almost identical results. Interestingly, a negative correlation was observed between the amount of coated COL4 and the coating volume.

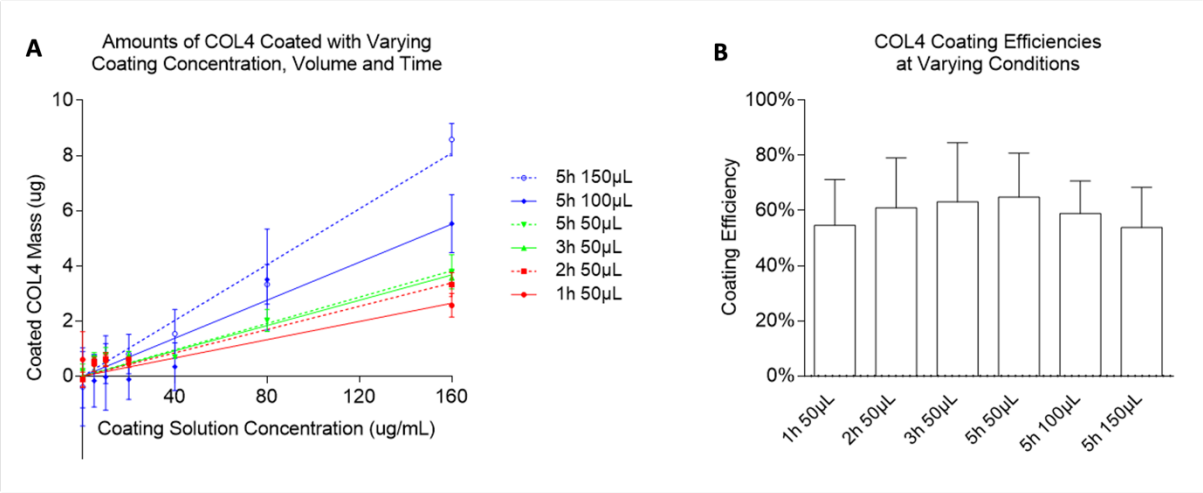

Figure 4. Analysis of collagen type IV coating efficiency across different concentrations. (A) Plot illustrating the relationship between the amount of coated collagen type IV and the coating concentration for each specific condition. (B) Bar chart comparing the coating efficiencies across the tested concentrations. Data points and bars represent the mean values for each concentration, with error bars indicating the standard error of the mean (SEM). Experiments were conducted in triplicate (n=3).

While longer coating durations increased the amount of COL4 coated onto the plates, the efficiency of coating plateaued after a certain point. This observation aligned with the principle of saturation kinetics, where a point of diminishing returns is reached beyond which additional

concentration does not significantly enhance the coating process. The inverse relationship between coating volume and efficiency is intriguing. It suggests that while increasing the volume might result in more COL4 being coated, the amount left in the residual solution also increased, leading to a diminishing efficiency. This could also be due to the limited surface area of the wells, which can only accommodate a certain amount of COL4 before becoming saturated. The linear relationship between coating concentration and the amount of COL4 coated underscores the importance of using concentrated solutions for efficient coating.

The results provided insights into the dynamics of COL4 coating under different conditions. One of the most salient practical implications derived is the optimal strategy for achieving the highest coating efficiency. Specifically, it was observed that the best results are obtained when using COL4 solutions of a smaller volume (50µL for a well of a 96-well plate, or around 155.5µL/cm^2) but at a higher concentration. Moreover, for the coating to be most effective, the solution should be incubated for a duration of 5 hours at 37°C before the removal of excess coating solution. While the data suggest that the amount of COL4 coated on the plate might continue to increase with higher coating concentrations, the highest concentration tested in this study was capped at 160µg/mL. This raises the question of whether there is a tangible benefit to using even higher concentrations of COL4 for coating. It may be theoretically possible to achieve a denser coating, but over-saturating the plate with coating might not be necessary or cost-efficient for subsequent experiments. While the physical efficiency is essential, the ultimate test of its efficacy lies in its impact on cell culture.

Collagen type IV (COL4) is an essential protein found abundantly in endothelial basement membranes, including the Descemet's membrane of the posterior cornea [165]. Its significance in the context of in vivo endothelial environments is underscored by its ability to facilitate rapid attachment of HCEC-12 cells to culture surfaces [16,17]. These cells were cultured over nine

passages, ranging from P4 to P12, on plates that had been coated with a range of concentrations of COL4. The plates were prepared using COL4 solutions at concentrations of 0, 20, 50, 100, and 150 μg/mL. By the time the cells reached P12, a comprehensive assessment was undertaken. This evaluation focused on key parameters such as cellular morphology, proliferation rates, and protein expression profiles. These metrics would provide an understanding of how varying COL4 coating amounts influence the behaviour and characteristics of HCEC-12 cells.

4.3.2 Cell Proliferation Increases with Coating Concentration

Cultured on different COL4 coatings, cellular activities of HCEC-12 cells were assessed using CCK-8 assays every other day post-seeding on day 0. A calibration curve was established, illustrating a positive linear correlation between the optical density at 450nm (OD_{450}) and the HCEC-12 cell number. This relationship was leveraged to compare the proliferation rates across five different coating conditions over a span of 9 days (Figure 5). While efforts were made to seed a consistent number of cells (5000/cm^2) for each condition on day 0, minor deviations were observed. These differences became more pronounced by days 7 and 9.

To account for these deviations and provide a fair comparison, the "doubling level" metric was introduced, calculated by:

$$Doubling\ Level = \frac{[Log(Day\ n) - Log(Day\ 1)]}{Log(2)}$$

This metric evaluates the number of times cells have doubled since day 1. All comparisons and calculations of doubling levels were based on OD_{450} values, given the established linear correlation with cell numbers and the fact that the optical density remained within the linear

range of the calibration curve. The doubling level chart (Figure 5C) revealed a mostly direct proportional relationship between the proliferation rate of HCEC-12 cells and the COL4 coating concentration. Notably, cells cultured on 100µg/mL and 150µg/mL COL4 coatings exhibited the highest proliferation rates, with both conditions showing comparable growth rates.

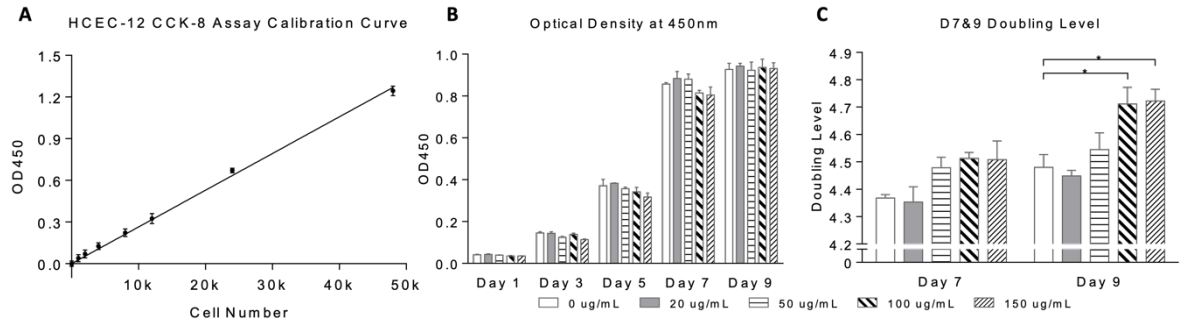

Figure 5. Evaluation of HCEC-12 P12 proliferation on culture surfaces coated with varying concentrations of collagen type IV using the CCK-8 assay. (A) Calibration curve depicting the relationship between optical density at 450nm (OD_{450}) and the number of cells in standard HCEC-12 suspensions. (B) Bar chart illustrating the OD_{450} values from day 1 to day 9, representing cell proliferation across different collagen type IV coating concentrations. (C) Bar chart showcasing the doubling levels of HCEC-12 on days 7 and 9 since day 1, providing insights into the growth rate of the cells on the coated surfaces. Data points and bars represent the mean values for each concentration, with error bars indicating the standard error of the mean (SEM). Experiments were conducted in triplicate (n=3). * denotes statistical significance with $P<0.05$.

The ability to culture corneal endothelial cells efficiently and maintain their proliferative capacity is crucial for their potential therapeutic applications. The CCK-8 assay, a widely recognised method for assessing cell viability and proliferation, provided valuable insights into the behaviour of HCEC-12 cells under different COL4 coating conditions. The establishment of a calibration curve, showing the linear relationship between OD_{450} and cell number, was a foundational step. This relationship allowed for a more nuanced understanding of cell proliferation rates, especially given the slight deviations in initial seeding densities. The introduction of doubling level was an approach to circumvent the challenges posed by these

deviations. By focusing on the number of times cells doubled since day 1, we could derive a more accurate representation of their proliferative capacity across different conditions.

The observed direct proportional relationship between HCEC-12 proliferation and COL4 coating concentration underscores the significance of the extracellular matrix in guiding cellular behaviour. COL4, a major component of the basement membrane, has been previously identified as a key factor in cellular adhesion and proliferation. Our findings further reinforce its role, suggesting that higher concentrations of COL4 provide a more conducive environment for HCEC-12 growth. Interestingly, the proliferation rates of cells cultured on 100 µg/mL and 150 µg/mL COL4 coatings were comparable, indicating a potential saturation point beyond which additional COL4 might not offer significant benefits. This observation could have implications for future experiments, suggesting that concentrations beyond 100µg/mL might not necessarily yield better results and could be resource inefficient.

4.3.3 Optimal Phenotypic Maintenance with High Coating Concentration

Upon reaching approximately 80% confluency, the HCEC-12 cells exhibited characteristic morphology, with cells displaying a "cobblestone-like" polygonal appearance. To gain deeper insights into the cellular phenotype and potential signs of endothelial-to-mesenchymal transition (EMT), the cells were fixed and subjected to immunostaining. Key markers associated with EMT, namely ZO-1, ATP1A1, and α-SMA, were visualised. The expression levels of these proteins serve as critical indicators of EMT. Additionally, F-actin staining was performed to delineate the cytoskeletal structure of the cells. To understand the potential influence of EMT on the extracellular matrix (ECM), the expression of specific ECM proteins, including COL1, COL4, and COL8, was also assessed. Micrographs (as shown in Figure 6) revealed that cells cultured on higher COL4 coating concentrations exhibited more consistent

expression of the tight junction protein ZO-1 and adherens junction protein ATP1A1. Furthermore, the morphology of cells, as indicated by α-SMA and F-actin staining, suggested that a COL4 concentration of 100 µg/mL promoted the most regular cellular shape — a tightly packed configuration with pronounced hexagonal or organised polygonal patterns, with minimal indications of a fibroblastic-like transformation. Notably, there was an observed increase in interconnections among the ECM proteins at higher COL4 coating concentrations, particularly for higher COL8 expression in cells cultured on 100 µg/mL COL4 coating. Collagen type VIII (COL8), a primary component of the Descemet's membrane, is known for its role in preserving a healthy corneal endothelium in vivo [215,216]. The short-chain ECM protein is typically secreted by HCECs as hexagonal lattices [217], potentially guiding HCEC-12 cell attachment and proliferation.

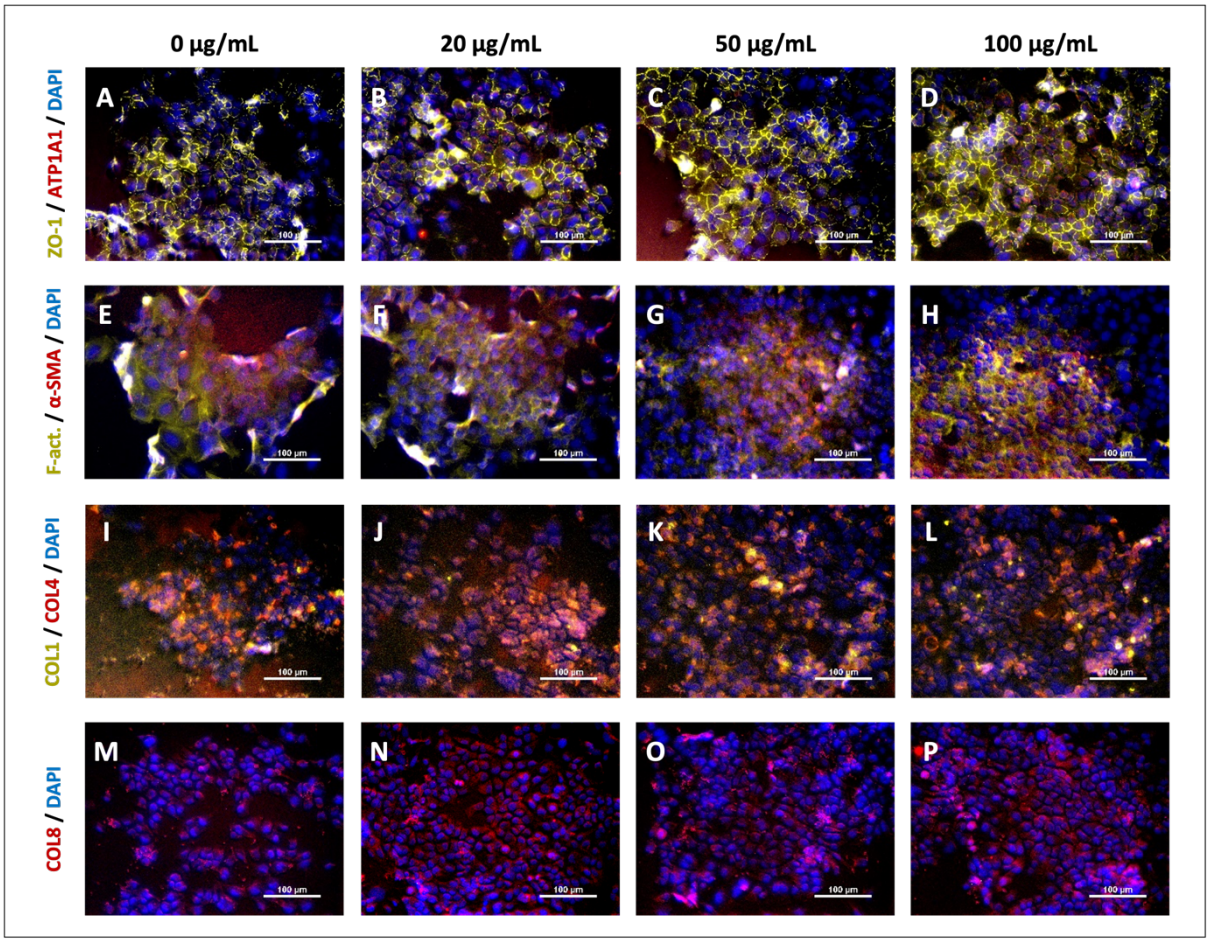

Figure 6. Immunofluorescence micrographs of HCEC-12 P12 cells cultured on surfaces coated with varying concentrations of collagen type IV (0-100µg/mL). (A-D) Visualisation of tight junction protein ZO-1 (yellow), adherens junction ATP1A1 (red), and cell nuclei (blue). (E-H) Depiction of cytoskeletal F-actin (yellow), fibroblast marker α-SMA (red), and cell nuclei (blue). (I-L) Imaging of extracellular matrix protein collagen type I (yellow), collagen type IV (red), and cell nuclei (blue). (M-P) Representation of collagen type VIII (red) in relation to cell nuclei (blue). All images are accompanied by scale bars representing 100µm, providing a reference for cell and protein structure sizes.

The morphology and behaviour of HCEC-12 cells in culture provide crucial insights into their health, phenotype, and potential for therapeutic applications. The observed cobblestone-like pattern at ~80% confluency is a typical hallmark of corneal endothelial cells and suggests that the cells were in a state of contact inhibition, a phenomenon where cells cease to proliferate upon forming sufficient contacts with neighbouring cells.

The immunostaining results offer a deeper understanding of the cellular phenotype, particularly in the context of EMT, a process where corneal endothelial cells lose their characteristic morphology and acquire mesenchymal traits. The consistent expression of ZO-1 in cells grown on higher COL4 concentrations underscores the protective role of COL4 in maintaining HCEC-12 culture. ZO-1, a tight junction protein, is pivotal for cell-cell adhesion and barrier function, and its robust expression is indicative of a healthy corneal endothelial phenotype. Conversely, the morphology suggested by α-SMA and F-actin staining provides insights into potential EMT events. α-SMA is a marker often associated with mesenchymal cells, and its increased expression in corneal endothelial cells can be indicative of EMT. The α-SMA expression in cells cultured on a 100μg/mL COL4 coating appears more structured, aligning with the hexagonal cell membranes. In contrast, cells undergoing EMT typically display a fibroblastic morphology with diminished ZO-1 and ATP1A1 expressions and increased α-SMA. The observation suggests that this concentration offers an optimal environment to suppress EMT. The enhanced interconnections among ECM proteins at higher COL4 concentrations further highlight the role of the ECM in guiding cellular behaviour. The ECM not only provides structural support but also modulates cellular signalling pathways, influencing cell proliferation, differentiation, and phenotype maintenance.

To assess protein expression levels, HCEC-12 cells, upon reaching approximately 80% confluency, were harvested by scraping. These cells were subsequently lysed to extract the total protein content. The bicinchoninic acid assay (BCA) assay was employed to determine the protein concentrations of these samples by comparing the optical density at 562 nm (OD_{562}) after the addition of the reagent against a calibration curve, as depicted in Figure 7A. Following concentration normalization, the protein samples were subjected to SDS-PAGE. The separated proteins were then transferred onto nitrocellulose membranes for immunoblotting, with the

results presented in Figure 7B. The immunoblots revealed a positive correlation between ZO-1 expression and COL4 coating concentration. In contrast, α-SMA expression exhibited a negative correlation with COL4 concentration. ATP1A1 expression remained relatively consistent across all five conditions. The bands corresponding to COL8A2 were faint, making accurate evaluation challenging, but it can still be seen that the uncoated group (or 0 µg/mL COL4) appeared to have the lowest COL8A2 expression level.

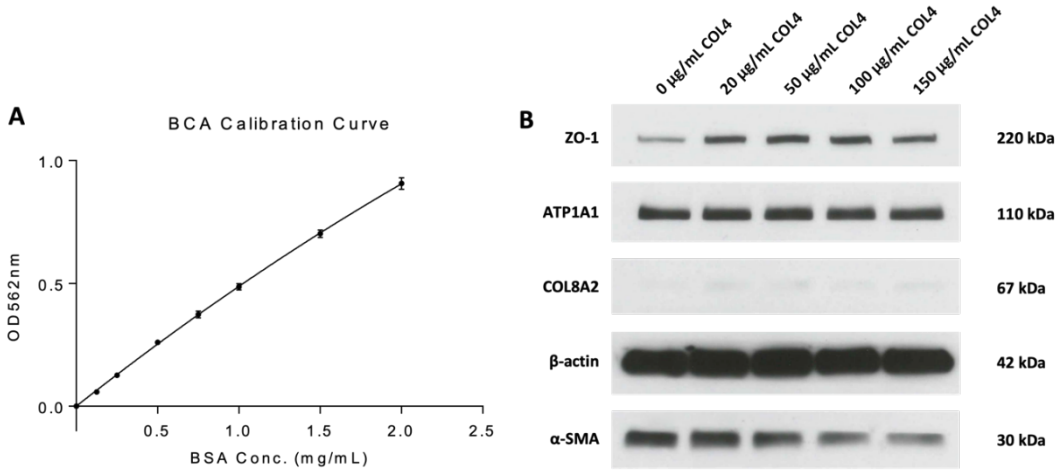

Figure 7. Comprehensive analysis of protein expressions in HCEC-12 P12 cells cultured on varying concentrations of collagen type IV. (A) BCA calibration curve showcasing the relationship between optical density at 562nm and a series of bovine serum albumin (BSA) concentrations ranging from 0 to 2mg/mL. Data points represent the mean optical density values for each BSA concentration, with error bars indicating standard deviation (SD), n=3. (B) Immunoblot analysis of total proteins extracted from the cultured HCEC-12 P12. Following electrophoresis, proteins with different molecular weights were transferred to a nitrocellulose membrane and subsequently probed with specific antibodies to visualise the expressions of ZO-1, ATP1A1, COL8A2, β-actin, and α-SMA. The bands provide insights into the relative protein expressions across the different collagen type IV coating concentrations.

The direct assessment of protein expression levels offers invaluable insights into the cellular responses to different culture conditions, particularly in the context of COL4 coating concentrations. The methodology employed, encompassing cell lysis, protein concentration determination, SDS-PAGE, and immunoblotting, is a robust approach to semi-quantitatively evaluate protein expression profiles.

The observed positive correlation between ZO-1 expression and COL4 coating concentration underscores the protective and supportive role of COL4 in maintaining endothelial integrity. ZO-1, a tight junction protein, is pivotal for cell-cell adhesion and barrier function. Its expression is often considered a hallmark of healthy endothelial cells, ensuring cell-cell adhesion and preventing paracellular leakage. The observed positive correlation between ZO-1 expression and COL4 concentration suggests that COL4 provides a conducive environment for maintaining endothelial integrity. Previous studies have highlighted the significance of the extracellular matrix, particularly basement membrane components like COL4, in guiding cellular behaviour and promoting tight junction formation [17,135].

Conversely, the inverse relationship between α-SMA expression and COL4 concentration is noteworthy. α-SMA is often associated with mesenchymal cells and its expression in endothelial cells can be indicative of endothelial-to-mesenchymal transition (EMT), a process where endothelial cells lose their characteristic morphology and acquire mesenchymal traits. EMT can be triggered by various factors, including changes in the extracellular matrix composition [19,218]. The reduced α-SMA expression at higher COL4 concentrations suggests that these conditions suppress EMT, further highlighting the protective role of COL4 as a coating substrate. This observation aligns with studies that have shown that a well-defined extracellular matrix can inhibit EMT by maintaining cell-matrix interactions and preventing the activation of EMT-inducing pathways [82,219].

The consistent expression of ATP1A1 across all conditions is intriguing. The Na^+/K^+ ATPase is essential for maintaining the ionic balance in corneal endothelial cells. This suggests that while the extracellular matrix can modulate certain cellular behaviours, the fundamental function of maintaining cellular homeostasis might be less influenced by the changes in culture substrate.

The faint bands corresponding to COL8A2, a key component of HCEC's basement membrane in vivo, pose challenges for accurate evaluation. However, the potential reduced expression of COL8A2 in the uncoated sample might suggest differences in ECM protein expression based on the coating conditions. Previous studies have indicated that the composition of the culture substrate can influence the deposition of ECM proteins, potentially due to feedback mechanisms or changes in cell-matrix interactions [11,220].

Flow cytometry was employed to further validate the protein expression profiles of three selected markers: ZO-1, ATP1A1, and α-SMA. The results are presented in Figure 8. P12 cells, once fixed, were stained using specific antibodies targeting these markers. The secondary antibodies utilised were conjugated to Alexa Fluor 488, a fluorochrome detectable in the FL1 channel of flow cytometers. The FL1 intensity histograms revealed a noticeable shift in all cells stained with antibodies compared to the blank controls, which lacked staining. To quantify this shift, a gating strategy was applied to each histogram, and the extent of the shift was represented as a percentage of shifted cells. Distinct shifts were observed based on the antibody staining and the coating condition. Specifically, cells stained for ZO-1 and ATP1A1 exhibited a positive correlation between FL1 intensity and coating concentration. In contrast, the α-SMA intensity remained relatively consistent across different coating conditions.

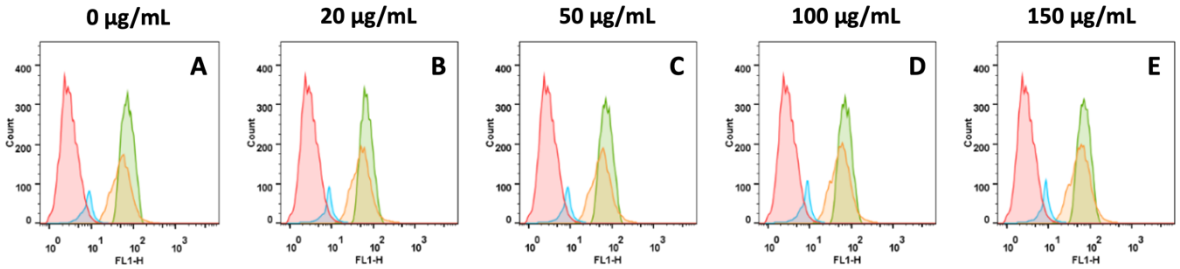

A	Sample	Freq. of HCEC-12
	Blank	100
	0 ug/mL ZO-1	13.4
	0 ug/mL ATP1A1	53.1
	0 ug/mL a-SMA	70.2

B	Sample	Freq. of HCEC-12
	Blank	100
	20 ug/mL ZO-1	12.5
	20 ug/mL ATP1A1	58.1
	20 ug/mL a-SMA	69.3

C	Sample	Freq. of HCEC-12
	Blank	100
	50 ug/mL ZO-1	13.6
	50 ug/mL ATP1A1	57.8
	50 ug/mL a-SMA	69.5

D	Sample	Freq. of HCEC-12
	Blank	100
	100 ug/mL ZO-1	15.7
	100 ug/mL ATP1A1	64.0
	100 ug/mL a-SMA	69.8

E	Sample	Freq. of HCEC-12
	Blank	100
	150 ug/mL ZO-1	14.7
	150 ug/mL ATP1A1	66.8
	150 ug/mL a-SMA	69.9

Figure 8. Flow cytometry histograms representing the protein expression intensities in HCEC-12 P12 cells cultured on surfaces with varying concentrations of collagen type IV. Cells were fixed and stained with specific antibodies targeting ZO-1 (blue), ATP1A1 (orange), and α-SMA (green). Additionally, cells not stained with any antibody served as a blank control (red). The combined histograms provide a comparative view of protein expression across the different coating concentrations: (A) Uncoated or 0µg/mL, (B) 20µg/mL, (C) 50µg/mL, (D) 100µg/mL, and (E) 150µg/mL. The x-axis represents the fluorescence intensity of the labelled proteins, while the y-axis indicates the frequency of HCEC-12 cells emitting the respective fluorescence, providing insights into the relative protein expressions for each coating concentration.

Both western blot and flow cytometry showed an increase in ZO-1 expression with increasing COL4 concentration, indicating a consistent observation across techniques, reinforcing the implication that higher COL4 coating concentration promotes a healthier endothelial phenotype in HCEC-12. However, a discrepancy between western blot and flow cytometry results for the expression of ATP1A1 and α-SMA was observed. The western blot experiment showed consistent ATP1A1 levels as COL4 coating concentration increased, while flow cytometry indicated an increase in the expression. This could be due to flow cytometry detecting a higher presence of ATP1A1 on individual cell's surface or in specific cellular compartments, which might not be as evident in the total protein content assessed by western blot. On the other hand, western blot showed a decrease in α-SMA with increasing COL4

coating concentration, suggesting suppression of EMT. The consistent levels of α-SMA observed in flow cytometry indicates that while the overall protein levels decrease, the distribution of α-SMA per cell remains relatively constant. The two experiments assessed the protein expressions of HCEC-12 through different perspectives and yielded slightly different results, which might also imply that the extracellular matrix's influence on EMT is more complex than previously thought.

While the focus has been predominantly on COL4 coatings, the experiments also underscore the utility of HCEC-12 as a reliable model for studying the process of EMT. Although primary cells are typically preferred, the findings from this study using HCEC-12 cells provide a harmonious blend of visual and quantifiable data, suggesting marker expressions akin to primary HCECs or animal corneal endothelial cells.

The economic implications of these findings cannot be understated. The experiments delineate that a 50μL of 100μg/mL collagen type IV solution incubated for 5 hours at 37°C for each well of a 96-well plate is both sufficient and optimal for HCEC-12 culturing. This coating not only sustains HCEC-12 proliferation and phenotype but also effectively curbs EMT. While this condition might be applicable to primary HCEC cultures, further validation is required. Ultimately, by utilising reduced COL4 amounts, the potential for cost-effective in vitro HCEC expansion becomes a tangible reality, paving the way for more affordable alternative treatments for corneal endothelial diseases.

4.4 Summary

This chapter described a comprehensive exploration of the effects of varying COL4 coating conditions on the behaviour and characteristics of HCEC-12, a human corneal endothelial cell

line. The study began with the establishment of an optimal coating procedure for COL4, which was found to be most efficient when using solutions of a smaller volume but at a higher concentration, incubated for 5 hours at 37°C. The subsequent cellular experiments provided a deeper understanding of the biological implications of these coatings. The amount of COL4 coated on the plate increased with higher coating concentrations, but the efficiency showed diminishing returns beyond a certain point. The HCEC-12 cells' response to these coatings, in terms of morphology, proliferation, and protein expressions, was pivotal in determining the biological relevance of the coating. The optimal concentration of COL4 coating solution for cellular experiments was found to be 100µg/mL. The expression levels of key proteins, such as ZO-1, ATP1A1, and α-SMA, provided insights into the cellular health and phenotype. The morphology of HCEC-12 cells, especially their "cobblestone-like" appearance, further reinforced the findings from protein expression studies. These findings underscore the importance of a holistic approach, where both the physical properties of the coatings and their biological implications are considered. In conclusion, this chapter has laid the groundwork for understanding the intricate relationship between COL4 coatings and HCEC-12 cell behaviour.

Chapter 5

Cell-Derived Decellularised Extracellular Matrix Supports HCEC-12 Culture

In this chapter, the potential of cell-derived decellularised extracellular matrices (dECMs) as substrates for the in vitro culture of a human corneal endothelial cell line, HCEC-12, was explored. The dECMs were characterised and compared against standard culture surfaces, namely tissue culture treated polystyrene (TCPS) surface and COL4 coating. The proliferation, phenotype maintenance, and response to endothelial-to-mesenchymal transition (EMT) induction of HCEC-12 cells on these substrates were meticulously assessed. Results revealed that dECMs, especially dECM-COL4 derived from healthy cells, significantly enhanced cell proliferation, and resistance to EMT compared to standard surfaces. This suggests that dECMs provide a more native-like environment, potentially mimicking the Descemet's membrane, which is pivotal for corneal endothelial cell function.

5.1 Introduction

The human corneal endothelium plays a pivotal role in maintaining the transparency and hydration of the cornea. However, unlike other cell types, human corneal endothelial cells possess limited regenerative capabilities [51]. This limitation has driven researchers to seek effective in vitro culture techniques to expand HCECs for therapeutic applications and research purposes. Traditional culture surfaces, such as COL4 coated culture surfaces have been widely

used for this purpose [17,135,221]. However, these surfaces may not fully recapitulate the native environment of HCECs, potentially affecting their phenotype and function.

The concept of using cell-derived decellularised extracellular matrices (dECMs) has emerged as a promising approach to provide cells with a more physiologically relevant environment in vitro [222,223]. dECMs, being products of cellular secretion, are believed to retain many of the biochemical and biomechanical cues of the native tissue, offering a substrate that might more optimally support cell attachment, growth, and function.

The primary objective of this chapter is to characterise dECMs derived from various cell sources and evaluate their impact on HCEC-12 cell behaviour. This includes assessing cell proliferation, phenotype maintenance, and the cells' response to endothelial-to-mesenchymal transition (EMT) induction, a process that can compromise the endothelial phenotype. By comparing the performance of HCEC-12 cells on dECMs with that on standard culture surfaces, this chapter aims to elucidate the potential benefits and challenges of using dECMs for HCEC culture. The findings from this investigation could pave the way for the development of improved culture techniques, bringing us a step closer to harnessing the therapeutic potential of HCECs.

5.2 Materials and Methods

5.2.1 Preparation of Cell-Derived Decellularised Extracellular Matrix

The process of preparing the cell-derived decellularised extracellular matrix (dECM) involved a series of steps to ensure the extraction of an intact ECM, while effectively removing the HCEC-12 cells that produced it. Two distinct types of culture surfaces were utilised for this

purpose: the standard tissue culture treated surface (TCPS) for generating dECM-TCPS, and a surface that had been pre-coated with 100µg/mL collagen type IV (COL4) for the creation of dECM-COL4. Initially, HCEC-12 cells were seeded onto these surfaces at a density of 1000 cells/cm^2. Over a span of 14 days, these cells were cultured using the method described in Chapter 3, with the medium being changed every 2-3 days to maintain optimal growth conditions. To enhance the secretion of extracellular matrix components by the cells, the medium was supplemented with 50µM L-ascorbic acid, starting from the third day of culture. On day 14, the cultures underwent a gentle rinse with phosphate-buffered saline (PBS) twice. This step was crucial to remove any non-adherent cells and potential debris. Following this, a decellularisation solution, comprising 0.5% Triton X-100 and 20mM NH_4OH, was introduced to the culture surfaces and incubate for 5 minutes at 37˚C to ensure effective cell lysis, leaving behind only the secreted ECM. To further refine the ECM and ensure the absence of any residual cell nuclei, the surfaces were treated with 10U/mL Benzonase® nuclease. After this treatment, another double rinse with PBS was performed to clear away the nuclease and any lingering cellular remnants. Once prepared, the dECM, now free from cells, was stored at 4˚C until being employed as a substrate for subsequent experiments. The maximum duration of storage was one week. All procedures were executed under aseptic conditions within a biosafety cabinet.

5.2.2 Analysis of dECM Components

Both dECM-TCPS and dECM-COL4 matrices were carefully extracted from 6-well plates by adding 200µL of 0.5M acetic acid per well and using cell scrapers to aid in the collection process. The concentrations of the reconstituted dECM samples were determined using a BCA assay, as described in Chapter 3. To facilitate the subsequent component analysis, the samples

were mixed with sample buffer before being loaded to the SDS-polyacrylamide gel. To quantify the amount of collagen types I (COL1) and IV (COL4) in the dECM-TCPS and dECM-COL4 samples, the intensities of the protein bands were compared with those of the controls. Three controls were loaded to the SDS-PAGE gel: 20µg COL1, 20µg COL4, and a mixture containing 10µg COL1 and 10µg COL4.

After electrophoresis, the proteins separated on the SDS-PAGE gel were effectively transferred to a nitrocellulose membrane. This membrane was then briefly stained with Ponceau S solution to visualise the total protein profile. Following the capture of the stained membrane's image, the membrane was rinsed five times with tris-buffered saline containing 0.1% Tween-20 (TBST) to remove the Ponceau S stain, thereby preparing the membrane for antibody probing. The membrane was blocked with 5% non-fat milk in TBST for 1 hour at room temperature to prevent non-specific binding. Following blocking, the membrane was incubated with primary antibodies against collagen type I, collagen type IV, and collagen type VIII overnight at 4°C. After washing three times with TBST, the membrane was incubated with appropriate horseradish peroxidase (HRP)-conjugated secondary antibodies for 1 hour at room temperature. The membrane was washed again, and the chemiluminescent protein bands were visualised on films.

5.2.3 Cellular Evaluation and EMT Induction

HCEC-12 cells were cultured following the method delineated in Chapter 3. Cells were seeded at a density of 6000 cells/cm^2 onto various substrates: dECM-TCPS, dECM-COL4, surfaces coated with 100µg/mL COL4 solution, and standard uncoated tissue culture treated surfaces (TCPS). HCEC-12 cultures were maintained until they achieved an approximate confluency of 90% before being employed in subsequent experiments to assess the impact of

the dECM matrices on HCEC-12 cells. The evaluation tools encompassed the CCK-8 proliferation assay, immunofluorescence imaging for markers ZO-1, α-SMA, and COL8A2, and western blot analyses focusing on ZO-1, ATP1A1, COL8A2, and α-SMA, using β-actin as the reference protein. To investigate whether the dECM matrices played a protective role against EMT in HCEC-12, these experiments were also performed to cells exposed to TGF-β1 for the induction of EMT. For EMT stimulation, the culture medium was supplemented with 5ng/mL transforming growth factor-beta 1 (TGF-β1) from the second day post-seeding. The medium was refreshed every alternate day to maintain consistent exposure and stimulate the EMT process.

5.3 Results

Although collagen type IV coating supports the growth of HCEC-12, it is far from the only ECM protein that contributes to keeping corneal endothelial cells healthy *in vivo*. The Descemet's membrane is a thin layer of the posterior cornea, a layer of ECM, produced by the human corneal endothelium. Thus, it is hypothesised here that the total ECM produced by cultured HCEC-12 would resemble the composition and the structure of the Descemet's membrane and even better support the growth of HCEC-12. The objective of this chapter was to delve into the influence of cell-derived extracellular matrix (dECM) on HCEC-12 cultures. Additionally, it is necessary to explore whether the dECMs, derived from various cell sources, show different influences in enhancing the proliferation and phenotype maintenance of HCEC-12 cells.

5.3.1 Obtaining Cell-Derived Decellularised Extracellular Matrix

HCEC-12 P4 cells were cultured on both uncoated tissue culture treated surfaces (TCPS) and surfaces coated with COL4. To enhance the production of the extracellular matrix (ECM), L-ascorbic acid was added to the culture medium. After two weeks, a decellularisation process was undertaken to obtain cell-derived ECMs. The efficacy of the decellularisation process was evaluated using DAPI staining, which is specific for cell nuclei. As depicted in Figure 9, post-decellularisation DAPI fluorescence was significantly reduced for both dECM-TCPS and dECM-COL4, suggesting successful removal of cells and nuclei. Furthermore, visible gelatinous sheets was observed on the culture-wares' bottom, indicative of the retained ECM as a continuous layer.

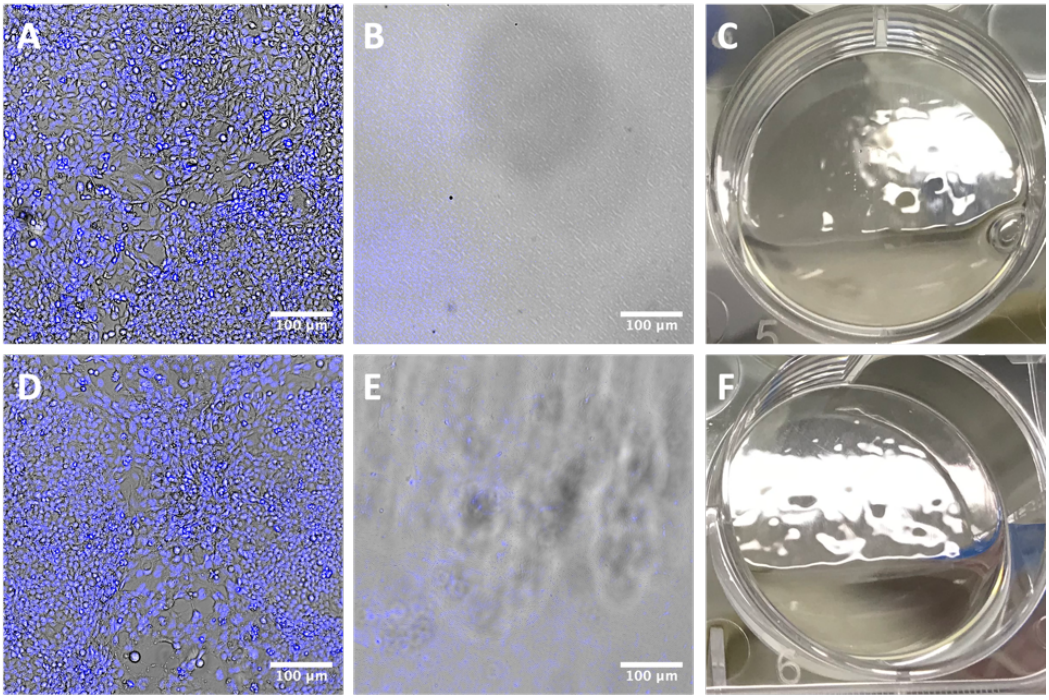

Figure 9. Fluorescence Micrographs and Photos of dECM Preparation. (A-C) HCEC-12 P4 cells cultured on TCPS and (D-F) on COL4 coating. (A, D) Fluorescence micrographs reveal HCEC-12 cells (brightfield) and their nuclei stained with DAPI (blue) prior to decellularisation. (B, E) Post-decellularisation images show minimal DAPI staining, confirming effective removal of cells and nuclear debris. Scale bars are 100µm. Adjacent photos depict the gelatinous matrices of (C) dECM-TCPS and (F) dECM-COL4 retained in the culture-wares following decellularisation.

The extracellular matrix is a complex network of proteins that provides structural and biochemical support to surrounding cells. The use of dECM is gaining prominence due to their ability to mimic the native microenvironment, thereby promoting cell attachment, proliferation, and differentiation [21]. During cell culture, the addition of L-ascorbic acid, a known stimulant for collagen synthesis [223], likely enhanced the deposition of ECM components. The minimal DAPI fluorescence observed post-decellularisation is crucial for future therapeutic purposes requiring reduce potential immunogenicity. The visible gelatinous layer of retained ECM can provide essential cues for cell proliferation and phenotype maintenance in subsequent cultures [222].

5.3.2 dECMs Contain Complex ECM Proteins

Following the extraction and reconstitution of the dECMs in 0.5M acetic acid, their protein concentrations were determined using the BCA assay. The dECM-TCPS and dECM-COL4 were found to have concentrations of 0.13±0.039µg/mL and 0.45±0.043µg/mL, respectively. SDS-PAGE was conducted on both dECM samples alongside collagen type I and IV controls. The dECM-TCPS sample did not yield any discernible bands post-electrophoresis, suggesting a low concentration of extracted matrix. In contrast, the dECM-COL4 sample displayed multiple protein bands upon Ponceau S staining, with bands observed at approximately 200kD, 70kD, 40kD, 30kD, 16kD, and 14kD molecular weights (Figure 10). However, when probed with anti-COL1, anti-COL4, and anti-COL8A2 antibodies, neither dECM-TCPS nor dECM-COL4 samples showed any bands.

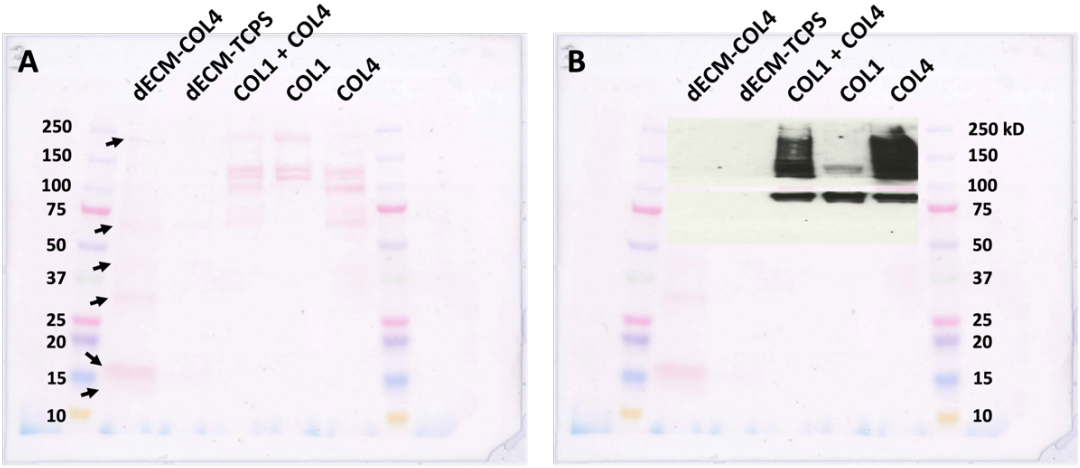

Figure 10. SDS-PAGE and western blot analysis of reconstituted dECM-COL4 and dECM-TCPS. Protein profiles of reconstituted dECM-COL4 and dECM-TCPS were compared against collagen types I and IV controls. (A) Post-electrophoresis, proteins were transferred to a nitrocellulose membrane and stained with Ponceau S, revealing the protein bands differentiated by molecular weight. Visible protein bands of the dECM-COL4 sample are denoted by arrows. (B) For western blot analysis, the membrane was incubated with antibodies to probe COL1, COL4, and COL8A2. The resultant blot is superimposed on the Ponceau S-stained membrane, providing a comparative view alongside the protein ladders.

The dECM-COL4 sample yielded multiple bands, indicating a diverse protein composition. The presence of a band at ~200kD in both the dECM-COL4 and COL1 control samples suggests the potential presence of a similar collagen chain in the dECM-COL4 sample. Similarly, the band at ~70kD in the dECM-COL4 and COL4 control samples hints at the presence of collagen type IV or a related protein. However, it can also be interpreted by the ~70kD band corresponds to the α2 chain of collagen type VIII (COL8A2) [224], a protein known to play a role in corneal endothelial health [19]. As previous research suggests, sufficiently high, but not aberrantly overproduced, levels of COL8 are often found in healthy DM [215,216,225]. The potential presence of COL8 in dECM-COL4 and the favourable results observed may hint at a correlation. It is plausible to hypothesise that an optimal culture substrate for human corneal endothelial cells can be formulated by mimicking the healthy Descemet's membrane's composition, where COL8 plays a pivotal role.

On the other hand, the absence of bands in the dECM-TCPS sample post-electrophoresis is intriguing. It suggests that the amount of matrix produced by HCEC-12 cells on uncoated TCPS might be minimal, leading to a concentration that was too low for detection via SDS-PAGE. This underscores the importance of the substrate on which cells are cultured, as it can influence the quantity and composition of the ECM they produce.

Despite the presence of these bands in the dECM-COL4 sample, the subsequent absence of bands when probed with specific antibodies for COL1, COL4, and COL8A2 is puzzling. Given that these collagens are among the most common ECM proteins secreted by corneal endothelial cells [226], their absence in the western blot is unexpected. It is plausible that the protein concentrations in the dECM samples were below the detection threshold of western blot, leading to a lack of significant chemiluminescence. This highlights the challenges of working with native ECMs, where protein concentrations can vary and may be below the detection limits of certain assays.

5.3.3 Increased Proliferation of HCEC-12 with dECMs

CCK-8 assays were utilised to evaluate the proliferation of HCEC-12 P4 cells when cultured on various surfaces: TCPS, COL4 coating, dECM-TCPS, and dECM-COL4. The optical density at 450nm was used as a representation of the number of HCEC-12 cells. As illustrated in Figure 11, on the third day of culture, the cell counts for both dECM-TCPS and dECM-COL4 were lower than that for the two control groups – TCPS and COL4 coating. However, from day 5 onwards, the dECM cultures exhibited higher cell counts than the controls. This indicates a longer lag phase in proliferation for HCEC-12 cells when cultured on dECMs. Although efforts were made to ensure a consistent seeding of cells across all conditions on day 0, slight variations were inevitable. These variations became more pronounced as the culture

period extended. When evaluating the doubling levels, by day 9, HCEC-12 cells cultured on dECM-TCPS and dECM-COL4 had doubled 4.46 and 4.48 times, respectively. In contrast, cells on TCPS and COL4 coating doubled 4.32 and 4.37 times, respectively. The proliferation rates for both dECM groups were statistically significantly higher than the control groups. This suggests that dECM-COL4 might support quicker HCEC-12 attachment initially and possibly offers guidance for cell expansion. This rapid attachment and guidance could be the reason why HCEC-12 cells grown on this matrix are less susceptible to EMT [227]. Specifically, both dECM groups exhibited increased proliferation compared to the TCPS group with a significance of $P<0.001$. Although not statistically significant, the dECM-COL4 culture showed a higher doubling level than the dECM-TCPS culture on both day 7 and day 9.

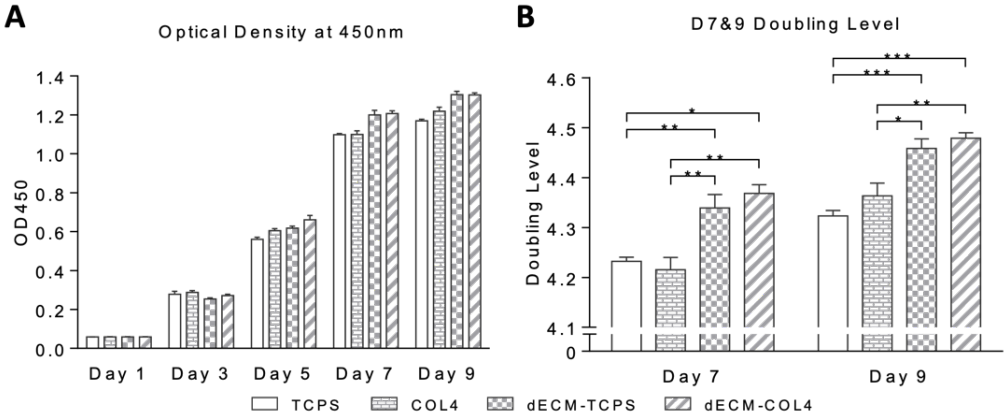

Figure 11. CCK-8 Proliferation Assay of HCEC-12 P4 on Various Culture Surfaces. HCEC-12 P4 cells were cultured on TCPS, COL4 coating, dECM-TCPS, and dECM-COL4. (A) Bar chart comparisons depict the optical density at 450nm (OD_{450}) from day 1 to day 9. (B) Doubling levels are illustrated for days 7 and 9, relative to day 1. Data are presented as means ± SEM, with n=4. Significance levels are indicated as * $P<0.05$, ** $P<0.01$, and *** $P<0.001$.

The CCK-8 assays provided a quantitative measure of cell growth. The proliferation of HCEC-12 cells on different surfaces was assessed using CCK-8, revealing interesting dynamics in cell growth patterns. The extracellular matrix plays a pivotal role in regulating cell behaviour, including proliferation. The initial lag in proliferation observed in cells cultured on

dECMs may be attributed to the cells acclimatising to the unique microenvironment provided by the dECMs [228]. This also suggests that the cells might be investing resources in adhering and spreading on the dECM surfaces before entering the exponential growth phase [229].

The significant increase in proliferation rates for cells on dECM surfaces compared to control surfaces underscores the potential benefits of using dECMs for HCEC-12 culture. It has been previously reported that cell derived ECM can enhance the cell attachment, growth, and function of cells from the same tissue type [230,231]. This could explain the enhanced proliferation observed in HCEC-12 cells on dECM surfaces. The lack of statistical significance in the doubling levels between the two dECM groups suggests that the source of the dECM, whether TCPS or COL4, might not have a pronounced effect on HCEC-12 proliferation – at least not within the timeframe of this study. It might also indicate that the inherent properties of the ECM sheet, rather than its source, play a more dominant role in influencing cell proliferation. This aligns with studies suggesting that both biochemical and biomechanical properties of the ECM can modulate cell functions [232]. Nevertheless, the slight edge observed for dECM-COL4 might be due to the presence of additional matrix proteins or growth factors specific to the COL4 environment.

5.3.4 dECM-COL4 Maintains Protein Expression in Normally Cultured HCEC-12

Upon reaching approximately 80% confluency, HCEC-12 cells cultured on TCPS, COL4 coating, dECM-TCPS, and dECM-COL4 were fixed and immunostained to visualise markers indicative of EMT, namely ZO-1, α-SMA, and COL8A2 (Figure 12). Observations highlighted variations in ZO-1 expression across the different surfaces. Cells cultured on COL4 coating, dECM-TCPS, and dECM-COL4 displayed pronounced ZO-1 expression at the cell membrane, forming distinct cellular boundaries in a hexagonal pattern, unlike those on TCPS. Notably,

cells on dECM-TCPS and dECM-COL4 were smaller in size, suggesting a denser cellular arrangement. Interestingly, α-SMA, a marker for EMT, was uniformly expressed across all four culture conditions. It localised to the cytoskeleton, revealing a hexagonal cell morphology in all conditions. Regarding COL8A2 expression, cells on TCPS exhibited a more scattered pattern, whereas those on the other three surfaces presented a continuous hexagonal distribution, with the dECM-COL4 group showing the most defined and continuous pattern.

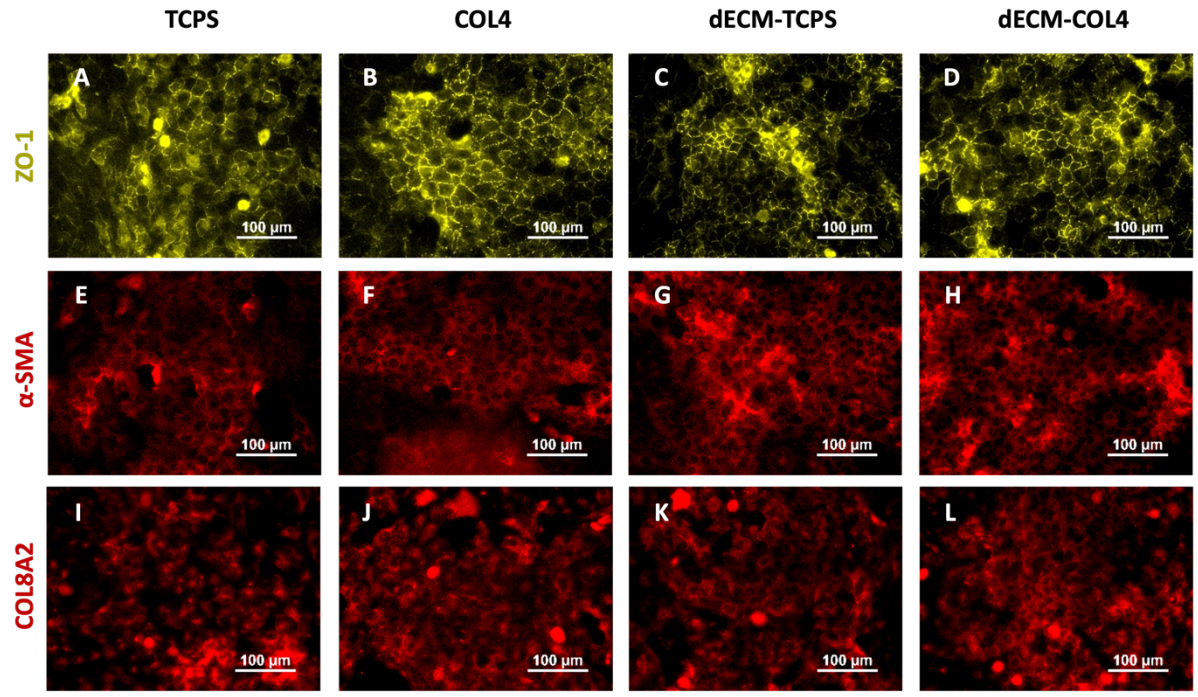

Figure 12. Immunofluorescence analysis of HCEC-12 P4 on various culture surfaces. Micrographs depict HCEC-12 P4 cells cultured on TCPS, COL4 coating, dECM-TCPS, and dECM-COL4. Specific antibody stainings visualise (A-D) ZO-1 (yellow), (E-H) α-SMA (red), and (I-L) COL8A2 (red). Each image is equipped with a scale bar of 100µm for size reference. Comprehensive immunofluorescence images, which combine staining of ZO-1, ATP1A1, α-SMA, F-actin, COL1, COL4, COL8, and DAPI-labelled nuclei, can be found in the supplementary material (Figure 28 in Appendix 2).

The observed variations in ZO-1 expression across different culture surfaces underscore the influence of the substrate on maintaining the characteristic morphology of corneal endothelial cells. ZO-1, a tight junction protein, is crucial for maintaining the barrier function of endothelial cells [103]. Its pronounced expression on COL4 coating, dECM-TCPS, and dECM-COL4

surfaces suggests enhanced cell-cell interactions and barrier integrity compared to TCPS. The consistent expression of α-SMA across all conditions is intriguing. Typically, α-SMA is associated with EMT, a process where endothelial cells acquire mesenchymal characteristics [15]. Its uniform expression might indicate that the cells, regardless of the surface, are in a transitional state or that other factors in the culture environment are influencing its expression. COL8A2's differential expression, especially its pronounced continuity in the dECM-COL4 culture, is noteworthy. COL8A2 is an essential component of the Descemet's membrane in the cornea [19]. Its enhanced expression on dECM surfaces might indicate a more native-like environment that promotes the deposition of this crucial ECM protein. The protein expressions in cells grown on dECM-COL4 and COL4 coating were strikingly similar, whereas those between dECM-COL4 and dECM-TCPS differed. This suggests that the dECMs obtained from healthy HCEC-12 cells cultured on COL4 coating and from those potentially undergoing EMT on uncoated surface (as previously found and explained in Chapter 4) might differ. This inherent difference in the ECMs could further influence the behaviour of cells grown on these matrices.

Upon reaching approximately 80% confluency, the cultured HCEC-12 cells were lysed to extract proteins which were then assessed via western blot, using β-actin as a reference for protein expression. The western blot results, as depicted in Figure 13, showcased the protein bands corresponding to ZO-1, ATP1A1, COL8A2, β-actin, and α-SMA. Notably, the ZO-1 protein bands from the COL4, dECM-TCPS, and dECM-COL4 conditions exhibited significantly stronger chemiluminescence compared to the TCPS condition, with the dECM-COL4 group showing the highest ZO-1 expression. ATP1A1 expression remained relatively consistent across all four conditions. The COL8A2 bands were faint for all conditions, though the COL4 group displayed a marginally more pronounced band. The highest α-SMA

expression was observed in the TCPS condition, with the dECM-TCPS group also showing a considerable expression. The COL4 group had the lowest α-SMA expression, with the dECM-COL4 group showing a slightly higher level.

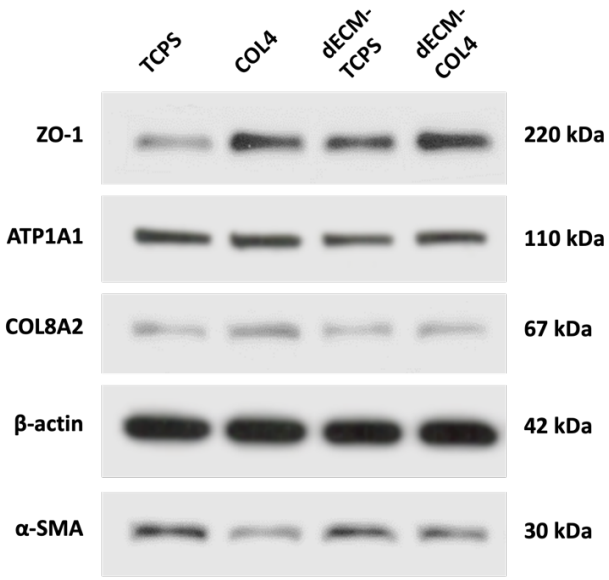

Figure 13. Western blot analysis of proteins from HCEC-12 P4 cultured on various surfaces. Protein extracts from HCEC-12 P4 cells cultured on TCPS, COL4 coating, dECM-TCPS, and dECM-COL4 were subjected to SDS-PAGE and subsequently transferred to a nitrocellulose membrane. The membrane was probed with antibodies to visualise the proteins ZO-1, ATP1A1, COL8A2, β-actin, and α-SMA. The corresponding molecular weight of each protein is indicated on the right side of the blot.

The pronounced expression of ZO-1 in the COL4, dECM-TCPS, and dECM-COL4 groups, especially the latter, aligns with the immunofluorescence imaging results. This suggested that matrices can enhance cellular functions and maintain the phenotype of HCEC-12. ZO-1 is a tight junction protein, and its enhanced expression suggests improved cell-cell adhesion and barrier function in these conditions compared to the standard TCPS. The consistent expression of ATP1A1 across all conditions indicates that this protein, essential for maintaining the ionic balance in corneal endothelial cells, is not significantly affected by the underlying culture substrate. The faint expression of COL8A2 across all conditions, with a slightly higher expression in the COL4 group, might suggest that the secretion of this ECM protein is not

robustly influenced by the culture substrate. However, the role of COL8A2 in corneal endothelial cells and its significance in maintaining corneal clarity is well-established [18,19,226]. The elevated α-SMA expression in the TCPS and dECM-TCPS groups compared to the COL4 and dECM-COL4 groups is indicative of potential EMT in these conditions. α-SMA is a marker for myofibroblast differentiation, and its elevated expression can suggest fibrotic changes and loss of the typical endothelial phenotype [233]. The lower α-SMA expression in the COL4 and dECM-COL4 groups suggests that these conditions might be more conducive to maintaining the corneal endothelial phenotype in the HCEC-12 cell line.

5.3.5 dECM-COL4 Maintains Protein Expression in EMT-induced HCEC-12

The molecular mechanisms through which dECM influences HCEC-12 behaviour can be attributed to various signalling pathways and gene expression profiles. TGF-β1, a known regulator of corneal endothelial to mesenchymal transition [15,234,235], was added to HCEC-12 cultures to intentionally induce EMT.

Upon the administration of 5ng/mL TGF-β1 to induce endothelial-to-mesenchymal transition in HCEC-12 cells, marked morphological and phenotypic alterations were evident across all culture conditions. As depicted in Figure 14, ZO-1 immunostaining revealed that the majority of cells in the TCPS and dECM-TCPS groups assumed irregular shapes, with their defining tight junctions becoming less distinguishable. While the COL4 and dECM-COL4 cultures also demonstrated adverse effects from the TGF-β1 treatment, they preserved a greater number of cells exhibiting the characteristic corneal endothelial phenotype. α-SMA, a signature marker of EMT, was expressed in pronounced filamentous patterns in both the TCPS and dECM-TCPS cultures. Conversely, the COL4 and dECM-COL4 cultures displayed diminished and less filamentous α-SMA expression, revealing the maintenance of the polygonal

cytoskeleton. Staining for COL8A2, representative of collagen type VIII secretion by HCEC-12 cells, showcased a filamentous arrangement in the TCPS group, with few discernible cellular boundaries. For the COL4, dECM-TCPS, and dECM-COL4 groups, the TGF-β1 exposure rendered the COL8A2 expression more dispersed, but the secretion patterns of individual cells remained distinguishable.

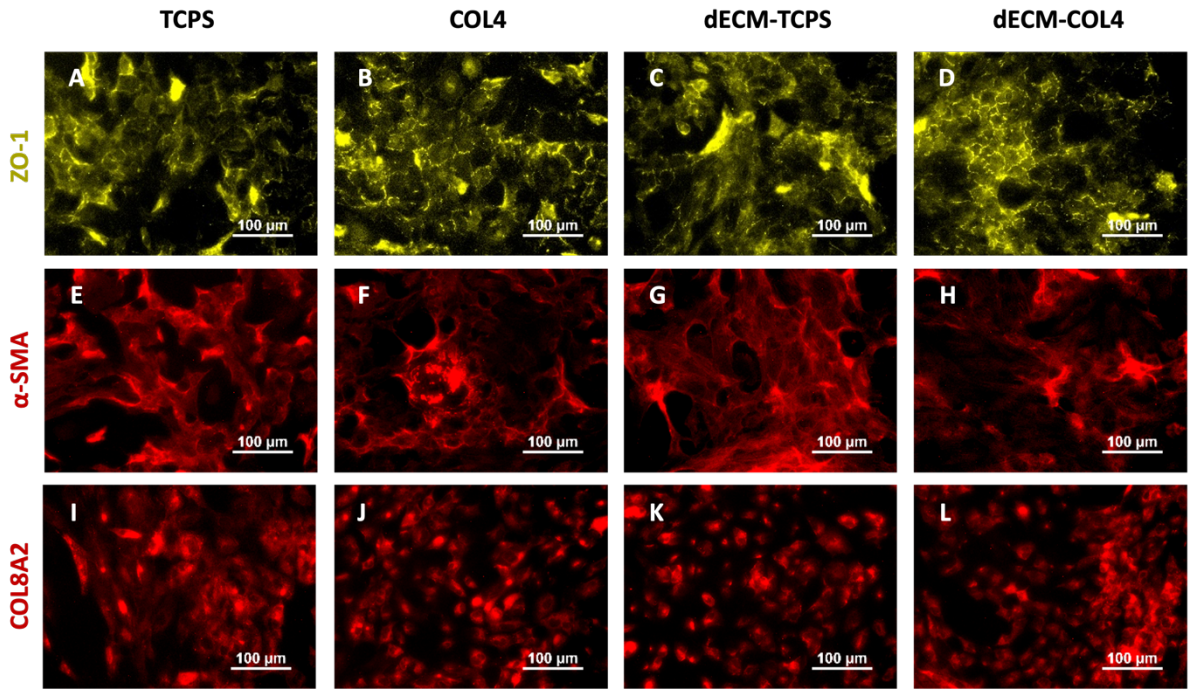

Figure 14. Immunofluorescence analysis of HCEC-12 P4, stimulated to undergo EMT, on various culture surfaces. Micrographs depict EMT-induced HCEC-12 P4 cells cultured on TCPS, COL4 coating, dECM-TCPS, and dECM-COL4. Specific antibody stainings visualise (A-D) ZO-1 (yellow), (E-H) α-SMA (red), and (I-L) COL8A2 (red). Each image is equipped with a scale bar of 100µm for size reference. Comprehensive immunofluorescence images, which combine staining of ZO-1, ATP1A1, α-SMA, F-actin, COL1, COL4, COL8, and DAPI-labelled nuclei, can be found in the supplementary material (Figure 29 in Appendix 3).

The administration of TGF-β1 is a well-established method to induce EMT in corneal endothelial cells, leading to a loss of endothelial characteristics and acquisition of mesenchymal traits [15,234]. The phosphorylation of Smads, facilitated by the TGF-β family [236], results in the activation of Snail, which plays a role in the deterioration of endothelial cell polarity, cytoskeleton remodelling, and increased cellular migration [237,238]. Furthermore, Smad

signalling elevates the level of ZEB, which might suppress the expression of tight junction and adherens junction proteins and activate the transcription of mesenchymal fibroblast markers [239].

The observed morphological changes in HCEC-12 cells, particularly the loss of the hexagonal shape and diminished ZO-1 expression, are consistent with the onset of EMT. The pronounced filamentous α-SMA expression in the TCPS and dECM-TCPS groups further corroborates this transition, as α-SMA is a key marker of mesenchymal cells. Interestingly, the COL4 and dECM-COL4 cultures demonstrated a relative resistance to TGF-β1-induced EMT. This suggests that the COL4 coating and the dECM-COL4 matrix might offer some protective effects against EMT, potentially by providing a more physiological microenvironment that supports the maintenance of the corneal endothelial phenotype. The distinct secretion patterns of COL8A2 across the different culture conditions further highlight the influence of the underlying matrix on cellular behaviour. The lack of distinct boundaries in the TCPS group, as evidenced by the COL8A2 staining, might indicate a more advanced stage of EMT, where cells lose their individuality, forming a more mesenchymal-like culture. In contrast, the distinct secretion patterns observed in the COL4, dECM-TCPS, and dECM-COL4 groups suggest that these matrices might slow down or partially reverse the EMT process, allowing cells to maintain some of their original characteristics.

Upon achieving approximately 80% confluency, EMT-induced HCEC-12 cells were lysed to extract proteins, which were subsequently assessed using western blot, with β-actin serving as a reference for protein expression. Figure 15 illustrates the protein bands corresponding to ZO-1, ATP1A1, COL8A2, β-actin, and α-SMA. Consistent with the immunofluorescence findings, cells cultured on TCPS exhibited the lowest ZO-1 expression and the highest α-SMA expression among the four conditions. ZO-1 expression in the dECM-TCPS group was slightly

elevated compared to the TCPS group but remained low. α-SMA expression was relatively uniform across the COL4, dECM-TCPS, and dECM-COL4 groups, with none reaching the elevated levels observed in the TCPS group. ATP1A1 expression remained consistent across all conditions, mirroring results from non-TGF-β1 treated HCEC-12 cultures. Similarly, COL8A2 expressions aligned with previous findings in HCEC-12 cells without EMT induction, with faint bands across all conditions, though the COL4 group exhibited a slightly more distinct band.

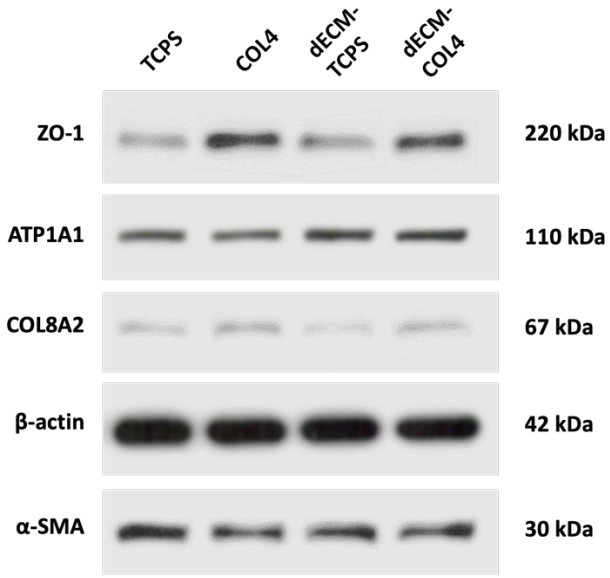

Figure 15. Western blot analysis of proteins from EMT-induced HCEC-12 P4 cultured on various surfaces. Total proteins were extracted from EMT-induced HCEC-12 P4 cells, cultured on TCPS, COL4 coating, dECM-TCPS, and dECM-COL4, with TGF-β1 supplementation in the culture medium. Following SDS-PAGE separation, the proteins were transferred to a nitrocellulose membrane. The membrane was probed with antibodies to visualise the proteins ZO-1, ATP1A1, COL8A2, β-actin, and α-SMA. The corresponding molecular weight of each protein is indicated on the right side of the blot.

The western blot results provide a molecular perspective on the phenotypic changes observed in HCEC-12 cells under different culture conditions post-EMT induction. The diminished ZO-1 expression in the TCPS and dECM-TCPS groups reinforces the notion that these surfaces may not be optimal for maintaining the corneal endothelial phenotype. The

reduced expression of the crucial tight junction protein ZO-1 suggests compromised barrier integrity. The elevated α-SMA expression, especially in the TCPS group, is indicative of the successful induction of EMT. The consistent ATP1A1 expression across all conditions suggests that the ion transport function, vital for corneal hydration, might be relatively unaffected by the culture surface or EMT induction. The consistent expression of COL8A2, even post-EMT induction suggests that the culture conditions, while influencing cellular phenotype, may not drastically alter the secretion of this vital ECM component.

5.4 Summary

This chapter embarked on a comprehensive exploration of the influence of cell-derived decellularised extracellular matrices (dECMs) on the behaviour of the immortalised human corneal endothelial cell line, HCEC-12. Through a series of meticulously conducted experiments, several pivotal findings emerged, each shedding light on the potential of dECM in corneal endothelial cell research.

The initial stages of the investigation successfully derived and characterised dECM from HCEC-12 cells cultured on TCPS (dECM-TCPS) and those cultured on surfaces coated with 100μg/mL COL4 (dECM-COL4). The presence of a gelatinous layer post-decellularisation confirmed the retention of the ECM. In the realm of proliferation, dECM substrates, especially dECM-COL4, emerged as superior platforms, outperforming the standard TCPS and COL4 coatings. This enhanced support for HCEC-12 proliferation suggests that dECMs, by closely mimicking the natural cellular microenvironment, offer a more conducive and physiologically relevant platform for cell growth. The immunostaining results, especially in the context of endothelial-to-mesenchymal transition (EMT) induced by TGF-β1, revealed the resilience of

cells cultured on dECM-COL4. These cells retained a significant proportion of their typical corneal endothelial phenotype, suggesting the inherent protective qualities of dECM against EMT. As found in western blot experiments, the preservation of characteristic protein profiles in HCEC-12 cells cultured on dECM-COL4 further emphasised the potential of dECM-COL4 in maintaining cellular integrity, even under challenging conditions.

In conclusion, it is unequivocally clear that dECMs, particularly those derived from healthy cells, offer immense potential for the in vitro culture of human corneal endothelial cells by providing a more native-like environment. The insights garnered from this chapter not only highlight the importance of dECM but also set the stage for subsequent investigations into whether an optimal culture substrate for corneal endothelial cells can be developed by emulating the Descemet's membrane.

Chapter 6

Development of a Novel Biomimetic Culture Substrate from Posterior Porcine Corneal Tissue

This chapter, along with the subsequent one, unveils the posterior porcine cornea (PPC) as an innovative substrate for HCEC-12 culture. The current chapter delineates the meticulous preparation and characterisation of PPC, setting the stage for the ensuing chapter that illustrates the outcomes of cell culture using PPC as a coating solution. The formulation of the coating solution necessitated the extraction of tissue from the posterior segment of porcine corneas, followed by a thorough decellularisation of the tissues and their subsequent reconstitution into a solution. A characterisation of the PPC constituents was undertaken, confirming the presence of collagen type VIII, a fundamental component of the Descemet's membrane. Furthermore, this study ventured into the scale-up of PPC decellularisation, culminating in the development of a prototype bioreactor that automates the process.

6.1 Introduction

Human corneal endothelial cells (HCECs) often struggle to be expanded beyond a couple of passages without a marked decline in their functional and phenotypic attributes [240,241]. This limitation is attributed to the endothelial-to-mesenchymal transition (EMT) that these cells undergo over passages [242,243]. Cells that have experienced EMT exhibit an elongated, fibrous morphology and a diminished expression of tight junction and adherens junction proteins [244,245].

Past research suggests that the cyclical disruption and reformation of cell-cell contacts during HCEC passaging might instigate EMT [8,9]. However, swiftly re-establishing confluency and cellular polarity might offer a solution to this challenge [13,14]. One promising strategy has been the coating of culture surfaces with specific extracellular matrix (ECM) proteins, which has demonstrated efficacy in bolstering cell adhesion, proliferation, and migration [246,247].

The Descemet's Membrane (DM), an integral component of the cornea, anchors the corneal endothelium to the stroma. Numerous studies have underscored the DM's pivotal role in sustaining corneal health [127,152]. The DM's rich composition of ECM proteins offers a corneal endothelial-specific microenvironment, hinting at its potential as an optimal substrate for in vitro culture [126,248]. For instance, collagen types IV (COL4) [16,247] and VIII (COL8) [249], both abundant in the DM, have been identified as potent culture substates for corneal endothelial cell culture.

Given the DM's significance in maintaining corneal health and its potential to support in vitro culture of HCECs, a DM-derived substrate for HCEC culture is created: posterior porcine cornea (PPC). Sourced from a pig's cornea, PPC represents a large portion of the cornea's posterior section, encompassing the DM.

6.2 Materials and Methods

6.2.1 Extracting PPC from Eyeballs

Porcine eyeballs were sourced immediately following the slaughter of the animals. To maintain the integrity of the tissues, the eyeballs were promptly transported to the laboratory on ice. Once in the lab, a meticulous dissection process was initiated. Using a sterile scalpel,

circular sections, approximately 15-20mm in diameter, were excised from the anterior side of the eyeballs. These sections encompassed the entire cornea and a fragment of the adjacent sclera. Following the dissection, the tissues were carefully inverted to present the posterior side. They were then securely mounted on a specially designed platform to ensure stability for the subsequent procedures. With the tissues firmly in place, a femtosecond laser lenticule extraction instrument (Wavelight FS200), calibrated to a depth of 100µm and 10mm diameter, was employed to slice a tissue disc from the posterior side of the cornea. The freshly obtained posterior porcine cornea (PPC) tissues were sealed in vacuum pouches for preservation at -20°C for up to six months, following thickness measurement using optical coherence tomography (Shenzhen Certainn OSLF-1500).

6.2.2 Decellularisation of Posterior Porcine Cornea (PPC)

The decellularisation of the PPC tissues was conducted using a rudimentary setup, designed to thoroughly remove cells from the PPCs while preserving the structural and biochemical integrity of the extracellular matrix. As illustrated in Figure 16, PPCs were placed into a cylindrical container perforated with holes (approximately 1.5mm in diameter) made using a solder iron. This container was then securely fastened to the base of a modified pipette box, with a large central portion of the box's lid removed for easier access. To facilitate the inflow and outflow of decellularisation solutions, two holes were made in the box's walls, accommodating silicone tubing connections. The entire assembly was elevated to create a fluid flow gradient, directing waste into a lower-positioned collection container.

The decellularisation process was driven by a peristaltic pump (Gilson, F155007), which introduced the solutions, and a plate rocker (Stuart, 1144190), which facilitated mass transfer. Gravity assisted in the drainage process. The outlet hole's strategic positioning maintained a

consistent liquid level inside the box, ensuring the PPCs were submerged during the shaking procedure.

A systematic sequence of solutions was employed to achieve optimal decellularisation. The decellularisation of PPC was initiated by treating the tissues with sodium dodecyl sulphate (SDS, Sigma-Aldrich, L3771). The tissues were first exposed to a prolonged circulating flow of 3L SDS for 12 hours at 25°C. This was followed by a continuous flow of 2L SDS for 3 hours at the same temperature. These steps were crucial in effectively removing cellular components from the tissue matrix. Subsequent to the SDS treatment, the tissues were subjected to a series of washes with PBS (Sigma-Aldrich, P3813) to eliminate any residual SDS. An initial circulating flow of 1L PBS was introduced for 4 hours at 25°C, followed by a continuous flow of 2L PBS for an additional 2 hours. To further enhance the decellularisation process, the tissues were treated with 1% Triton X-100 (Sigma-Aldrich, T8787) for 3 hours at 25°C, aiding in the removal of cellular lipids. Post treatment, the tissues were again washed with PBS, first with a circulating flow for 4 hour and then with a continuous flow for 1 hour, both at 25°C. To ensure the complete degradation of any lingering nucleic acids, the tissues were treated with 10U/mL Benzonase® nuclease (Sigma-Aldrich, E1014) for 1 hour at a temperature of 37°C. This was followed by another sequence of PBS wash, initially with a circulating flow for 4 hour and subsequently with a circulating flow containing 1% penicillin/streptomycin (ThermoFisher, 15070063) for 1 hour, both at 25°C.

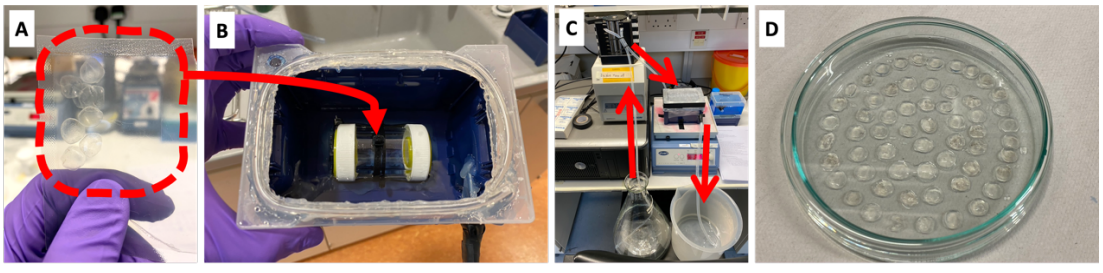

Figure 16. Decellularisation Apparatus and Process for PPCs. This figure illustrates the sequence and components of the decellularisation process for PPC tissues. (A) Shows the initial

step where vacuum-sealed PPC tissues are prepared for decellularisation. (B) Depicts these tissues being transferred to the tank of a custom-built decellularisation setup. (C) Demonstrates the flow of decellularisation reagents, facilitated by a peristaltic pump, which moves the reagents from a conical flask through the tank (where the tissues are agitated on a rocking bed, as indicated by the arrows), and finally to a waste beaker for collection. (D) Displays the decellularised PPCs post-process, laid out in a glass petri dish for visual inspection.

6.2.3 Automating Decellularisation of PPC

To automate the decellularisation of PPC tissues, a bioreactor was designed using Autodesk Inventor, as shown in Figure 17. The bioreactor's core component is a rotatable cylinder, measuring 82mm in length and 35mm in diameter, fitted with filter units at each end to contain the PPC tissues. Internally, the cylinder features four evenly spaced baffles, each 2mm wide and 3.5mm tall, to facilitate agitation. It is capped on both ends and mounted between two stands, with rotation driven by a DC motor via a timing belt.

Reagents required for decellularisation are introduced into the cylinder by a peristaltic dosing pump (Treedix, U-PLP-0001). Control over the reagent flow is achieved through solenoid valves (Sourcingmap, a14010700ux0266) at both the inlet and outlet. Components in direct contact with reagents were 3D printed using resin (Formlabs Form 2), while supporting structures were created with PLA using fused deposition modelling (Makerbot Replicator 2).

A programmed Arduino Uno R3 controls the sequential delivery of reagents, operating the pump, motor, and valves. Two modes were programmed for each solution: ‘static’, where the outlet valve is closed to allow complete filling and soaking of tissues, and ‘continuous’, where solutions flow through the cylinder. The initial decellularisation involves treating tissues with SDS in static mode thrice, each for 4 hours at 25°C, followed by a 3-hour continuous flow of SDS. Post-SDS, tissues undergo multiple PBS washes to remove residual SDS, including twenty 5-minute static washes and a 2-hour continuous flow. Further decellularisation involves

a 3-hour Triton X-100 treatment at 25°C to remove cellular lipids, followed by similar PBS washing steps. To degrade nucleic acids, the tissues are statically submerged in 10U/mL Benzonase® nuclease for 1 hour at 37°C, and then subjected to final PBS washes: fifty 5-minute static cycles and a continuous flow for 2 hours. Finally, the PPC tissues are removed and rinsed with PBS containing 1% penicillin/streptomycin.

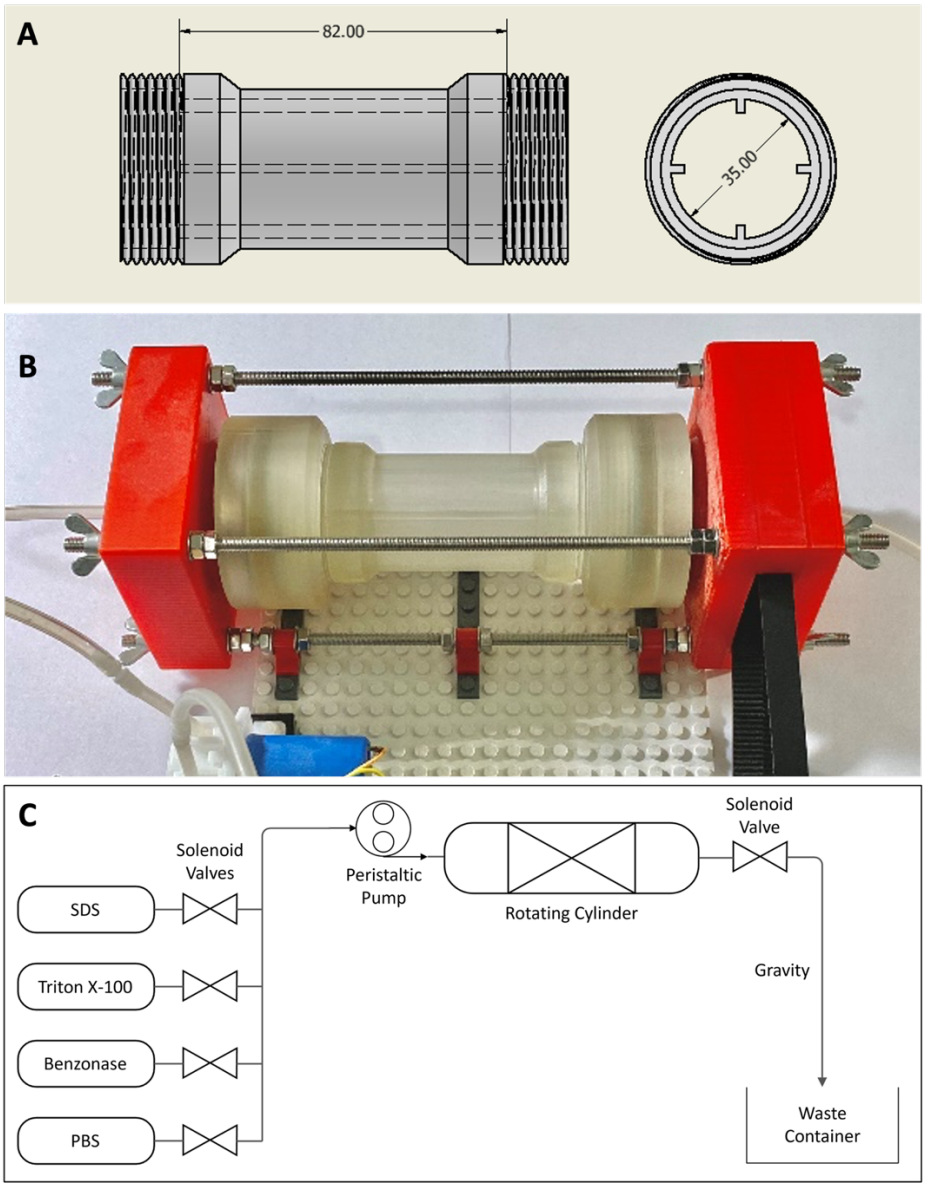

Figure 17. Design and illustration of a working prototype of the PPC decellularisation bioreactor. (A) Showcases the design of the rotating cylinder of the bioreactor. (B) Displays

the assembly of the bioreactor. (C) Presents a flowchart detailing the operational setup of the decellularisation process. This includes solenoid valve-controlled introduction of four reagents - SDS, Triton X-100, Benzonase, and PBS - into the rotating cylinder, following the decellularisation protocol. Another solenoid valve at the outlet end regulates the outflow of reagents to a waste container.

6.2.4 Hematoxylin and Eosin (H&E) Staining of PPCs

Both native and decellularised PPCs were fixed using 10% formalin for a duration of 24 hours at ambient room temperature. Following fixation, the tissues were subjected to a series of washes using phosphate-buffered saline (PBS) to remove any residual formalin. The fixed PPCs were then methodically dehydrated through a graded ethanol series, transitioning from lower to higher concentrations. Subsequent to dehydration, the tissues underwent a clearing process using benzene, which aids in removing any residual water and prepares the tissue for embedding. The cleared PPCs were then embedded in paraffin wax, ensuring they were fully encapsulated and protected. Once embedded, the paraffin blocks containing the PPCs were carefully inspected and, if deemed necessary, trimmed to ensure optimal sectioning. Using a microtome, the blocks were then sectioned into thin slices, each measuring approximately 4µm in thickness.

The obtained paraffin sections underwent a deparaffinisation process to remove the wax, followed by a rehydration sequence to prepare them for staining. The sections were then stained using hematoxylin, which imparts a blue-purple hue to the nuclei, and eosin, which stains the cytoplasm and extracellular matrix with a pink hue. This combination, referred to as H&E staining, provides a clear contrast between different cellular and tissue components. Post-staining, the sections were sealed using a resin-based medium to preserve the stain and provide a clear viewing surface. Once air-dried, these stained sections were meticulously observed

under a microscope to assess the efficacy of the decellularisation process, comparing the cellular components in native versus decellularised PPCs.

6.2.5 Reconstituting PPC for Coating

Decellularised PPCs were first subjected to a freeze-drying process. This ensured the removal of any residual moisture, and once thoroughly dried, the weight of the PPCs was meticulously recorded. To achieve a uniform consistency suitable for subsequent processes, these tissues were mechanically processed. This involved an initial shredding phase, followed by a thorough grinding, resulting in a fine powder-like texture. The next step involved the enzymatic digestion of the processed PPC tissues. For this purpose, pepsin was employed. A specific ratio was maintained where for every milligram of tissue, 500U of pepsin (Sigma-Aldrich, P7000) was added in a 10mM HCl solution (Sigma-Aldrich, 320331). To ensure comprehensive digestion, the mixture was kept in a gentle rocking motion for a duration spanning 3 to 5 days at a consistent temperature of 4°C. Simultaneously, a gentle rocking motion was maintained for a duration spanning 3 to 5 days. The completion of this phase was marked by the total dissolution of all visible tissue fragments within the solution. Post-digestion, the concentration of PPC proteins in the resultant solution was determined using bicinchoninic acid assay (BCA, ThermoFisher, 1859078), a colorimetric assay. The intensity of the colour change is directly proportional to the protein concentration, and this was quantified spectrophotometrically using a plate reader (Molecular Devices, SpectraMax i3x). To ensure the accuracy of this assay, a blank control was set using a pepsin/10mM HCl solution.

6.2.6 Analysis of dECM Components

Reconstituted solutions of PPC tissues decellularised using both the rudimentary setup and the bioreactor were analysed. The concentrations of the reconstituted dECM samples were determined using a BCA assay, as described in Chapter 3. To facilitate the subsequent component analysis, the samples were mixed with sample buffer before being loaded to the SDS-polyacrylamide gel. To quantify the amount of collagen types I (COL1) and IV (COL4) in the dECM-TCPS and dECM-COL4 samples, the intensities of the protein bands were compared with those of the controls. Three controls were loaded to the SDS-PAGE gel: 20µg COL1, 20µg COL4, and a mixture containing 10µg COL1 and 10µg COL4.

After electrophoresis, the proteins separated on the SDS-PAGE gel were effectively transferred to a nitrocellulose membrane. This membrane was then briefly stained with Ponceau S solution to visualise the total protein profile. Following the capture of the stained membrane's image, the membrane was rinsed five times with tris-buffered saline containing 0.1% Tween-20 (TBST) to remove the Ponceau S stain, thereby preparing the membrane for antibody probing. The membrane was blocked with 5% non-fat milk in TBST for 1 hour at room temperature to prevent non-specific binding. Following blocking, the membrane was incubated with primary antibodies against collagen type I, collagen type IV, and collagen type VIII overnight at 4°C. After washing three times with TBST, the membrane was incubated with appropriate horseradish peroxidase (HRP)-conjugated secondary antibodies for 1 hour at room temperature. The membrane was washed again, and the chemiluminescent protein bands were visualised on films.

6.3 Results

6.3.1 Uneven Thickness at Different Regions of PPC

The experiments were designed to investigate the potential of Descemet's Membrane (DM) to support the in vitro regeneration of corneal endothelial cells, given its known capacity in corneal endothelial regeneration [127,152]. The experiments focused on whether a substrate derived from DM could provide a conducive environment for the culture of HCEC-12. Porcine corneas were utilised to extract extracellular matrix (ECM) proteins, specifically from their posterior sections. This extraction involved delicately separating thin tissue slices from the posterior side of the porcine corneas using a laser lenticule extraction instrument. The thicknesses of these tissues were subsequently determined using ocular coherence tomography (OCT). Despite setting the separation depth at 100µm, there was a noticeable variation in thickness from the centre to the periphery of the PPC tissues. Measurements were taken across different regions on six individual pieces of PPC (N=6). The results revealed average thicknesses of 108.83 ± 2.27µm in the centre (n=1), 130.08 ± 1.09µm in the intermediate region (n=8), and 106.88 ± 2.02µm towards the edge (n=8) (Figure 18A). Taking into account the areas of the measured regions, the overall average thickness was calculated to be 120.62 ± 1.51 µm. In contrast, a typical DM is only about 10µm thick [250] – considerably thinner than the PPC. This indicates that a significant portion of the PPC tissue was, in fact, stromal tissue from the porcine cornea.

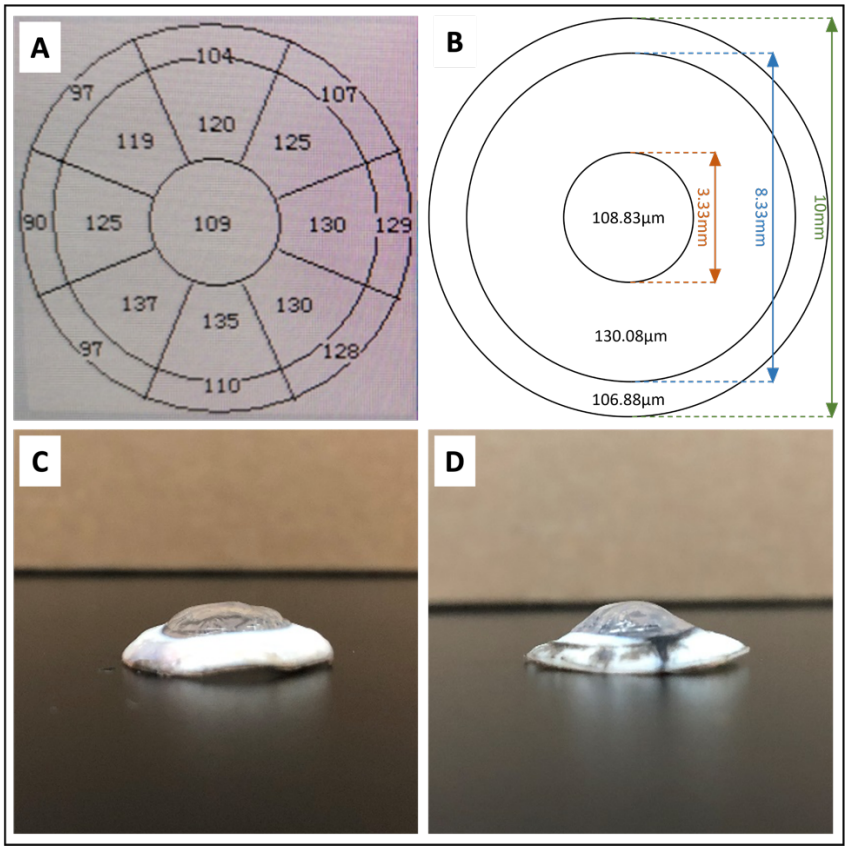

Figure 18. Visual representation of the thickness measurements of PPC tissues from porcine corneas. Optical coherence tomography (OCT) was utilised to determine the thickness, with images (A) showcasing the operating software's interface and (B) presenting the average thicknesses derived from six individual PPC samples, with measurements taken across varied regions. (C) A photograph depicting a whole porcine cornea along with the adjacent sclera, excised from the eyeball, showcasing its natural appearance. (D) The same cornea but inverted to display its posterior side.

Typically, a laser lenticule extraction instrument is adept at slicing tissue with uniform thickness from the anterior side of a cornea. However, the topography of the acquired PPCs in this study was reminiscent of a ripple. This irregularity could potentially be attributed to surface warping that occurs when the naturally dome-shaped corneas (Figure 18B) are inverted. This inversion transforms the concave side of the cornea to a convex shape (Figure 18C), thereby exposing the posterior surface to the laser. A similar deformation can be observed when a contact lens is inverted, resulting in a bell shape. This phenomenon of surface warping and its impact on tissue thickness is not unique to this study [251].

6.3.2 Successful Decellularisation of PPC

The acquired PPCs were decellularised using the rudimentary setup described in section 6.2.2 or the bioreactor described in section 6.2.3. This was to ensure the resultant tissues were devoid of any cellular components that might interfere with cell seeding or elicit an immune response, which can potentially lead to graft rejection upon implantation. The efficacy of both decellularisation methods was verified through examining hematoxylin and eosin (H&E) stained paraffin sections of the tissues, as depicted in Figure 19. A comparative analysis between the native and treated PPCs revealed a notable absence of intact cells and cellular remnants in the tissues treated using both methods. In contrast, the collagenous fibres inherent to the extracellular matrix remained intact and discernible. The images demonstrates the bioreactor was able to achieve the same decellularisation efficacy in an automated manner and using less reagent.

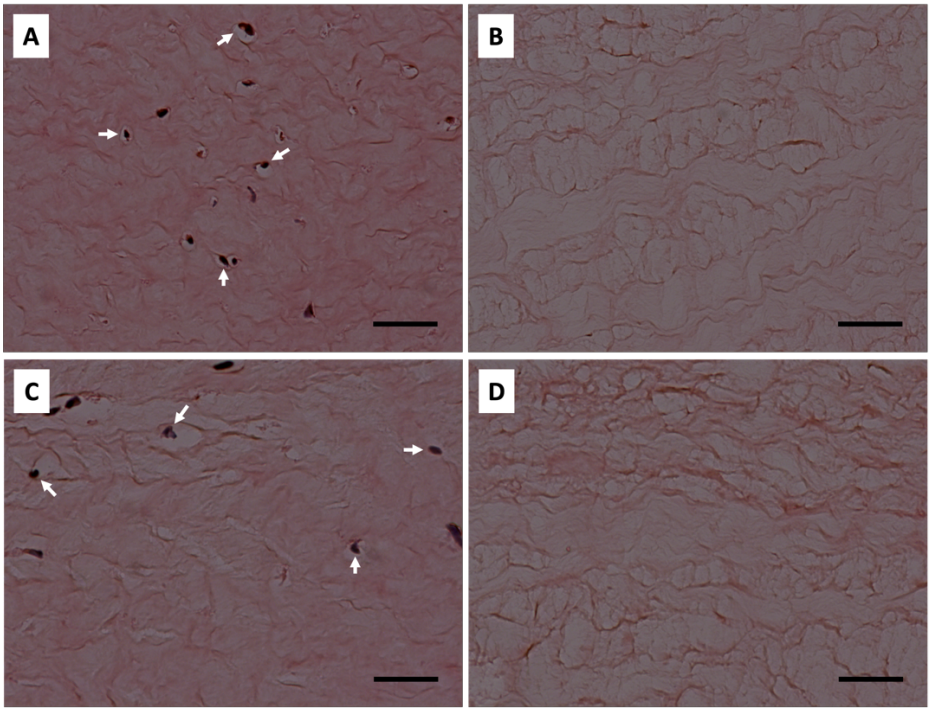

Figure 19. Histological analysis of PPC tissues. This figure presents representative histological images of native and decellularised PPC tissues. (A) and (C) show native PPC tissues prior to decellularisation using the rudimentary setup and the bioreactor, respectively, highlighting intact cells (indicated by white arrows). (B) and (D) depict PPC tissues post-

decellularisation, treated using the rudimentary setup and the bioreactor, respectively, illustrating the absence of cells. All images were stained with haematoxylin and eosin to highlight cellular and matrix structures. Scale bars in each image represent 50µm.

6.3.3 PPC's Complex Protein Profile

The major collagen components of PPC were characterised to understand its protein composition. Reconstituted solutions of PPC were assayed through SDS-PAGE, which separated protein bands based on their molecular weights, and the result was visualised on a Coomassie Brilliant Blue stained gel (Figure 20A). The gel displayed distinct protein bands for recombinant collagen type IV, PPC, and the control (the digesting solvent for PPC). The COL4 lane exhibited a series of protein bands with molecular weights ranging from approximately 55kD to over 250kD. In contrast, the PPC sample presented a more diverse protein profile, with bands spanning from below 10kD to above 250kD. The control lane showed a prominent protein band at around 37kD, corresponding to the molecular weight of pepsin [256].

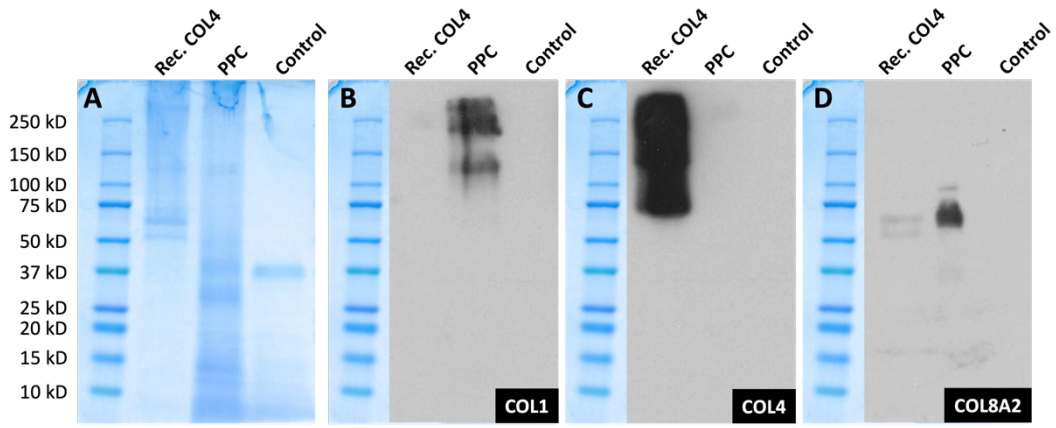

Figure 20. Protein component analysis of PPC. (A) Representative SDS-PAGE gel image showcasing protein separation, stained with Coomassie Brilliant Blue. (B-D) Western blot results for the identification of specific collagen types in PPC. The blots were probed with antibodies against (B) COL1, (C) COL4, and (D) COL8A2. For clarity, images of the stained nitrocellulose membrane are superimposed on the gel, providing a visual reference for molecular weight determination. In all panels, the lanes are designated as follows: lane 1 - protein ladder, serving as a molecular weight reference; lane 2 - recombinant COL4, used as a positive control for collagen type IV; lane 3 - reconstituted PPC, representing the protein profile

of the treated porcine cornea; lane 4 - control sample, consisting of the PPC dissolvent (pepsin/HCl solution).

Further characterisation was carried out by transferring the separated proteins onto a nitrocellulose membrane. The major collagenous components in the PPC solution, namely collagen types I (COL1), IV (COL4), and VIII's α2 chain (COL8A2), were identified using specific antibodies and visualised through chemiluminescence. The distinct bands corresponding to these collagens are illustrated in Figure 20B-D. The findings from the SDS-PAGE and subsequent immunoblotting provide valuable insights into the collagen composition of the PPC. As anticipated, the PPC solution predominantly contained COL1, which is primarily derived from the corneal stroma [31], and COL8A2 from the Descemet's membrane (DM) [249]. However, an unexpected observation was the absence of COL4 in the PPC solution. Collagen type IV is known to be a component of the DM, and its absence in the PPC suggests that its presence might be minimal or even negligible in the DM or stroma of the porcine cornea. This finding challenges the conventional understanding of the collagen composition of the DM and highlights the importance of thorough characterisation when working with tissue-derived products.

6.4 Summary

This chapter provides a comprehensive overview of the methods and results involved in the extraction of proteins from posterior porcine cornea (PPC) tissues. The innovative procedures include sourcing and dissecting porcine eyeballs, employing a femtosecond laser for slicing, decellularising the obtained tissues, and methods to reconstitute a coating solution. Two approaches are described for the decellularisation of PPC tissues: a semi-automated, rudimentary setup and an automated bioreactor system. The methodologies aim to ensure the

thorough removal of cellular components while maintaining the structural integrity of the extracellular matrix. Hematoxylin and eosin (H&E) staining reveal the effectiveness of the decellularisation process. The complex protein profile of PPC is elucidated through protein assays and Western blotting. Interestingly, the absence of collagen type IV in the PPC solution raises questions about the conventional understanding of the collagen composition in porcine cornea. These findings are essential for understanding the potential of PPC in corneal endothelial tissue engineering.

Chapter 7

Effective Maintenance of HCEC-12 Culture Using PPC Coating

Recognising the limitations of current cultivation techniques, this study introduces the posterior porcine cornea (PPC) as a pioneering substrate for the culture of the HCEC-12 human corneal endothelial cell line. The method in this chapter involves the meticulous decellularisation of tissues extracted from the porcine cornea's posterior segment, followed by their transformation into a viable coating solution. In comparative assessments, HCEC-12 cells cultured on PPC-coated surfaces demonstrated superior performance across several metrics, including cell adherence, proliferation, cell density, functional protein expression, and wound recovery. Central to the findings is the revelation that PPC coating effectively inhibits the endothelial-to-mesenchymal transition (EMT), thus optimising HCEC-12 culture. The encouraging result suggests PPC holds immense potential to advance corneal endothelial cell culture techniques.

7.1 Introduction

The cornea, the transparent front part of the eye, plays an indispensable role in vision by refracting light and protecting the inner ocular structures. Central to its function is the corneal endothelium, a monolayer of hexagonal cells situated on the innermost surface of the cornea. These cells are responsible for preserving corneal clarity by regulating fluid and nutrient

exchange between the aqueous humour and the corneal stroma [5]. However, their limited regenerative capability in humans means that any damage or disease affecting these cells can culminate in corneal oedema and, consequently, vision impairment [252].

A significant hurdle in corneal endothelial tissue engineering is the in vitro expansion of these cells. Human corneal endothelial cells (HCECs) often struggle to be expanded beyond a couple of passages without a marked decline in their functional and phenotypic attributes [240,241]. This limitation is attributed to the endothelial-to-mesenchymal transition (EMT) that these cells undergo over passages [242,243]. Cells that have experienced EMT exhibit an elongated, fibrous morphology and a diminished expression of tight junction and adherens junction proteins [244,245]. Past research suggests that the cyclical disruption and reformation of cell-cell contacts during HCEC passaging might instigate EMT [8,9]. However, swiftly re-establishing confluency and cellular polarity might offer a solution to this challenge [13,14]. One promising strategy has been the coating of culture surfaces with specific extracellular matrix (ECM) proteins, which has demonstrated efficacy in bolstering cell adhesion, proliferation, and migration [246,247].

The Descemet's Membrane (DM), an integral component of the cornea, anchors the corneal endothelium to the stroma. Numerous studies have underscored the DM's pivotal role in sustaining corneal health [127,152]. The DM's rich composition of ECM proteins offers a corneal endothelial-specific microenvironment, hinting at its potential as an optimal substrate for in vitro culture [126,248]. For instance, collagen types IV (COL4) [16,247] and VIII (COL8) [249], both abundant in the DM, have been identified as potent culture substates for corneal endothelial cell culture.

Given the DM's significance in maintaining corneal health and its potential to maintain in vitro culture of HCECs, a DM-derived substrate for HCEC culture is created: posterior porcine

cornea (PPC). Sourced from a pig's cornea, PPC represents a large portion of the cornea's posterior section, encompassing the DM. By systematically examining the interactions between HCEC-12 cells and this substrate, this chapter seeks to elucidate the potential of PPC in advancing corneal endothelial cell culture techniques. Subsequent experiments are designed to determine whether this substrate can promote cell adherence, proliferation, and phenotype maintenance, thereby potentially suppressing the EMT process. Furthermore, with the increasing demand for corneal transplants and the scarcity of donor corneas, there is a pressing need to develop alternative solutions. This chapter, therefore, also delves into the creation of a transplantable model using cultured HCEC-12 cells on these substrates. Such a model holds promise for future applications in corneal endothelial tissue engineering and transplantation.

7.2 Materials and Methods

7.2.1 PPC Coating for Cell Culture

To prepare PPC coated surfaces for HCEC-12 cell culture, a working solution of reconstituted PPC was formulated. This involved diluting the stock PPC solution to achieve a final working concentration of 100µg/mL, using 10mM HCl as the diluent. For the coating process, specific volumes of the working PPC solution were allocated based on the surface area of the culture-ware. For instance, a 96-well plate received 50µL per well, which translates to 155.5µL/cm^2. In the case of a T-75 flask, 11.66mL of the solution was deemed appropriate. The culture-ware, now containing the coating solution, was then incubated for 5 hours at 37°C. This ensured adequate adsorption of the PPC proteins onto the culture surface, providing an optimal environment for HCEC-12 cell attachment and growth.

Post-incubation, the next step was to prepare the coated surface for cell seeding. The residual PPC solution was carefully discarded from the culture-ware. To neutralise any remaining pepsin activity, which could potentially harm the cells, the culture surface was rinsed twice with a 1mM NH_4OH solution. This was followed by a subsequent rinse with PBS (ThermoFisher, 10010-023) to remove any traces of the NH_4OH solution. The final preparatory step involved sterilising the culture-ware to ensure a contamination-free environment for the cells. This was achieved by exposing the culture-ware to UV radiation within a biosafety cabinet for a duration of one hour. With the culture surface now primed, it was ready for the seeding and culture of HCEC-12 cells.

7.2.2 Scratch Assay

To evaluate the ability of HCEC-12 cells to recover from inflicted damage, a scratch assay was conducted using a similar method described in previous articles [253,254]. This assay serves as a standard method to assess cell migration and wound healing capabilities in vitro. Initially, HCEC-12 cells were cultured until they reached a confluent monolayer. Using a Nikon Eclipse Ti widefield microscope coupled with the NIS Elements AR software, images of the cultured cells were captured to establish a baseline.

For the initiation of the scratch assay, a sterile 200µL pipette tip was employed. With gentle pressure, a scratch was made across the confluent monolayer of HCEC-12 cells, simulating a wound or damage. This action created a clear, cell-free gap or "wound" within the monolayer. Following the creation of the scratch, the cultures were placed under the microscope, and images were captured at 5-minute intervals. The primary focus during imaging was the scratched region, capturing the dynamics of cell migration into the cell-free gap. Post imaging, the captured images were processed to delineate the boundaries of the cell-free regions. The

edges of the gaps were manually outlined to clearly demarcate the wounded area from the surrounding intact cell monolayer. For quantification purposes, the software ImageJ was utilised. The areas of the cell-free regions in the images were analysed to determine the extent of wound closure over time. This meticulous approach ensured a comprehensive understanding of the wound healing capabilities of HCEC-12 cells under the given conditions.

7.2.3 Assessment of Contact Inhibition of Locomotion (CIL)

To investigate contact inhibition of locomotion (CIL) in HCEC-12 cells, a time-lapse imaging technique was employed. Using a Nikon Eclipse Ti widefield microscope, images were captured at a 20x magnification. The cells cultured on TCPS, COL4 coating, and PPC coating, were continuously imaged for a span of 64 hours. These images were taken at regular intervals of 15 minutes. The initiation of the time-lapse was set 4 hours post-seeding, allowing the cells adequate time to adhere to their respective culture surfaces at a maintained temperature of 37°C. For the purpose of ensuring repeatability, the experiment was conducted thrice. In each iteration, HCEC-12 cells were cultured in a 24-well plate. Each of the three groups - TCPS, COL4 coating, and PPC coating - was allocated four wells. Prior to seeding the cells, six random locations on the culture surface of each well were distinctly marked using a needle. These markings served as reference points during the time-lapse imaging, ensuring consistent observation of the same locations throughout the experiment.

The primary objective of this study was to determine CIL by observing if cells either changed their trajectory upon encountering other cells or if they clumped together. The latter behaviour, cell clumping, indicates a lack of CIL expression. Observations were documented using a binary metric: the presence or absence of cell clumping in each of the pre-marked regions. Based on these observations, the frequency of absence of CIL was computed. It is

crucial to highlight that the results from this methodology do not represent the frequency of CIL in individual cells. Instead, the data provides an understanding of the likelihood that a region, when observed under a 20x magnification lens, would display an absence of CIL.

7.2.4 Cell Culture on RAFT™ Cell Carrier

To explore the potential of creating a transplantable model using expanded HCEC-12 cells, the RAFT™ 3D cell culture kit (Lonza, 016-1R24) was employed. This kit facilitates the generation of a plastically compressed collagen type I hydrogel, which serves as a cell carrier, mimicking a more in vivo-like environment for the cells. The process commenced with the preparation of the initial hydrogel within a 24-well plate. A stock solution of collagen type I was mixed thoroughly with a neutralising solution provided in the kit. This mixture was then aliquoted into the wells of the plate and incubated at 37°C for a duration of 15 minutes. This incubation allowed the collagen to polymerise, forming a soft hydrogel. Using the absorber provided in the RAFT™ kit, the majority of the moisture content within the hydrogel was extracted. This action resulted in the compression of the hydrogel, transforming it into a disc with a thickness of approximately 120µm. This compressed hydrogel disc, now residing at the bottom of the well, provided a suitable substrate for cell culture. With the cell carrier ready, HCEC-12 cells were seeded at a high density of 30,000 cell/cm^2 onto the exposed surface of the compressed hydrogel. The cells were then cultured for three days, ensuring a dense and uniform layer of cells on the hydrogel's surface. Brightfield images were taken one and three days after seeding, and immunostaining of ZO-1 and cell nuclei with fluorescence images taken on the third day post-seeding. This setup, with HCEC-12 cells cultured on the RAFT™ system, aimed to replicate a transplantable model that could be utilised in further experiments and potential therapeutic applications.

7.3 Results and Discussion

7.3.1 HCEC-12 Cells Adhere Faster on PPC

Upon seeding HCEC-12 cells onto TCPS, COL4 coating, and PPC coating, a distinct difference in cell adherence was observed. Microscopic examination post-seeding revealed a more rapid flattening of individual cells in the COL4 and PPC groups. Within the first hour post-seeding, a majority of cells in these groups had already begun extending their contact with the culture surfaces, indicated by a transition from a spherical to a flattened morphology. In contrast, cells on the TCPS remained predominantly round (Figure 21).

This difference in attachment speed was further quantified using CCK-8 assays. Unadhered cells were aspirated, and the culture surfaces were gently rinsed with PBS at varying time intervals post-inoculation (Figure 21G). Consistent with the microscopic observations, the number of adhered cells was higher in the COL4 and PPC groups compared to the TCPS group at all tested time points. Two hours after seeding, the COL4 and PPC groups exhibited 32.96 ± 5.33% and 37.58 ± 4.70% more attached cells, respectively, than the TCPS group. These differences were statistically significant, with p-values of <0.01 for the COL4 group and <0.001 for the PPC group. However, the cell adhesion rates between the COL4 and PPC groups were comparable.

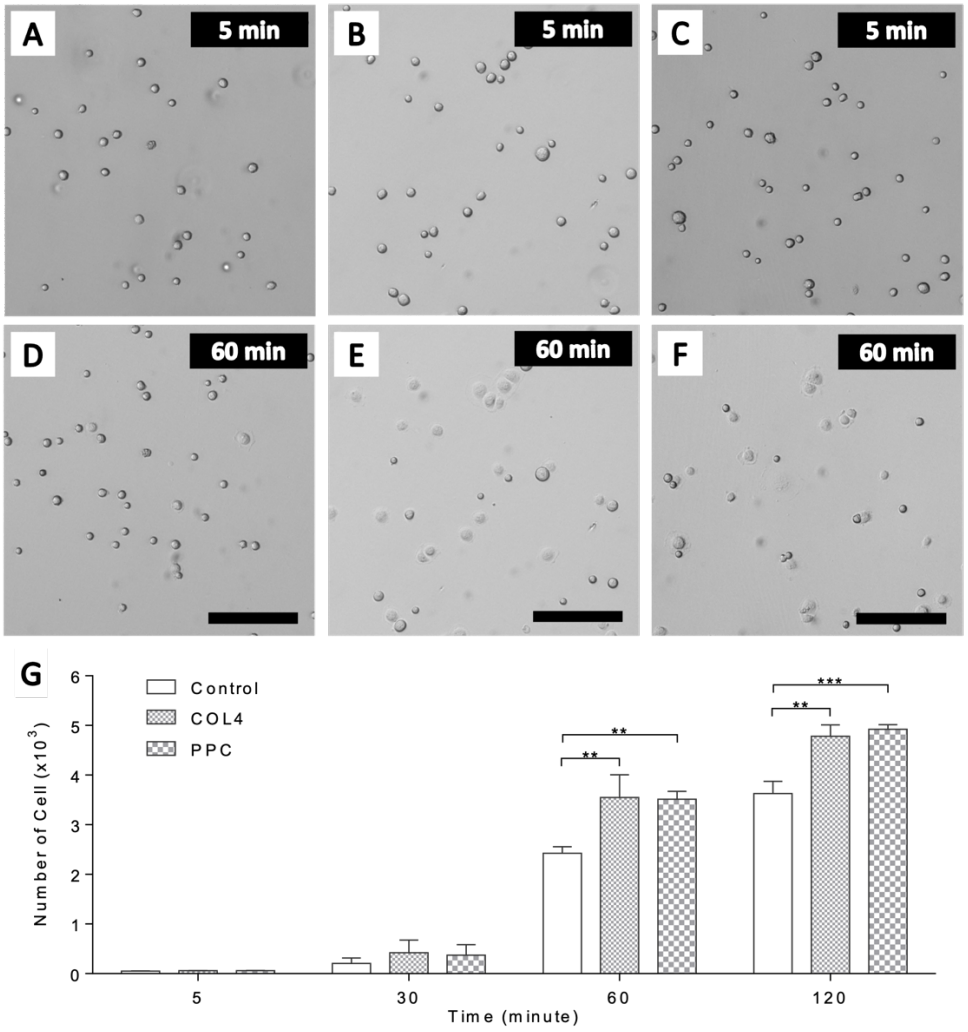

Figure 21. Characterisation of HCEC-12 cell adhesion on different substrates. (A-F) Representative brightfield microscopic images depicting HCEC-12 cells on TCPS (A, D), COL4 coating (B, E), and PPC coating (C, F) at two time points: 5 minutes (A-C) and 60 minutes (D-F) post-seeding. The images highlight the differences in cell attachment across the three surfaces. Scale bars represent 100µm. (G) A column chart illustrating the comparative analysis of the number of HCEC-12 cells that stably adhered to the culture surfaces in the TCPS, COL4, and PPC groups at four distinct time intervals: t=5, 30, 60, and 120 minutes. Each group consisted of four samples (N=4). Statistical significance was determined using two-way ANOVA, denoted by ** $p < 0.01$ and *** $p < 0.001$.

The observed differences in cell adhesion across the three surfaces highlight the significance of the substrate in influencing cellular behaviour. The rapid spreading of HCEC-12 cells on COL4 and PPC coatings suggest that these surfaces offer a more conducive environment for cell adhesion compared to TCPS. This could be attributed to the inherent biochemical properties of the coatings, which might mimic the natural extracellular matrix more closely,

thereby promoting cell attachment. The similarity in adhesion rates between the PPC and COL4 groups is intriguing. It suggests that the PPC, despite being derived from a different source, possesses properties comparable to COL4 in promoting cell adhesion.

7.3.2 Increased HCEC-12 Proliferation on PPC

The proliferation of HCEC-12 cells was significantly influenced by the type of substrate they were cultured on. Cells from passage 7 were seeded on TCPS, COL4 coating, and PPC coating, and their growth was monitored over a period of 9 days. CCK-8 assay, which was performed every other day, was employed to quantify the number of cells (Figure 22). As the days progressed, the beneficial effects of both the COL4 and PPC coatings on HCEC-12 proliferation became increasingly evident. By day 5, PPC coating demonstrated a significant advantage in supporting cell proliferation, and by day 7, the COL4 coating showed similar benefits. By the time the exponential growth phase reached a plateau on day 9, the cell counts in the PPC and COL4 groups were found to be 22.60 ± 2.53% and 12.74 ± 2.28% higher, respectively, than those in the TCPS group. These differences were statistically significant, with p-values of <0.01 for the PPC group and <0.0001 for the COL4 group when compared to the TCPS group. Furthermore, the PPC coating also showed a statistically significant advantage over the COL4 coating, with 9.20 ± 2.65% more cells on day 9 ($p<0.05$).

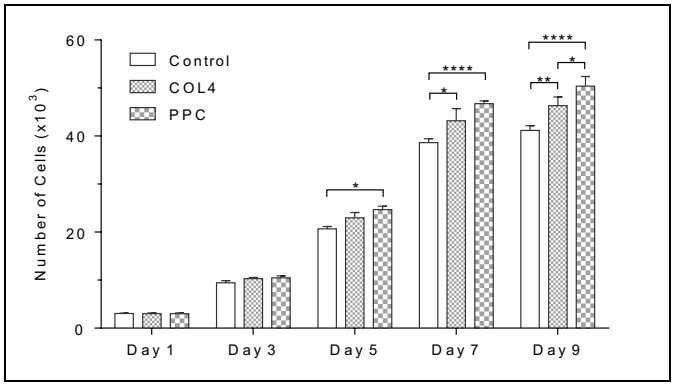

Figure 22. Comparative analysis of HCEC-12 cell proliferation on different substrates. The chart displays the growth rates of HCEC-12 cells cultured on TCPS, COL4 coating, and PPC coating over a period of 9 days. Cell counts were determined using CCK-8 assays, conducted every other day starting 12 hours post-seeding. Each experimental group consisted of four replicates (N=4). Statistical differences between groups were determined through two-way ANOVA, with significance denoted by *$p < 0.05$, **$p < 0.01$, and ****$p < 0.0001$.

The observed differences in cell proliferation across the three substrates indicate the importance of the underlying matrix in influencing cellular behaviours. The presence of COL8 in PPC might be a contributing factor, as it has been associated with enhanced endothelial cell proliferation and phenotypic maintenance in other studies [19,249,255]. It is well-established that the extracellular matrix plays a pivotal role in regulating various cellular functions, including proliferation, differentiation, and migration. The findings from this experiment align with previous research that has highlighted the significance of substrate composition in influencing cell growth [21,256].

The superior performance of PPC coating in supporting HCEC-12 cell proliferation, compared to the COL4 coating, is intriguing and warrants a deeper exploration. One plausible explanation lies in the inherent composition of PPC. As previously characterised, PPC is not just a single collagenous matrix but a complex combination of various ECM components. While COL4 is a major component of basement membranes and has been shown to support cell adhesion and growth, PPC offers a more holistic representation of the corneal ECM environment. PPC retains collagen type I from the corneal stroma as well as collagen type VIII from Descemet's membrane (DM). Collagen type I provides structural integrity [257] and has been associated with cell attachment and proliferation in various cell types [258,259]. Collagen type VIII, on the other hand, plays a role in endothelial cell function and is crucial for the maintenance of corneal transparency [19,249]. The presence of both these collagen types in PPC might create a synergistic environment that is more conducive to HCEC-12 growth than a

single type of collagen, as in the COL4 coating. Moreover, aside from collagens, PPC likely retains other ECM components, such as proteoglycans, glycoproteins. These components can modulate cell behaviour, offering binding sites for cell receptors, and providing signals that can influence cell proliferation, migration, and differentiation. The diverse protein profile of PPC, as evidenced by the SDS-PAGE results, suggests a rich milieu of proteins that might collectively enhance cell-matrix interactions, leading to improved cell proliferation.

7.3.3 HCEC-12 Morphology Maintained by PPC Across Passages

Cultured corneal endothelial cells are prone to morph into fibroblast-like cells, losing their natural function in a process called endothelial-to-mesenchymal transition (EMT). HCEC-12 cells were cultured under each experimental condition for five passages. To investigate whether PPC maintains the healthy phenotype of corneal endothelial, reconstituted solution of PPC was coated on culture-wares and its cellular influences were examined. TCPS and COL4 coating were used as control conditions for cell culture. Morphological evaluations were conducted on the fifth day post-seeding for each passage, with representative findings captured in Figure 23. Initially, at the first passage, cells across all groups presented a robust, closely arranged, hexagonal appearance. However, as the passages progressed, the inherent advantages of the ECM protein coatings became increasingly evident. By the second passage, cells cultured on TCPS began to exhibit a marked morphological heterogeneity. A significant portion of these cells underwent a transformation, adopting an elongated, fibroblast-like appearance indicative of endothelial-to-mesenchymal transition (EMT). This EMT phenomenon became more pronounced in the TCPS group with each subsequent passage. By the fifth passage, while the COL4 and PPC groups largely retained their healthy cellular morphology, the TCPS group

displayed a stark contrast. The culture was less dense, with a predominant presence of EMT cells interspersed among the few remaining hexagonal cell colonies.

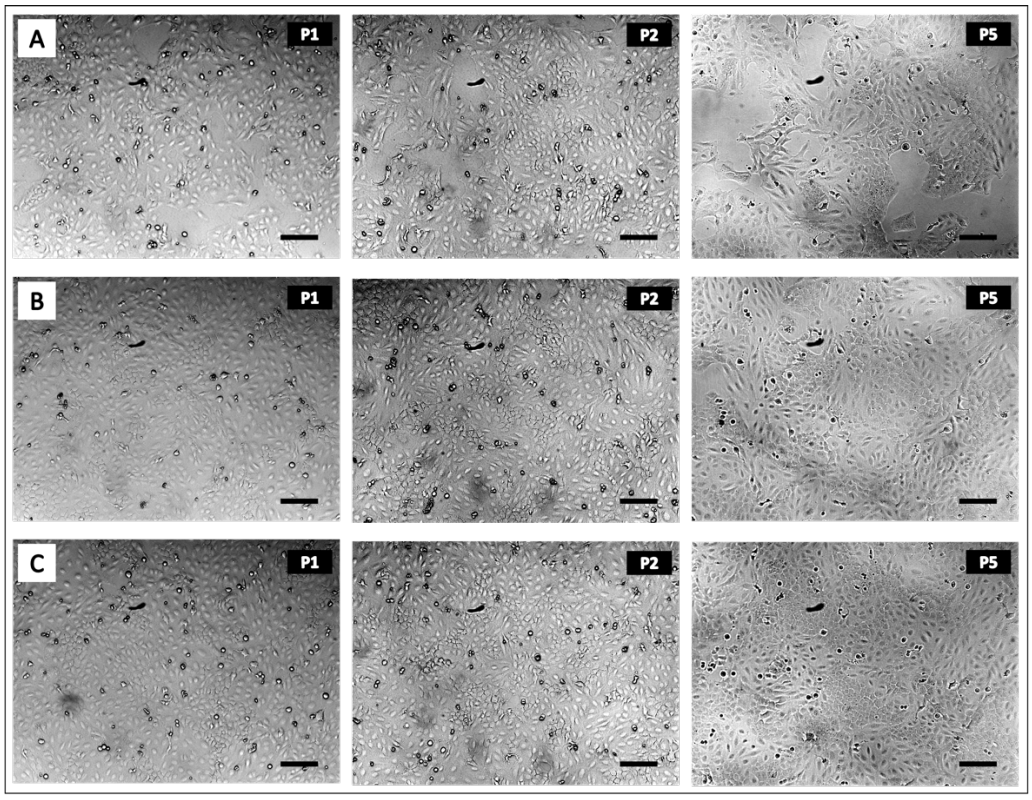

Figure 23. Morphological assessment of HCEC-12 cells across multiple passages. Representative brightfield microscopic images depict the cellular morphology of HCEC-12 cells at passages P1, P2, and P5 when cultured on different substrates: TCPS (A), COL4 coating (B), and PPC coating (C). All images were taken 5 days post-seeding for each respective passage. Scale bars represent 100µm for all images.

The observed morphological changes in the TCPS group, reveals the importance of the substrate in influencing cell behaviour. EMT is often associated with pathological conditions and can compromise the functionality of corneal endothelial cells. The pronounced EMT observed in the TCPS group suggests that the absence of a biomimetic substrate can adversely affect the maintenance of the endothelial phenotype over extended culture periods. On the other hand, the COL4 and PPC coatings appeared to provide a more conducive environment for the preservation of the hexagonal phenotype. This could be attributed to the presence of specific ECM components in these coatings that play a pivotal role in cell-matrix interactions, thereby

influencing cell behaviour. The PPC, in particular, contains a rich composition of ECM proteins, including collagen type VIII, which has been previously discussed for its potential role in supporting endothelial cell function.

7.3.4 Higher Tight Junction Protein Expression on PPC

The abnormal phenotypic drift of cultured HCEC-12 cells became increasingly observable over passages. Upon reaching approximately 80% confluency at their fifth passage, the cells were harvested to evaluate the expression of the membrane protein zonula occludens-1 (ZO-1), a marker for the formation of tight junctions between corneal endothelial cells. Disrupted cellular morphology and loss of tight junction ZO-1 expression are both commonly recognised signs of corneal EMT [260]. Western blot analysis was conducted on the extracted total proteins from these cells and the band intensities were quantified using ImageJ software (Figure 24A). When the expression of ZO-1 was normalised to the reference protein β-actin, the ratios were determined to be 0.3155±0.0209 for the TCPS group, 0.6784±0.0126 for the COL4 group, and 0.7762±0.0139 for the PPC group. Both the COL4 and PPC coatings significantly enhanced the ZO-1 expression in HCEC-12 cultures compared to the TCPS group. However, while the PPC cultures exhibited a higher ZO-1 expression than the COL4 cultures, the difference was not statistically significant.

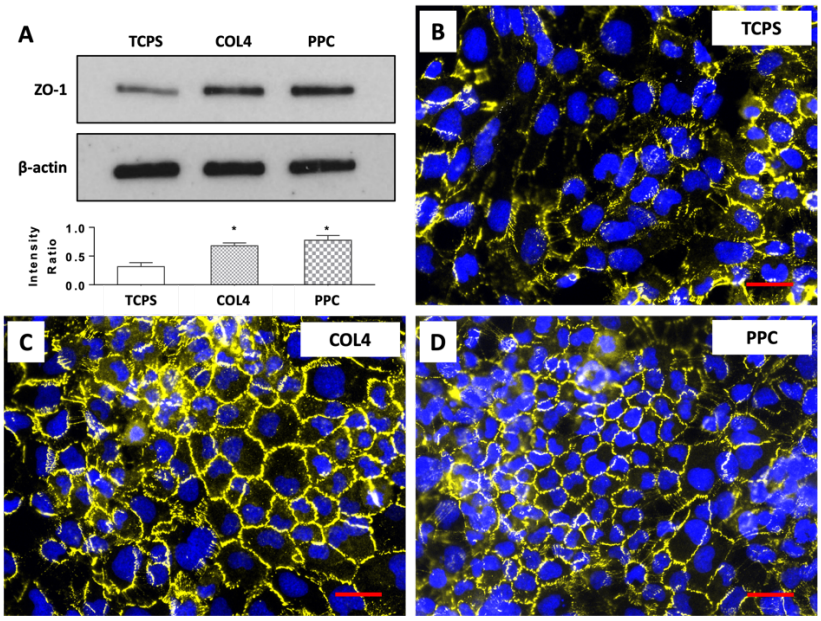

Figure 24. Evaluation of ZO-1 protein expression in HCEC-12 cells. (A) Western blot analysis showcasing ZO-1 expression in cells cultured for five passages on TCPS (left lane), COL4 coating (middle lane), and PPC coating (right lane). B-actin, stained as a reference protein, is used for normalisation. The column chart illustrates the ratios of ZO-1 to β-actin expression, with significance determined using a t-test in comparison to the TCPS group (* $p<0.05$). (b-d) Immunofluorescence images of HCEC-12 cells after 5 days of culture at the fifth passage on TCPS (B), COL4 coating (C), and PPC coating (D). The images highlight ZO-1 expression (yellow) on the cellular membrane and the cellular nuclei (blue). Scale bars represent 50µm.

Immunostaining of HCEC-12 cells followed by fluorescence microscopy (Figure 24B-D) further confirmed the presence of ZO-1 on the cellular membrane, with the formation of tight junctions being evident in both the COL4 and PPC coated cultures, unlike the TCPS cells. The expression of ZO-1 is a critical marker for the formation of tight junctions in corneal endothelial cells. Its consistent expression in cells cultured on COL4 and PPC coatings suggests the suppression of EMT, a process that can lead to the loss of the corneal endothelial phenotype. The TCPS group, on the other hand, exhibited a pronounced EMT, as evidenced by the heterogeneous morphologies and the presence of elongated, fibroblast-like cells. Previous research supports the notion that a bioengineered substrate mimicking the chemo-mechanical properties of Descemet's membrane can enhance the in vitro expansion of corneal endothelial cells while preserving their phenotype [17]. In the current study, PPC coating, which contains

collagen type VIII, demonstrated superior performance in maintaining the hexagonal morphology of HCEC-12 cells and promoting ZO-1 expression. The denser packing of cells in the PPC group, in line with the observation in the proliferation assessment earlier, further underscores the potential of PPC as a promising substrate for corneal endothelial tissue engineering.

7.3.5 HCEC-12 Migrate Faster on PPC

The scratch assay, a widely recognised method for evaluating cell migration and proliferation, was employed to determine the recolonisation ability of HCEC-12 cells on different substrates: TCPS, COL4 coating, and PPC coating. Following the creation of a gap in the cell monolayer using a pipette tip, the cultures were observed for cell migration into the cell-free area (Figure 25). While all cultures demonstrated migration towards the gap, a more rapid closure was evident in the COL4 and PPC coated cultures compared to the TCPS group. Initial measurements at t=0hr showed cell-free areas of $9.79\times10^4 \pm 1.90\times10^3$ μm^2, $9.67\times10^4 \pm 1.10\times10^3$ μm^2, and $9.71\times10^4 \pm 1.71\times10^3$ μm^2 for TCPS, COL4, and PPC cultures, respectively. After 36 hours, these areas reduced to $8.30\times10^4 \pm 2.45\times10^3$ μm^2, $7.00\times10^4 \pm 2.27\times10^3$ μm^2, and $6.82\times10^4 \pm 1.22\times10^3$ μm^2, respectively. This translates to a recolonisation of $15.28 \pm 0.95\%$ for TCPS, $27.78 \pm 1.50\%$ for COL4, and $29.59 \pm 1.59\%$ for PPC cultures.

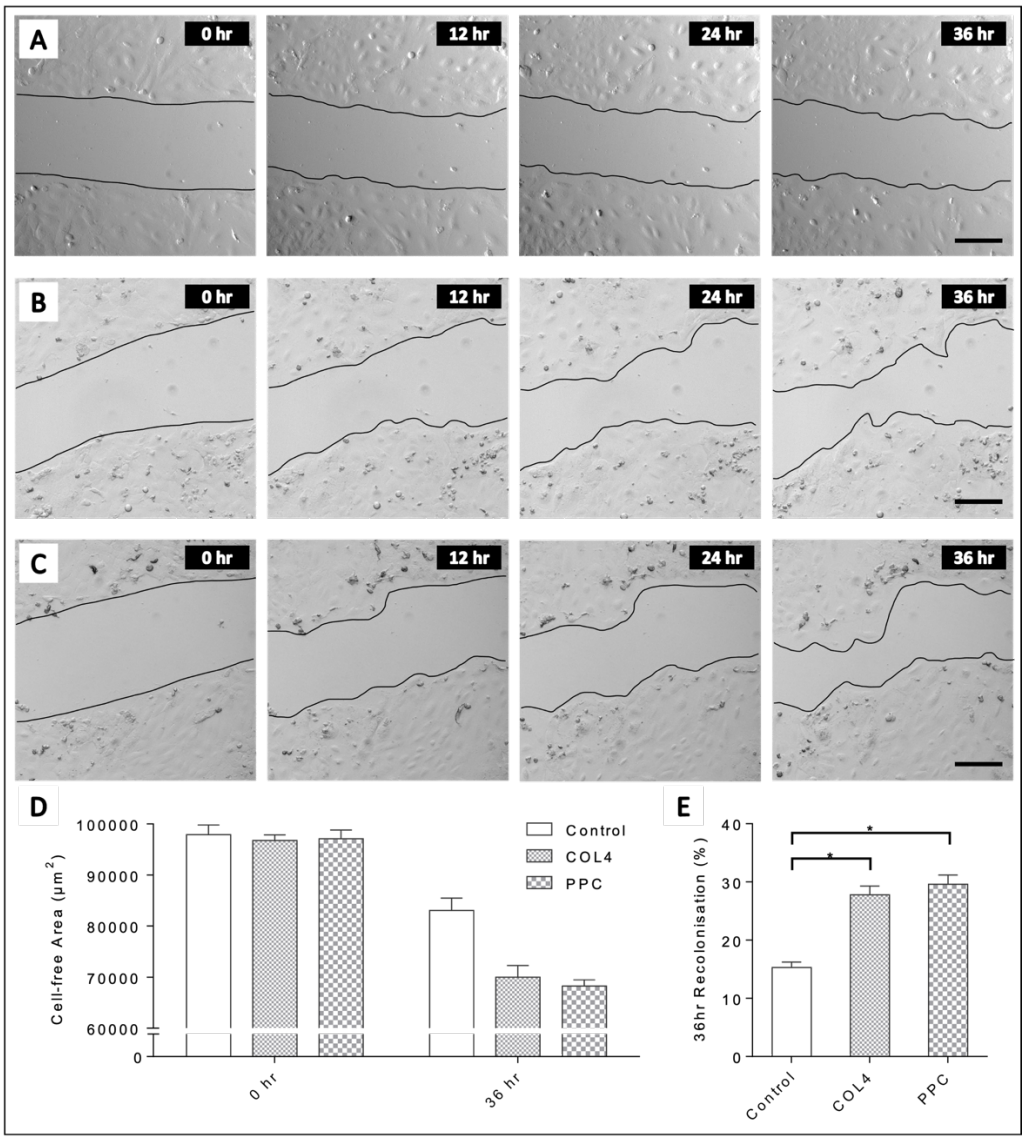

Figure 25. Evaluation of HCEC-12 cell proliferation and migration in an in vitro scratch assay. (A-C) Representative timelapse images depict the progression of HCEC-12 cells on (A) TCPS, (B) COL4 coating, and (C) PPC coating, at intervals of 0, 12, 24, and 36 hours post-scratching. The boundaries of the created gaps are highlighted for clarity. Scale bars represent 100µm. (D) A chart illustrating the quantified cell-free areas at the start (t=0hr) and end (t=36hr) of the observation period, determined using ImageJ software. (E) A subsequent chart displays the percentage of the gap area that was recolonised by cells at t=36hr. Statistical significance was ascertained using two-way ANOVA, with * indicating $p < 0.05$.

The statistically significant enhance in recolonisation observed in the COL4 and PPC coated cultures suggests that these coatings provide a more conducive environment for HCEC-12 cell migration and proliferation compared to standard TCPS. The PPC coating demonstrated a

slightly superior performance over the COL4 coating. This could be attributed to the presence of collagen type VIII, which might play a role in promoting cell migration and proliferation [249].

7.3.6 PPC Promotes Contact Inhibition of Locomotion

HCEC-12 cells were cultured for a duration of 64 hours on TCPS, COL4 coating, and PPC coating, and their behaviour was meticulously observed and captured in timelapse images (Figure 26). The primary objective was to discern the frequency of contact inhibition of locomotion (CIL) in these cells. CIL is a key characteristic of endothelial cells, allowing them to spread evenly over a surface. On TCPS, HCEC-12 cells often moved freely until they encountered another cell, after which many tended to cluster together. However, in the COL4 and PPC coatings, many cells displayed CIL and changed their path upon contact. In the designated observation regions, cells cultured on TCPS displayed a lack of CIL in 66.67 ± 25.62% of the observed locations. In statistically significant contrast, cells on COL4 coating and PPC coating showed a non-occurrence of CIL in 45.83 ± 17.59% and 40.28 ± 19.41% of the locations, respectively.

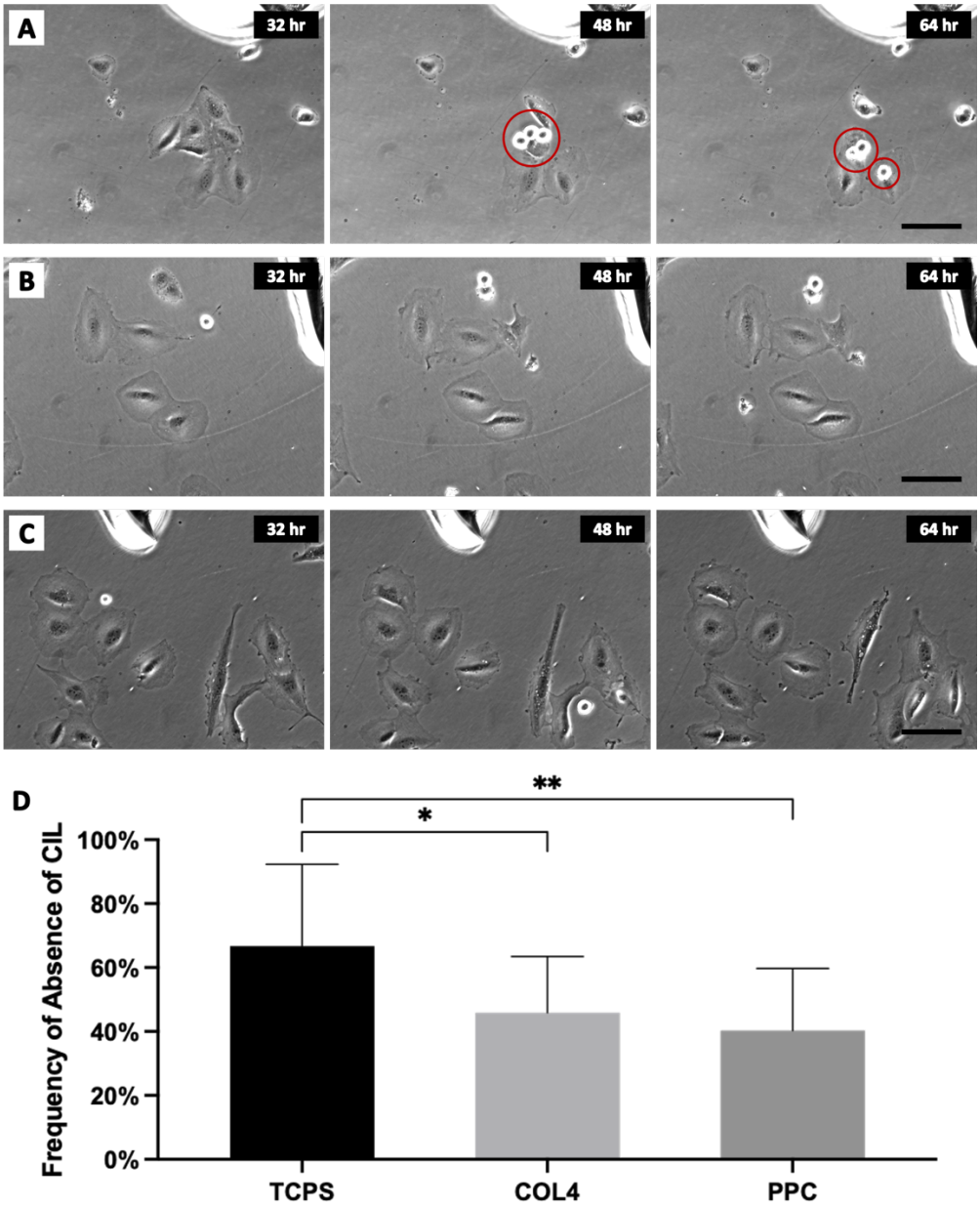

Figure 26. Evaluation of contact inhibition of locomotion in HCEC-12 cultures. (A-C) Representative timelapse images showcasing HCEC-12 cells on (A) TCPS, (B) COL4 coating, and (C) PPC coating, at intervals of 32, 48, and 64 hours after seeding. Cells observed clumping, and traversing over other cells are highlighted with red circles. Each scale bar corresponds to 20µm. (D) A column chart presenting the frequency at which the absence of contact inhibition of locomotion was observed in HCEC-12 cells across the different substrates. The data were derived from three separate experiments (N=3), with each experiment comprising 4 distinct wells for every condition. Each well contained 6 designated observation regions, culminating in a total of 24 observations (n=24). Statistical significance was ascertained using one-way ANOVA, with significance denoted by * $p<0.05$ and ** $p<0.01$.

CIL is a fundamental cellular behaviour that plays a crucial role in various physiological processes [261]. The absence or presence of CIL can significantly influence the behaviour of cells

in culture, especially in terms of their movement, interactions, and overall morphology. In the context of endothelial cells, CIL ensures that cells spread uniformly over a surface, leading to the formation of a tightly packed monolayer. This behaviour is essential for the proper functioning of endothelial cells, as they form the inner lining of blood vessels and play a vital role in controlling the passage of substances between the bloodstream and the surrounding tissues [262,263]. The observed lack of CIL in HCEC-12 cells cultured on TCPS suggests that these cells are more prone to clump together, which can disrupt the formation of a uniform monolayer. On the other hand, the presence of CIL in cells cultured on COL4 and PPC coatings indicates that these surfaces promote more natural endothelial cell behaviour.

7.3.7 Cells Expanded with PPC Used to Construct a Transplantable Model

HCEC-12 cells, after being expanded for five passages on TCPS, COL4 coating, and PPC coating, were harvested and subsequently seeded at a high density of 30,000/cm^2 onto RAFT™, a commercially available, plastically compressed type I collagen hydrogel. It offers a biomimetic environment that closely resembles the natural corneal stroma. By seeding HCEC-12 cells onto this hydrogel, the study aimed to create a construct that not only supports cell growth and function but also facilitates transplantation. Brightfield images captured on days 1 and 3 post-seeding and immunofluorescent images taken on day 3 provided insights into cell behaviour on the hydrogel (Figure 27). On the day after seeding, cells attached to the hydrogel flattened and initiated connections with adjacent cells. Notably, cells derived from COL4 and PPC coated cultures exhibited more uniform morphology, with distinct polygonal shapes. In contrast, cells from the TCPS group displayed a mix of hexagonal and elongated morphologies. By the third day of growth on RAFT™, the cell number in the TCPS group was visibly lower than in the COL4 and PPC groups. Both the COL4 and PPC groups showcased cells that had

grown to form distinct hexagonal shapes. Tight junctions, as indicated by ZO-1 staining, were evident across all groups. However, cells from the TCPS group were noticeably larger and irregular in shape. In contrast, both coated groups demonstrated efficient cell packing in a single layer, with hexagonal patterns. The PPC group, in particular, displayed cells with a smaller, more hexagonal morphology compared to the COL4 group.

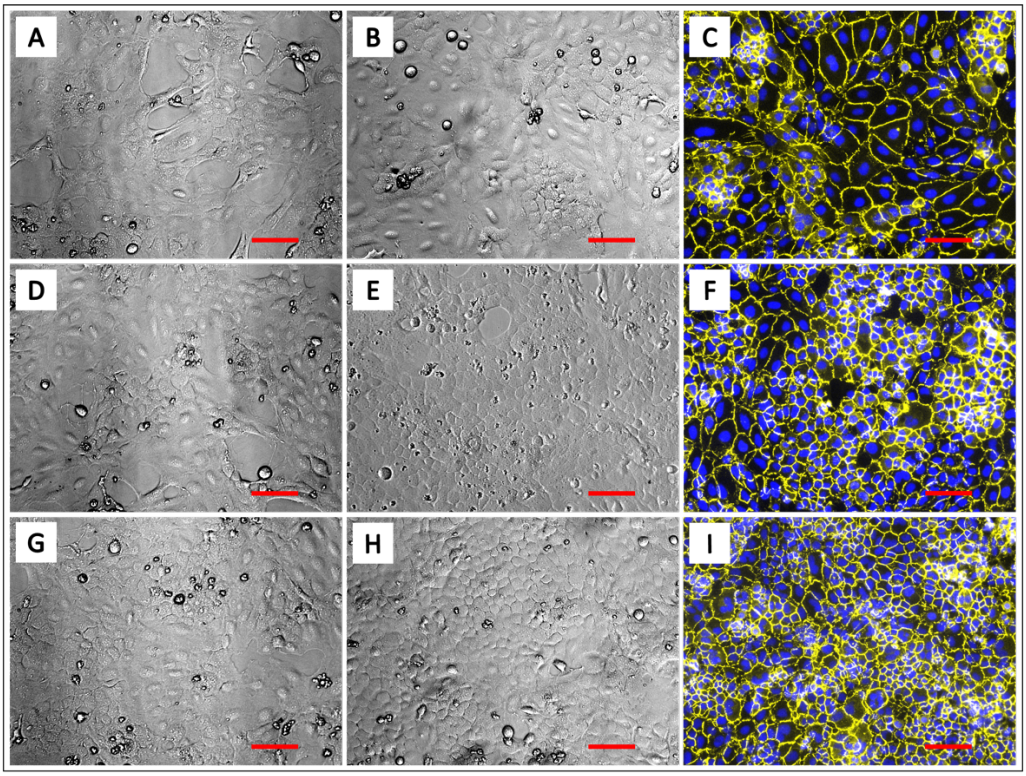

Figure 27. Morphology and protein expression assessment of HCEC-12 cells seeded on RAFT™. Representative images of HCEC-12 cells derived from cultures on (A-C) TCPS, (D-F) COL4 coating, and (G-I) PPC coating, and subsequently expanded on RAFT™. (A, D, G) Brightfield images captured one day and (B, E, H) three days post-seeding showcase the cellular morphology and proliferation. (C, F, I) Immunofluorescence images taken on the third day highlight the expression of the tight junction protein ZO-1 (yellow) and the cellular nuclei (blue). Scale bars represent 100µm.

The use of RAFT™, a type I collagen hydrogel, offers a promising avenue for corneal tissue engineering. Type I collagen is a major component of the corneal stroma and has been shown to support corneal endothelial cell growth [197]. The observed differences in cell morphology and proliferation between the groups can be attributed to the initial culture conditions. The

enhanced performance of cells from the COL4 and PPC coatings suggests that these coatings provide a more conducive environment for maintaining the inherent properties of HCEC-12 cells. The phenomenon of cells from the TCPS group displaying both hexagonal and elongated morphologies might be indicative of EMT, which can compromise the functionality of the seeded cells, making them unsuitable for transplantation. The consistent hexagonal morphology observed in the COL4 and PPC groups, especially the latter, underscores the importance of the initial culture conditions. The PPC coating, with its unique composition, seems to offer an environment that closely mimics the natural niche of human corneal endothelial cells, thereby preserving the phenotype of HCEC-12 during expansion.

While the positive findings associated with PPC is intriguing, it is crucial to note that PPC does not entirely represent the DM. The significant presence of corneal stroma in the PPC means the coating contains a substantial amount of collagen type I (COL1) and other stroma-predominant proteins [31]. In contrast, the DM primarily comprises COL4 and COL8 [31,264]. Both COL1 and COL4 have been utilised as coatings in corneal endothelial cell culture. While opinions vary regarding COL1's effect in corneal endothelial cell culture [172,265], COL4, an endothelial basement membrane-specific collagen, has been reported to preserve HCEC phenotype and boost proliferation [135,221,266]. A study contrasting the use of COL1, COL4, laminin, and fibronectin revealed that a combination of 50kPa silicone and COL4 coating inhibited EMT, whereas cells cultured with COL1 or other proteins lost their phenotype [17]. The role of COL8 coating in HCEC cultures remains relatively unexplored, though a study that knocked down the COL8A2 gene in corneal endothelial cells observed corneal opacity in vivo and disturbed cell culture in vitro [19]. One hypothesis for PPC's supportive role in HCEC-12 culture could be the unique presence of COL8 in the DM. However, the abundant COL1 dilutes

COL8's presence. Future experiments should aim to extract COL8 and investigate its impact on corneal endothelial cell culture.

7.4 Summary

In this chapter, a comprehensive exploration was undertaken of the potential of posterior porcine cornea (PPC), a substrate derived from the Descemet's Membrane (DM) and corneal stroma, as a supportive matrix for the in vitro culture of HCEC-12 cells. Experimental results revealed the advantage of PPC, particularly in promoting cell adherence, proliferation, and the maintenance of the corneal endothelial phenotype. The presence of collagen type VIII (COL8) in PPC, a characteristic protein of the DM, further underscored the biomimetic nature of this substrate.

The observed benefits of PPC over traditional tissue culture polystyrene (TCPS) and even the optimised COL4 coating highlight its potential as a superior substrate for corneal endothelial cell culture. The cells not only adhered faster but also displayed a more consistent hexagonal morphology and exhibited a higher level of hallmark protein expression. These categories are vital for the proper functioning of the corneal endothelium. The development of a transplantable model using RAFT™, a type I collagen hydrogel, in conjunction with HCEC-12 cells cultured on PPC, opens promising avenues for future corneal endothelial tissue engineering and transplantation.

While the results are encouraging, they also pave the way for further investigations, particularly into the specific role of COL8 and the intricate cell-cell and cell-matrix interactions that underpin the observed cellular behaviours. As this chapter concludes, it becomes evident that the journey of harnessing the potential of DM and its derived substrates for corneal

endothelial cell culture is only just beginning. The insights gained here lay a robust foundation for future endeavours aimed at revolutionising corneal transplantation and regenerative medicine.

Chapter 8

General Discussion and Concluding Remarks

The corneal endothelium plays a pivotal role in maintaining ocular clarity, and its limited regenerative capacity in humans necessitates innovative therapeutic strategies. This thesis embarked on a comprehensive journey to explore effective and sustainable methods for the in vitro culture and application of the immortalised human corneal endothelial cell line, HCEC-12. The overarching aim was to advance the field of corneal endothelial tissue engineering by investigating various substrates and their influence on HCEC-12 behaviour, morphology, and functionality. The research journey was divided into four main research chapters, each focusing on a distinct substrate and its implications.

The inaugural research chapter (Chapter 4) delved into the intricate relationship between collagen type IV (COL4) coatings and HCEC-12 cell behaviour. COL4, an essential protein abundantly found in endothelial basement membranes, including the Descemet's membrane, holds significance due to its ability to facilitate rapid attachment of HCEC-12 cells to culture surfaces. The study began with the establishment of an optimal coating procedure for COL4, which was found to be most efficient when using solutions of a smaller volume but at a higher concentration, incubated for 5 hours at 37°C.

The subsequent cellular experiments provided a deeper understanding of the biological implications of these coatings. As the COL4 coating concentration increased, there was a notable rise in the expression levels of the tight junction protein ZO-1 and adherens junction protein ATP1A1, while the mesenchymal-related marker α-SMA decreased. This indicated that higher COL4 concentrations fostered an environment conducive for HCEC-12 cells to express

elevated levels of intercellular junction proteins and reduced fibroblast markers. Immunofluorescence imaging further reinforced these findings, revealing that HCEC-12 cells on a 100µg/mL COL4 coating exhibited a tightly packed configuration with pronounced hexagonal patterns. The economic implications of these findings were also significant, suggesting that a 50µL of 100µg/mL collagen type IV solution incubated for 5 hours at 37°C for each well of a 96-well plate is both sufficient and optimal for HCEC-12 culturing. This coating not only sustains HCEC-12 proliferation and phenotype but also effectively curbs EMT, paving the way for more affordable alternative treatments for corneal endothelial diseases.

The next chapter embarked on a comprehensive exploration of the potential benefits of using dECMs for HCEC-12 culture. dECMs, derived from various cell sources, have shown promise in enhancing the proliferation and phenotype maintenance of HCEC-12 cells. The initial stages of the investigation successfully derived and characterised dECM from HCEC-12 cells cultured on TCPS (dECM-TCPS) and those cultured on surfaces coated with 100µg/mL COL4 (dECM-COL4). The presence of a gelatinous layer post-decellularisation confirmed the retention of the ECM.

In terms of proliferation, dECM substrates, especially dECM-COL4, emerged as superior platforms, outperforming the standard TCPS and COL4 coatings. This enhanced support for HCEC-12 proliferation suggests that dECMs, by closely mimicking the natural cellular microenvironment, offer a more conducive and physiologically relevant platform for cell growth. The resilience of cells cultured on dECM-COL4, especially in the context of endothelial-to-mesenchymal transition (EMT) induced by TGF-β1, was particularly noteworthy. These cells retained a significant proportion of their typical corneal endothelial phenotype, suggesting the inherent protective qualities of dECM against EMT. Preservation of characteristic protein profiles in HCEC-12 cells cultured on dECM-COL4 further emphasised

the potential of dECM-COL4 in maintaining cellular integrity, even under challenging conditions.

The composition analysis of the dECMs revealed that the amount of ECM proteins in dECM-COL4 was higher than in dECM-TCPS. Ponceau S staining confirmed this by showing diverse protein bands in dECM-COL4 and undetectable bands in dECM-TCPS. The potential presence of COL8 in dECM-COL4 and the favourable results observed may hint at a correlation. It is plausible to hypothesise that an optimal culture substrate for human corneal endothelial cells can be formulated by mimicking the healthy Descemet's membrane's composition, where COL8 plays a pivotal role.

The final two research chapters focused on a detailed investigation into the potential of posterior porcine cornea (PPC) as a substrate for the in vitro culture of HCEC-12 cells. The Descemet's Membrane (DM), an integral component of the cornea, plays a pivotal role in anchoring the corneal endothelium to the stroma and regulating the flow of water and macromolecules. Given the DM's significance in maintaining corneal health, this chapter aimed to explore whether PPC, a DM-derived substrate, could foster a healthy in vitro culture of these cells.

The initial steps of the research involved the extraction and decellularisation of PPC. Using a femtosecond laser, sections from the posterior side of the porcine corneas were extracted. The thickness of these sections indicated that a significant portion of the PPC tissue was stromal tissue from the porcine cornea. The acquired PPCs were then decellularised, ensuring the resultant tissues were devoid of any cellular components. The reconstituted solution of PPC was characterised to understand its composition, and the presence of collagen type VIII (COL8), a hallmark protein of the DM, was identified.

The experiments revealed that PPC offers significant advantages over traditional tissue culture polystyrene (TCPS) and even the optimised COL4 coating process. HCEC-12 cells cultured on PPC not only adhered faster but also displayed a more consistent hexagonal morphology and exhibited a higher level of hallmark protein expression. The proliferation studies further cemented PPC's potential, with HCEC-12 cells cultured on PPC showing a significant advantage in proliferation over those on TCPS and COL4 coating. The presence of COL8 in PPC might be a contributing factor, as it has been associated with enhanced endothelial cell proliferation and phenotypic maintenance in other studies. The development of a transplantable model using the RAFT™ system, combined with HCEC-12 cells cultured on PPC, showcased the potential of PPC in corneal endothelial tissue engineering. The cells harvested from PPC-coated cultures exhibited superior morphology and functionality when seeded on RAFT™, indicating its potential for future corneal transplants.

However, it is essential to note that PPC does not entirely represent the DM due to the significant presence of corneal stroma. While the positive findings associated with PPC are intriguing, future experiments should aim to extract COL8 and investigate its impact on corneal endothelial cell culture, given its potential significance in maintaining a healthy corneal endothelium.

In this comprehensive study of corneal endothelial tissue engineering, the thesis explored deep into the intricacies of culturing the immortalised human corneal endothelial cell line, HCEC-12, under various conditions and substrates. From the foundational work with collagen type IV (COL4) coatings to the innovative strides made with cell-derived extracellular matrix (dECM) and the promising potential of the novel posterior porcine cornea (PPC), the research underscored the paramount importance of a biomimetic approach. Each investigation, distinct yet interconnected, collectively illuminated the path towards optimising HCEC-12 culture,

emphasising the need for an environment that closely mirrors the in vivo conditions of the corneal endothelium. The development of a transplantable model, combined with the insights into the protective qualities of substrates against EMT, not only paves the way for addressing the global donor cornea shortage but also heralds a new era of affordable and effective treatments for corneal endothelial dysfunctions.

References

1 Geneva, W. H. O. *World Report on Vision*. (2019).

2 Gaum, L. *et al.* Tissue and corneal donation and transplantation in the UK. *Br J Anaesth* **108 Suppl 1**, i43-47 (2012). https://doi.org:10.1093/bja/aer398

3 Sridhar, M. S. Anatomy of cornea and ocular surface. *Indian J Ophthalmol* **66**, 190-194 (2018). https://doi.org:10.4103/ijo.IJO_646_17

4 Peh, G. S., Beuerman, R. W., Colman, A., Tan, D. T. & Mehta, J. S. Human corneal endothelial cell expansion for corneal endothelium transplantation: an overview. *Transplantation* **91**, 811-819 (2011). https://doi.org:10.1097/TP.0b013e3182111f01

5 Srinivas, S. P. Dynamic regulation of barrier integrity of the corneal endothelium. *Optom Vis Sci* **87**, E239-254 (2010). https://doi.org:10.1097/OPX.0b013e3181d39464

6 Feizi, S. Corneal endothelial cell dysfunction: etiologies and management. *Ther Adv Ophthalmol* **10**, 2515841418815802 (2018). https://doi.org:10.1177/2515841418815802

7 Price, M. O. & Price, F. W., Jr. Endothelial keratoplasty - a review. *Clin Exp Ophthalmol* **38**, 128-140 (2010). https://doi.org:10.1111/j.1442-9071.2010.02213.x

8 Grisanti, S. & Guidry, C. Transdifferentiation of retinal pigment epithelial cells from epithelial to mesenchymal phenotype. *Invest Ophthalmol Vis Sci* **36**, 391-405 (1995).

9 Miyoshi, J. & Takai, Y. Structural and functional associations of apical junctions with cytoskeleton. *Biochimica et biophysica acta* **1778**, 670-691 (2008). https://doi.org:10.1016/j.bbamem.2007.12.014

10 Wheelock, M. J., Shintani, Y., Maeda, M., Fukumoto, Y. & Johnson, K. R. Cadherin switching. *J Cell Sci* **121**, 727-735 (2008). https://doi.org:10.1242/jcs.000455

11 Zagorski, Z. & Naumann, G. O. Reactive production of extracellular matrix (ECM) by corneal endothelial cells. *Acta Ophthalmol (Copenh)* **70**, 366-370 (1992). https://doi.org:10.1111/j.1755-3768.1992.tb08581.x

12 Ali, M., Raghunathan, V., Li, J. Y., Murphy, C. J. & Thomasy, S. M. Biomechanical relationships between the corneal endothelium and Descemet's membrane. *Exp Eye Res* **152**, 57-70 (2016). https://doi.org:10.1016/j.exer.2016.09.004

13 Arita, T. *et al.* Density dependent growth of corneal endothelial cells cultured in vitro. *Cell Differ* **22**, 61-69 (1987).

14 Peh, G. S. *et al.* Optimization of human corneal endothelial cell culture: density dependency of successful cultures in vitro. *BMC Res Notes* **6**, 176 (2013). https://doi.org:10.1186/1756-0500-6-176

15 Roy, O., Leclerc, V. B., Bourget, J. M., Theriault, M. & Proulx, S. Understanding the process of corneal endothelial morphological change in vitro. *Invest Ophthalmol Vis Sci* **56**, 1228-1237 (2015). https://doi.org:10.1167/iovs.14-16166

16 Choi, J. S. *et al.* In vitro evaluation of the interactions between human corneal endothelial cells and extracellular matrix proteins. *Biomed Mater* **8**, 014108 (2013). https://doi.org:10.1088/1748-6041/8/1/014108

17 Palchesko, R. N., Lathrop, K. L., Funderburgh, J. L. & Feinberg, A. W. In vitro expansion of corneal endothelial cells on biomimetic substrates. *Sci Rep* **5**, 7955 (2015). https://doi.org:10.1038/srep07955

18 Biswas, S. *et al.* Missense mutations in COL8A2, the gene encoding the alpha2 chain of type VIII collagen, cause two forms of corneal endothelial dystrophy. *Hum Mol Genet* **10**, 2415-2423 (2001). https://doi.org:10.1093/hmg/10.21.2415

19 Hwang, J. S., Ma, D. J., Choi, J. & Shin, Y. J. COL8A2 Regulates the Fate of Corneal Endothelial Cells. *Invest Ophthalmol Vis Sci* **61**, 26 (2020). https://doi.org:10.1167/iovs.61.11.26

20 Bednarz, J., Teifel, M., Friedl, P. & Engelmann, K. Immortalization of human corneal endothelial cells using electroporation protocol optimized for human corneal endothelial and human retinal pigment epithelial cells. *Acta Ophthalmol Scan* **78**, 130-136 (2000). https://doi.org:DOI 10.1034/j.1600-0420.2000.078002130.x

21 Parekh, M. *et al.* Human corneal endothelial cells from older donors can be cultured and passaged on cell-derived extracellular matrix. *Acta Ophthalmol* **99**, e512-e522 (2021). https://doi.org:10.1111/aos.14614

22 Cassin, B. & Rubin, M. L. *Dictionary of eye terminology*. 4th edn, (Triad Pub. Co., 2001).

23 Goldstein, E. B. *Sensation and perception*. 5th edn, (Brooks/Cole Pub., 1999).

24 Vaiciuliene, R., Rylskyte, N., Baguzyte, G. & Jasinskas, V. Risk factors for fluctuations in corneal endothelial cell density (Review). *Exp Ther Med* **23**, 129 (2022). https://doi.org:10.3892/etm.2021.11052

25 Whitcher, J. P., Srinivasan, M. & Upadhyay, M. P. Corneal blindness: a global perspective. *Bull World Health Organ* **79**, 214-221 (2001).

26 Mimura, T., Yamagami, S. & Amano, S. Corneal endothelial regeneration and tissue engineering. *Prog Retin Eye Res* **35**, 1-17 (2013). https://doi.org:10.1016/j.preteyeres.2013.01.003

27 Mobaraki, M. *et al.* Corneal Repair and Regeneration: Current Concepts and Future Directions. *Front Bioeng Biotechnol* **7**, 135 (2019). https://doi.org:10.3389/fbioe.2019.00135

28 Oie, Y. & Nishida, K. Regenerative medicine for the cornea. *Biomed Res Int* **2013**, 428247 (2013). https://doi.org:10.1155/2013/428247

29 Riley, M. V. The role of the epithelium in control of corneal hydration. *Exp Eye Res* **12**, 128-137 (1971). https://doi.org:10.1016/0014-4835(71)90137-0

30 Swamynathan, S., Kenchegowda, D., Piatigorsky, J. & Swamynathan, S. Regulation of corneal epithelial barrier function by Kruppel-like transcription factor 4. *Invest Ophthalmol Vis Sci* **52**, 1762-1769 (2011). https://doi.org:10.1167/iovs.10-6134

31 Espana, E. M. & Birk, D. E. Composition, structure and function of the corneal stroma. *Exp Eye Res* **198**, 108137 (2020). https://doi.org:10.1016/j.exer.2020.108137

32 Zavala, J., Lopez Jaime, G. R., Rodriguez Barrientos, C. A. & Valdez-Garcia, J. Corneal endothelium: developmental strategies for regeneration. *Eye (Lond)* **27**, 579-588 (2013). https://doi.org:10.1038/eye.2013.15

33 Weston, J. A. The migration and differentiation of neural crest cells. *Adv Morphog* **8**, 41-114 (1970). https://doi.org:10.1016/b978-0-12-028608-9.50006-5

34 Tuft, S. J. & Coster, D. J. The corneal endothelium. *Eye (Lond)* **4 (Pt 3)**, 389-424 (1990). https://doi.org:10.1038/eye.1990.53

35 Murphy, C., Alvarado, J., Juster, R. & Maglio, M. Prenatal and postnatal cellularity of the human corneal endothelium. A quantitative histologic study. *Invest Ophthalmol Vis Sci* **25**, 312-322 (1984).

36 Yee, R. W., Matsuda, M., Schultz, R. O. & Edelhauser, H. F. Changes in the normal corneal endothelial cellular pattern as a function of age. *Curr Eye Res* **4**, 671-678 (1985). https://doi.org:10.3109/02713688509017661

37 Whiteley, H. E. & Peiffer, R. L. in *Handbook of Toxicologic Pathology (Second Edition)* (eds Wanda M. Haschek, Colin G. Rousseaux, & Matthew A. Wallig) 539-584 (Academic Press, 2002).

38 Waring, G. O., 3rd, Bourne, W. M., Edelhauser, H. F. & Kenyon, K. R. The corneal endothelium. Normal and pathologic structure and function. *Ophthalmology* **89**, 531-590 (1982).

39 Faye, P. A. *et al.* Focus on cell therapy to treat corneal endothelial diseases. *Exp Eye Res* **204**, 108462 (2021). https://doi.org:10.1016/j.exer.2021.108462

40 Griffiths, S. N., Drasdo, N., Barnes, D. A. & Sabell, A. G. Effect of epithelial and stromal edema on the light scattering properties of the cornea. *Am J Optom Physiol Opt* **63**, 888-894 (1986). https://doi.org:10.1097/00006324-198611000-00005

41 Bonanno, J. A. Molecular mechanisms underlying the corneal endothelial pump. *Exp Eye Res* **95**, 2-7 (2012). https://doi.org:10.1016/j.exer.2011.06.004

42 Dawson, D. G. & Edelhauser, H. F. in *Ocular Disease* (eds Leonard A. Levin & Daniel M. Albert) 64-73 (W.B. Saunders, 2010).

43 Aiello, F., Gallo Afflitto, G., Ceccarelli, F., Cesareo, M. & Nucci, C. Global Prevalence of Fuchs Endothelial Corneal Dystrophy (FECD) in Adult Population: A Systematic Review and Meta-Analysis. *J Ophthalmol* **2022**, 3091695 (2022). https://doi.org:10.1155/2022/3091695

44 Elhalis, H., Azizi, B. & Jurkunas, U. V. Fuchs endothelial corneal dystrophy. *Ocul Surf* **8**, 173-184 (2010). https://doi.org:10.1016/s1542-0124(12)70232-x

45 Asbell, P. & Brocks, D. in *Encyclopedia of the Eye* (ed Darlene A. Dartt) 522-531 (Academic Press, 2010).

46 Singh, G., Bohnke, M. & Draeger, J. Endothelial wound healing in organ-cultured pig corneae after mechanical trauma. *Fortschr Ophthalmol* **81**, 293-295 (1984).

47 Van Horn, D. L. & Hyndiuk, R. A. Endothelial wound repair in primate cornea. *Exp Eye Res* **21**, 113-124 (1975). https://doi.org:10.1016/0014-4835(75)90076-7

48 Van Horn, D. L., Sendele, D. D., Seideman, S. & Buco, P. J. Regenerative capacity of the corneal endothelium in rabbit and cat. *Invest Ophthalmol Vis Sci* **16**, 597-613 (1977).

49 Fitch, K. L., Nadakavukaren, M. J. & Richardson, A. Age-related changes in the corneal endothelium of the rat. *Exp Gerontol* **17**, 179-183 (1982). https://doi.org:10.1016/0531-5565(82)90023-7

50 Geroski, D. H., Matsuda, M., Yee, R. W. & Edelhauser, H. F. Pump function of the human corneal endothelium. Effects of age and cornea guttata. *Ophthalmology* **92**, 759-763 (1985). https://doi.org:10.1016/s0161-6420(85)33973-8

51 Joyce, N. Proliferative capacity of the corneal endothelium. *Progress in Retinal and Eye Research* **22**, 359-389 (2003). https://doi.org:10.1016/s1350-9462(02)00065-4

52 Babushkina, A. & Lwigale, P. Periocular neural crest cell differentiation into corneal endothelium is influenced by signals in the nascent corneal environment. *Dev Biol* **465**, 119-129 (2020). https://doi.org:10.1016/j.ydbio.2020.06.012

53 Joyce, N. C., Harris, D. L. & Mello, D. M. Mechanisms of mitotic inhibition in corneal endothelium: contact inhibition and TGF-beta2. *Invest Ophthalmol Vis Sci* **43**, 2152-2159 (2002).

54 Yoshida, K. *et al.* Involvement of p27KIP1 in the proliferation of the developing corneal endothelium. *Invest Ophthalmol Vis Sci* **45**, 2163-2167 (2004). https://doi.org:10.1167/iovs.03-1238

55 Toslak, D., Thapa, D., Erol, M. K., Chen, Y. & Yao, X. Smartphone-based imaging of the corneal endothelium at sub-cellular resolution. *J Mod Opt* **64**, 1229-1232 (2017). https://doi.org:10.1080/09500340.2016.1267815

56 Araki-Sasaki, K., Danjo, S., Kawaguchi, S., Hosohata, J. & Tano, Y. Human hepatocyte growth factor (HGF) in the aqueous humor. *Jpn J Ophthalmol* **41**, 409-413 (1997). https://doi.org:10.1016/s0021-5155(97)00081-6

57 Schultz-Cherry, S., Lawler, J. & Murphy-Ullrich, J. E. The type 1 repeats of thrombospondin 1 activate latent transforming growth factor-beta. *The Journal of biological chemistry* **269**, 26783-26788 (1994).

58 Joyce, N. C. & Zieske, J. D. Transforming growth factor-beta receptor expression in human cornea. *Invest Ophthalmol Vis Sci* **38**, 1922-1928 (1997).

59 Chen, K. H., Hsu, W. M., Chiang, C. C. & Li, Y. S. Transforming growth factor-beta2 inhibition of corneal endothelial proliferation mediated by prostaglandin. *Curr Eye Res* **26**, 363-370 (2003). https://doi.org:10.1076/ceyr.26.5.363.15442

60 Kim, T. Y., Kim, W. I., Smith, R. E. & Kay, E. D. Role of p27(Kip1) in cAMP- and TGF-beta2-mediated antiproliferation in rabbit corneal endothelial cells. *Invest Ophthalmol Vis Sci* **42**, 3142-3149 (2001).

61 Guell, J. L., El Husseiny, M. A., Manero, F., Gris, O. & Elies, D. Historical Review and Update of Surgical Treatment for Corneal Endothelial Diseases. *Ophthalmol Ther* **3**, 1-15 (2014). https://doi.org:10.1007/s40123-014-0022-y

62 Nanavaty, M. A., Wang, X. & Shortt, A. J. Endothelial keratoplasty versus penetrating keratoplasty for Fuchs endothelial dystrophy. *Cochrane Database Syst Rev* **2**, CD008420 (2014). https://doi.org:10.1002/14651858.CD008420.pub3

63 Fernandez, M. M. & Afshari, N. A. Endothelial Keratoplasty: From DLEK to DMEK. *Middle East Afr J Ophthalmol* **17**, 5-8 (2010). https://doi.org:10.4103/0974-9233.61210

64 Melles, G. R., Wijdh, R. H. & Nieuwendaal, C. P. A technique to excise the descemet membrane from a recipient cornea (descemetorhexis). *Cornea* **23**, 286-288 (2004).

65 Price, F. W., Jr. & Price, M. O. Descemet's stripping with endothelial keratoplasty in 50 eyes: a refractive neutral corneal transplant. *J Refract Surg* **21**, 339-345 (2005).

66 Gorovoy, M. S. Descemet-stripping automated endothelial keratoplasty. *Cornea* **25**, 886-889 (2006). https://doi.org:10.1097/01.ico.0000214224.90743.01

67 Melles, G. R., Ong, T. S., Ververs, B. & van der Wees, J. Descemet membrane endothelial keratoplasty (DMEK). *Cornea* **25**, 987-990 (2006). https://doi.org:10.1097/01.ico.0000248385.16896.34

68 Price, M. O., Giebel, A. W., Fairchild, K. M. & Price, F. W., Jr. Descemet's membrane endothelial keratoplasty: prospective multicenter study of visual and refractive outcomes and endothelial survival. *Ophthalmology* **116**, 2361-2368 (2009). https://doi.org:10.1016/j.ophtha.2009.07.010

69 Flockerzi, E. *et al.* Trends in Corneal Transplantation from 2001 to 2016 in Germany: A Report of the DOG-Section Cornea and its Keratoplasty Registry. *Am J Ophthalmol* **188**, 91-98 (2018). https://doi.org:10.1016/j.ajo.2018.01.018

70 Gain, P. *et al.* Global Survey of Corneal Transplantation and Eye Banking. *JAMA Ophthalmol* **134**, 167-173 (2016). https://doi.org:10.1001/jamaophthalmol.2015.4776

71 Wong, E. N. & Mehta, J. S. Cell therapy in corneal endothelial disease. *Curr Opin Ophthalmol* **33**, 275-281 (2022). https://doi.org:10.1097/ICU.0000000000000853

72 Okumura, N., Kinoshita, S. & Koizumi, N. Cell-based approach for treatment of corneal endothelial dysfunction. *Cornea* **33 Suppl 11**, S37-41 (2014). https://doi.org:10.1097/ICO.0000000000000229

73 Mimura, T. *et al.* Necessary prone position time for human corneal endothelial precursor transplantation in a rabbit endothelial deficiency model. *Curr Eye Res* **32**, 617-623 (2007). https://doi.org:10.1080/02713680701530589

74 Moysidis, S. N. *et al.* Magnetic field-guided cell delivery with nanoparticle-loaded human corneal endothelial cells. *Nanomedicine* **11**, 499-509 (2015). https://doi.org:10.1016/j.nano.2014.12.002

75 Mimura, T. *et al.* Long-term outcome of iron-endocytosing cultured corneal endothelial cell transplantation with magnetic attraction. *Exp Eye Res* **80**, 149-157 (2005). https://doi.org:10.1016/j.exer.2004.08.021

76 Xia, X. *et al.* Magnetic Human Corneal Endothelial Cell Transplant: Delivery, Retention, and Short-Term Efficacy. *Invest Ophthalmol Vis Sci* **60**, 2438-2448 (2019). https://doi.org:10.1167/iovs.18-26001

77 Okumura, N. *et al.* Rho kinase inhibitor enables cell-based therapy for corneal endothelial dysfunction. *Sci Rep* **6**, 26113 (2016). https://doi.org:10.1038/srep26113

78 Okumura, N. *et al.* Enhancement on primate corneal endothelial cell survival in vitro by a ROCK inhibitor. *Invest Ophthalmol Vis Sci* **50**, 3680-3687 (2009). https://doi.org:10.1167/iovs.08-2634

79 Kinoshita, S. *et al.* Injection of Cultured Cells with a ROCK Inhibitor for Bullous Keratopathy. *N Engl J Med* **378**, 995-1003 (2018). https://doi.org:10.1056/NEJMoa1712770

80 Numa, K. *et al.* Five-Year Follow-up of First 11 Patients Undergoing Injection of Cultured Corneal Endothelial Cells for Corneal Endothelial Failure. *Ophthalmology* **128**, 504-514 (2021). https://doi.org:10.1016/j.ophtha.2020.09.002

81 Liu, Y. *et al.* Human Corneal Endothelial Cells Expanded In Vitro Are a Powerful Resource for Tissue Engineering. *Int J Med Sci* **14**, 128-135 (2017). https://doi.org:10.7150/ijms.17624

82 Okumura, N. *et al.* Inhibition of TGF-beta signaling enables human corneal endothelial cell expansion in vitro for use in regenerative medicine. *PloS one* **8**, e58000 (2013). https://doi.org:10.1371/journal.pone.0058000

83 Hsueh, Y. J. *et al.* Ascorbic acid ameliorates corneal endothelial dysfunction and enhances cell proliferation via the noncanonical GLUT1-ERK axis. *Biomed Pharmacother* **144**, 112306 (2021). https://doi.org:10.1016/j.biopha.2021.112306

84 Gordon, S. R., Reaume, D. R. & Perkins, T. R. Insulin and IGF-2 support rat corneal endothelial cell growth and wound repair in the organ cultured tissue. *Growth Factors* **38**, 269-281 (2020). https://doi.org:10.1080/08977194.2021.1963721

85 Li, X., Li, Z., Qiu, L., Zhao, C. & Hu, Z. Nerve growth factor modulate proliferation of cultured rabbit corneal endothelial cells and epithelial cells. *J Huazhong Univ Sci Technolog Med Sci* **25**, 575-577 (2005). https://doi.org:10.1007/BF02896022

86 Couch, J. M., Cullen, P., Casey, T. A. & Fabre, J. W. Mitotic activity of corneal endothelial cells in organ culture with recombinant human epidermal growth factor. *Ophthalmology* **94**, 1-6 (1987). https://doi.org:10.1016/s0161-6420(87)33512-2

87 Weant, J. *et al.* Regenerative responses of rabbit corneal endothelial cells to stimulation by fibroblast growth factor 1 (FGF1) derivatives, TTHX1001 and TTHX1114. *Growth Factors* **39**, 14-27 (2021). https://doi.org:10.1080/08977194.2021.2012468

88 Peh, G. S. *et al.* The effects of Rho-associated kinase inhibitor Y-27632 on primary human corneal endothelial cells propagated using a dual media approach. *Sci Rep* **5**, 9167 (2015). https://doi.org:10.1038/srep09167

89 Li, Z. *et al.* Nicotinamide inhibits corneal endothelial mesenchymal transition and accelerates wound healing. *Exp Eye Res* **184**, 227-233 (2019). https://doi.org:10.1016/j.exer.2019.04.012

90 Valtink, M., Gruschwitz, R., Funk, R. H. & Engelmann, K. Two clonal cell lines of immortalized human corneal endothelial cells show either differentiated or precursor cell characteristics. *Cells Tissues Organs* **187**, 286-294 (2008). https://doi.org:10.1159/000113406

91 Konomi, K., Zhu, C., Harris, D. & Joyce, N. C. Comparison of the proliferative capacity of human corneal endothelial cells from the central and peripheral areas. *Invest Ophthalmol Vis Sci* **46**, 4086-4091 (2005). https://doi.org:10.1167/iovs.05-0245

92 Senoo, T. & Joyce, N. C. Cell cycle kinetics in corneal endothelium from old and young donors. *Invest Ophthalmol Vis Sci* **41**, 660-667 (2000).

93 Joyce, N. C., Zhu, C. C. & Harris, D. L. Relationship among oxidative stress, DNA damage, and proliferative capacity in human corneal endothelium. *Invest Ophthalmol Vis Sci* **50**, 2116-2122 (2009). https://doi.org:10.1167/iovs.08-3007

94 Joyce, N. C. & Zhu, C. C. Human Corneal Endothelial Cell Proliferation: Potential for Use in Regenerative Medicine. *Cornea* **23**, S8-S19 (2004). https://doi.org:10.1097/01.ico.0000136666.63870.18

95 Chen, P. *et al.* Treatment with retinoic acid and lens epithelial cell-conditioned medium in vitro directed the differentiation of pluripotent stem cells towards corneal endothelial cell-like cells. *Exp Ther Med* **9**, 351-360 (2015). https://doi.org:10.3892/etm.2014.2103

96 Theerakittayakorn, K. *et al.* Differentiation Induction of Human Stem Cells for Corneal Epithelial Regeneration. *Int J Mol Sci* **21** (2020). https://doi.org:10.3390/ijms21217834

97 Liang, G. & Zhang, Y. Embryonic stem cell and induced pluripotent stem cell: an epigenetic perspective. *Cell Res* **23**, 49-69 (2013). https://doi.org:10.1038/cr.2012.175

98 Wagoner, M. D. *et al.* Feeder-free differentiation of cells exhibiting characteristics of corneal endothelium from human induced pluripotent stem cells. *Biol Open* **7** (2018). https://doi.org:10.1242/bio.032102

99 Zhao, J. J. & Afshari, N. A. Generation of Human Corneal Endothelial Cells via In Vitro Ocular Lineage Restriction of Pluripotent Stem Cells. *Invest Ophthalmol Vis Sci* **57**, 6878-6884 (2016). https://doi.org:10.1167/iovs.16-20024

100 Bosch, B. M. *et al.* Discovering the Potential of Dental Pulp Stem Cells for Corneal Endothelial Cell Production: A Proof of Concept. *Front Bioeng Biotechnol* **9**, 617724 (2021). https://doi.org:10.3389/fbioe.2021.617724

101 Hatou, S. *et al.* Transplantation of iPSC-derived corneal endothelial substitutes in a monkey corneal edema model. *Stem Cell Res* **55**, 102497 (2021). https://doi.org:10.1016/j.scr.2021.102497

102 Li, Z. *et al.* Rapid Differentiation of Multi-Zone Ocular Cells from Human Induced Pluripotent Stem Cells and Generation of Corneal Epithelial and Endothelial Cells. *Stem cells and development* **28**, 454-463 (2019). https://doi.org:10.1089/scd.2018.0176

103 Okumura, N. *et al.* Cell surface markers of functional phenotypic corneal endothelial cells. *Invest Ophthalmol Vis Sci* **55**, 7610-7618 (2014). https://doi.org:10.1167/iovs.14-14980

104 Medvedev, S. P., Shevchenko, A. I. & Zakian, S. M. Induced Pluripotent Stem Cells: Problems and Advantages when Applying them in Regenerative Medicine. *Acta Naturae* **2**, 18-28 (2010).

105 Stone, R. A., Kuwayama, Y., Laties, A. M. & Marangos, P. J. Neuron-specific enolase-containing cells in the rhesus monkey trabecular meshwork. *Invest Ophthalmol Vis Sci* **25**, 1332-1334 (1984).

106 Raviola, G. Schwalbe line's cells: a new cell type in the trabecular meshwork of Macaca mulatta. *Invest Ophthalmol Vis Sci* **22**, 45-56 (1982).

107 Yam, G. H. *et al.* Characterization of Human Transition Zone Reveals a Putative Progenitor-Enriched Niche of Corneal Endothelium. *Cells* **8** (2019). https://doi.org:10.3390/cells8101244

108 McGowan, S. L., Edelhauser, H. F., Pfister, R. R. & Whikehart, D. R. Stem cell markers in the human posterior limbus and corneal endothelium of unwounded and wounded corneas. *Mol Vis* **13**, 1984-2000 (2007).

109 Hara, S. *et al.* Identification and potential application of human corneal endothelial progenitor cells. *Stem cells and development* **23**, 2190-2201 (2014). https://doi.org:10.1089/scd.2013.0387

110 Mimura, T. *et al.* Sphere therapy for corneal endothelium deficiency in a rabbit model. *Invest Ophthalmol Vis Sci* **46**, 3128-3135 (2005). https://doi.org:10.1167/iovs.05-0251

111 Shen, L. *et al.* Therapy of corneal endothelial dysfunction with corneal endothelial cell-like cells derived from skin-derived precursors. *Sci Rep* **7**, 13400 (2017). https://doi.org:10.1038/s41598-017-13787-1

112 Yamashita, K. *et al.* Corneal Endothelial Regeneration Using Mesenchymal Stem Cells Derived from Human Umbilical Cord. *Stem cells and development* **27**, 1097-1108 (2018). https://doi.org:10.1089/scd.2017.0297

113 Ju, C., Zhang, K. & Wu, X. Derivation of corneal endothelial cell-like cells from rat neural crest cells in vitro. *PloS one* **7**, e42378 (2012). https://doi.org:10.1371/journal.pone.0042378

114 Ren, G. *et al.* Mesenchymal stem cell-mediated immunosuppression occurs via concerted action of chemokines and nitric oxide. *Cell stem cell* **2**, 141-150 (2008). https://doi.org:10.1016/j.stem.2007.11.014

115 Acquart, S. *et al.* Endothelial morphometry by image analysis of corneas organ cultured at 31 degrees C. *Invest Ophthalmol Vis Sci* **51**, 1356-1364 (2010). https://doi.org:10.1167/iovs.08-3103

116 Chng, Z. *et al.* High throughput gene expression analysis identifies reliable expression markers of human corneal endothelial cells. *PloS one* **8**, e67546 (2013). https://doi.org:10.1371/journal.pone.0067546

117 Frausto, R. F. *et al.* Phenotypic and functional characterization of corneal endothelial cells during in vitro expansion. *Sci Rep* **10**, 7402 (2020). https://doi.org:10.1038/s41598-020-64311-x

118 Wu, Q., Ouyang, C., Xie, L., Ling, Y. & Huang, T. The ROCK inhibitor, thiazovivin, inhibits human corneal endothelial-to-mesenchymal transition/epithelial-to-mesenchymal transition and increases ionic transporter expression. *Int J Mol Med* **40**, 1009-1018 (2017). https://doi.org:10.3892/ijmm.2017.3103

119 Toda, M. *et al.* Production of Homogeneous Cultured Human Corneal Endothelial Cells Indispensable for Innovative Cell Therapy. *Invest Ophthalmol Vis Sci* **58**, 2011-2020 (2017). https://doi.org:10.1167/iovs.16-20703

120 Van den Bogerd, B. *et al.* Corneal Endothelial Cells Over the Past Decade: Are We Missing the Mark(er)? *Transl Vis Sci Technol* **8**, 13 (2019). https://doi.org:10.1167/tvst.8.6.13

121 Hatou, S. *et al.* Functional corneal endothelium derived from corneal stroma stem cells of neural crest origin by retinoic acid and Wnt/beta-catenin signaling. *Stem cells and development* **22**, 828-839 (2013). https://doi.org:10.1089/scd.2012.0286

122 Smeringaiova, I., Utheim, T. P. & Jirsova, K. Ex vivo expansion and characterization of human corneal endothelium for transplantation: a review. *Stem cell research & therapy* **12**, 554 (2021). https://doi.org:10.1186/s13287-021-02611-3

123 Catala, P. *et al.* Approaches for corneal endothelium regenerative medicine. *Prog Retin Eye Res* **87**, 100987 (2022). https://doi.org:10.1016/j.preteyeres.2021.100987

124 Parekh, M. *et al.* Biomaterials for corneal endothelial cell culture and tissue engineering. *Journal of tissue engineering* **12**, 2041731421990536 (2021). https://doi.org:10.1177/2041731421990536

125 Patel, S., Marshall, J. & Fitzke, F. W., 3rd. Refractive index of the human corneal epithelium and stroma. *J Refract Surg* **11**, 100-105 (1995). https://doi.org:10.3928/1081-597X-19950301-09

126 Amano, S. Transplantation of cultured human corneal endothelial cells. *Cornea* **22**, S66-74 (2003).

127 Lange, T. M., Wood, T. O. & McLaughlin, B. J. Corneal endothelial cell transplantation using Descemet's membrane as a carrier. *J Cataract Refract Surg* **19**, 232-235 (1993). https://doi.org:10.1016/s0886-3350(13)80947-9

128 Ishino, Y. *et al.* Amniotic membrane as a carrier for cultivated human corneal endothelial cell transplantation. *Invest Ophthalmol Vis Sci* **45**, 800-806 (2004). https://doi.org:10.1167/iovs.03-0016

129 Yoeruek, E. *et al.* Human anterior lens capsule as carrier matrix for cultivated human corneal endothelial cells. *Cornea* **28**, 416-420 (2009). https://doi.org:10.1097/ICO.0b013e31818c2c36

130 Li, K. Y. *et al.* Fish-Scale Collagen Membrane Seeded with Corneal Endothelial Cells as Alternative Graft for Endothelial Keratoplasty Transplantation. *ACS Biomater Sci Eng* **6**, 2570-2577 (2020). https://doi.org:10.1021/acsbiomaterials.9b00562

131 Arnalich-Montiel, F. *et al.* Treatment of corneal endothelial damage in a rabbit model with a bioengineered graft using human decellularized corneal lamina and cultured human corneal endothelium. *PloS one* **14**, e0225480 (2019). https://doi.org:10.1371/journal.pone.0225480

132 He, Z. *et al.* Cutting and Decellularization of Multiple Corneal Stromal Lamellae for the Bioengineering of Endothelial Grafts. *Invest Ophthalmol Vis Sci* **57**, 6639-6651 (2016). https://doi.org:10.1167/iovs.16-20256

133 Zhang, Y. *et al.* Tissue-Engineered Corneal Endothelial Sheets Using Ultrathin Acellular Porcine Corneal Stroma Substrates for Endothelial Keratoplasty. *ACS Biomater Sci Eng* **8**, 1301-1311 (2022). https://doi.org:10.1021/acsbiomaterials.2c00039

134 Proulx, S. *et al.* Tissue engineering of feline corneal endothelium using a devitalized human cornea as carrier. *Tissue engineering. Part A* **15**, 1709-1718 (2009). https://doi.org:10.1089/ten.tea.2008.0208

135 Madden, P. W. *et al.* Human corneal endothelial cell growth on a silk fibroin membrane. *Biomaterials* **32**, 4076-4084 (2011). https://doi.org:10.1016/j.biomaterials.2010.12.034

136 Cen, Y. J. & Feng, Y. Constructing a Novel Three-Dimensional Biomimetic Corneal Endothelium Graft by Culturing Corneal Endothelium Cells on Compressed Collagen Gels. *Chin Med J (Engl)* **131**, 1710-1714 (2018). https://doi.org:10.4103/0366-6999.235883

137 Hadlock, T., Singh, S., Vacanti, J. P. & McLaughlin, B. J. Ocular cell monolayers cultured on biodegradable substrates. *Tissue engineering* **5**, 187-196 (1999). https://doi.org:10.1089/ten.1999.5.187

138 Himmler, M., Garreis, F., Paulsen, F., Schubert, D. W. & Fuchsluger, T. A. Optimization of polycaprolactone - based nanofiber matrices for the cultivation of corneal endothelial cells. *Sci Rep* **11**, 18858 (2021). https://doi.org:10.1038/s41598-021-98426-6

139 Madathil, B. K., Kumar, P. R. & Kumary, T. V. N-isopropylacrylamide-co-glycidylmethacrylate as a thermoresponsive substrate for corneal endothelial cell sheet engineering. *Biomed Res Int* **2014**, 450672 (2014). https://doi.org:10.1155/2014/450672

140 Liu, X. N. *et al.* Acellular ostrich corneal stroma used as scaffold for construction of tissue-engineered cornea. *International journal of ophthalmology* **9**, 325-331 (2016). https://doi.org:10.18240/ijo.2016.03.01

141 Gonzalez-Andrades, M. *et al.* Generation of bioengineered corneas with decellularized xenografts and human keratocytes. *Invest Ophthalmol Vis Sci* **52**, 215-222 (2011). https://doi.org:10.1167/iovs.09-4773

142 Li, S. *et al.* Healing characteristics of acellular porcine corneal stroma following therapeutic keratoplasty. *Xenotransplantation* **27**, e12566 (2020). https://doi.org:10.1111/xen.12566

143 Tian, B. S. *et al.* The lived experiences of patients undergoing acellular porcine corneal stroma transplantation. *International journal of ophthalmology* **11**, 1716-1720 (2018). https://doi.org:10.18240/ijo.2018.10.22

144 Zheng, J. *et al.* Short-term results of acellular porcine corneal stroma keratoplasty for herpes simplex keratitis. *Xenotransplantation* **26**, e12509 (2019). https://doi.org:10.1111/xen.12509

145 Fu, R. *et al.* Generation of GGTA1-/-beta2M-/-CIITA-/- Pigs Using CRISPR/Cas9 Technology to Alleviate Xenogeneic Immune Reactions. *Transplantation* **104**, 1566-1573 (2020). https://doi.org:10.1097/TP.0000000000003205

146 Chakraborty, J. *et al.* Modulation of Macrophage Phenotype, Maturation, and Graft Integration through Chondroitin Sulfate Cross-Linking to Decellularized Cornea. *ACS Biomater Sci Eng* **5**, 165-179 (2019). https://doi.org:10.1021/acsbiomaterials.8b00251

147 Levy, S. G., McCartney, A. C. & Moss, J. The distribution of fibronectin and P component in Descemet's membrane: an immunoelectron microscopic study. *Curr Eye Res* **14**, 865-870 (1995). https://doi.org:10.3109/02713689508995810

148 Grant, D. S. & Leblond, C. P. Immunogold quantitation of laminin, type IV collagen, and heparan sulfate proteoglycan in a variety of basement membranes. *J Histochem Cytochem* **36**, 271-283 (1988). https://doi.org:10.1177/36.3.2963856

149 Ljubimov, A. V. *et al.* Human corneal basement membrane heterogeneity: topographical differences in the expression of type IV collagen and laminin isoforms. *Lab Invest* **72**, 461-473 (1995).

150 Kapoor, R., Bornstein, P. & Sage, E. H. Type VIII collagen from bovine Descemet's membrane: structural characterization of a triple-helical domain. *Biochemistry* **25**, 3930-3937 (1986). https://doi.org:10.1021/bi00361a029

151 Okumura, N. *et al.* Laminin-511 and -521 enable efficient in vitro expansion of human corneal endothelial cells. *Invest Ophthalmol Vis Sci* **56**, 2933-2942 (2015). https://doi.org:10.1167/iovs.14-15163

152 Lu, Q. *et al.* Evaluation of reconstructed human corneal endothelium sheets made with porcine Descemet's membrane in vitro and in vivo. *Exp Eye Res* **197**, 108125 (2020). https://doi.org:10.1016/j.exer.2020.108125

153 Halfter, W. *et al.* The human Descemet's membrane and lens capsule: Protein composition and biomechanical properties. *Exp Eye Res* **201**, 108326 (2020). https://doi.org:10.1016/j.exer.2020.108326

154 Spinozzi, D. *et al.* In Vitro Evaluation and Transplantation of Human Corneal Endothelial Cells Cultured on Biocompatible Carriers. *Cell Transplant* **29**, 963689720923577 (2020). https://doi.org:10.1177/0963689720923577

155 Stefaniu, G. I., Chiotoroiu, S. M., Secureanu, F. A., Purcarea, V. L. & Zemba, M. Use of amniotic membrane in bullous keratopathy palliative care. *J Med Life* **7 Spec No. 2**, 88-91 (2014).

156 Zhang, L. *et al.* An Ultra-thin Amniotic Membrane as Carrier in Corneal Epithelium Tissue-Engineering. *Sci Rep* **6**, 21021 (2016). https://doi.org:10.1038/srep21021

157 Koizumi, N. & Kinoshita, S. Ocular surface reconstruction, amniotic membrane, and cultivated epithelial cells from the limbus. *Br J Ophthalmol* **87**, 1437-1439 (2003). https://doi.org:10.1136/bjo.87.12.1437-a

158 Wencan, W. *et al.* Using basement membrane of human amniotic membrane as a cell carrier for cultivated cat corneal endothelial cell transplantation. *Curr Eye Res* **32**, 199-215 (2007). https://doi.org:10.1080/02713680601174165

159 Kim, H. J., Ryu, Y. H., Ahn, J. I., Park, J. K. & Kim, J. C. Characterization of immortalized human corneal endothelial cell line using HPV 16 E6/E7 on lyophilized human amniotic membrane. *Korean J Ophthalmol* **20**, 47-54 (2006). https://doi.org:10.3341/kjo.2006.20.1.47

160 Zhao, J., Fan, T., Ma, X. & Hu, X. Construction of a high cell density human corneal endothelial equivalent and its transplantation in primate models. *Xenotransplantation* **26**, e12514 (2019). https://doi.org:10.1111/xen.12514

161 Malhotra, C. & Jain, A. K. Human amniotic membrane transplantation: Different modalities of its use in ophthalmology. *World J Transplant* **4**, 111-121 (2014). https://doi.org:10.5500/wjt.v4.i2.111

162 Chen, B. *et al.* The mechanical properties of amniotic membrane influence its effect as a biomaterial for ocular surface repair. *Soft Matter* **8**, 8379-8387 (2012). https://doi.org:10.1039/C2SM26175H

163 van Essen, T. H. *et al.* Biocompatibility of a fish scale-derived artificial cornea: Cytotoxicity, cellular adhesion and phenotype, and in vivo immunogenicity. *Biomaterials* **81**, 36-45 (2016). https://doi.org:10.1016/j.biomaterials.2015.11.015

164 Parekh, M., Van den Bogerd, B., Zakaria, N., Ponzin, D. & Ferrari, S. Fish Scale-Derived Scaffolds for Culturing Human Corneal Endothelial Cells. *Stem Cells Int* **2018**, 8146834 (2018). https://doi.org:10.1155/2018/8146834

165 Nakayasu, K., Tanaka, M., Konomi, H. & Hayashi, T. Distribution of types I, II, III, IV and V collagen in normal and keratoconus corneas. *Ophthalmic Res* **18**, 1-10 (1986). https://doi.org:10.1159/000265406

166 Merrett, K. *et al.* Tissue-engineered recombinant human collagen-based corneal substitutes for implantation: performance of type I versus type III collagen. *Invest Ophthalmol Vis Sci* **49**, 3887-3894 (2008). https://doi.org:10.1167/iovs.07-1348

167 Minami, Y., Sugihara, H. & Oono, S. Reconstruction of cornea in three-dimensional collagen gel matrix culture. *Invest Ophthalmol Vis Sci* **34**, 2316-2324 (1993).

168 Orwin, E. J. & Hubel, A. In vitro culture characteristics of corneal epithelial, endothelial, and keratocyte cells in a native collagen matrix. *Tissue engineering* **6**, 307-319 (2000). https://doi.org:10.1089/107632700418038

169 Koizumi, N. *et al.* Cultivated corneal endothelial transplantation in a primate: possible future clinical application in corneal endothelial regenerative medicine. *Cornea* **27 Suppl 1**, S48-55 (2008). https://doi.org:10.1097/ICO.0b013e31817f2298

170 Brown, R. A., Wiseman, M., Chuo, C. B., Cheema, U. & Nazhat, S. N. Ultrarapid Engineering of Biomimetic Materials and Tissues: Fabrication of Nano- and Microstructures by Plastic Compression. *Advanced Functional Materials* **15**, 1762-1770 (2005). https://doi.org:https://doi.org/10.1002/adfm.200500042

171 Levis, H. J., Menzel-Severing, J., Drake, R. A. & Daniels, J. T. Plastic compressed collagen constructs for ocular cell culture and transplantation: a new and improved technique of confined fluid loss. *Curr Eye Res* **38**, 41-52 (2013). https://doi.org:10.3109/02713683.2012.725799

172 Levis, H. J. *et al.* Plastic compressed collagen as a novel carrier for expanded human corneal endothelial cells for transplantation. *PloS one* **7**, e50993 (2012). https://doi.org:10.1371/journal.pone.0050993

173 Lai, J. Y., Chen, K. H. & Hsiue, G. H. Tissue-engineered human corneal endothelial cell sheet transplantation in a rabbit model using functional biomaterials. *Transplantation* **84**, 1222-1232 (2007). https://doi.org:10.1097/01.tp.0000287336.09848.39

174 Jumblatt, M. M., Maurice, D. M. & Schwartz, B. D. A gelatin membrane substrate for the transplantation of tissue cultured cells. *Transplantation* **29**, 498-499 (1980). https://doi.org:10.1097/00007890-198006000-00013

175 Pan, T., Song, W., Cao, X. & Wang, Y. 3D Bioplotting of Gelatin/Alginate Scaffolds for Tissue Engineering: Influence of Crosslinking Degree and Pore Architecture on Physicochemical Properties. *Journal of Materials Science & Technology* **32**, 889-900 (2016). https://doi.org:https://doi.org/10.1016/j.jmst.2016.01.007

176 Schwartz, B. D. & McCulley, J. P. Morphology of transplanted corneal endothelium derived from tissue culture. *Invest Ophthalmol Vis Sci* **20**, 467-480 (1981).

177 Yang, G. *et al.* Assessment of the characteristics and biocompatibility of gelatin sponge scaffolds prepared by various crosslinking methods. *Sci Rep* **8**, 1616 (2018). https://doi.org:10.1038/s41598-018-20006-y

178 Niu, G. *et al.* Heparin-modified gelatin scaffolds for human corneal endothelial cell transplantation. *Biomaterials* **35**, 4005-4014 (2014). https://doi.org:10.1016/j.biomaterials.2014.01.033

179 Kimoto, M. *et al.* Development of a bioengineered corneal endothelial cell sheet to fit the corneal curvature. *Invest Ophthalmol Vis Sci* **55**, 2337-2343 (2014). https://doi.org:10.1167/iovs.13-13167

180 Stenevi, U., Gwin, T., Harfstrand, A. & Apple, D. Demonstration of Hyaluronic Acid Binding to Corneal Endothelial Cells in Human Eye-Bank Eyes. *European journal of Implant and Refractive Surgery* **5**, 228-232 (1993). https://doi.org:https://doi.org/10.1016/S0955-3681(13)80162-1

181 Parekh, M., Ahmad, S., Ruzza, A. & Ferrari, S. Human Corneal Endothelial Cell Cultivation From Old Donor Corneas With Forced Attachment. *Sci Rep* **7**, 142 (2017). https://doi.org:10.1038/s41598-017-00209-5

182 Lai, J. Y., Cheng, H. Y. & Ma, D. H. Investigation of Overrun-Processed Porous Hyaluronic Acid Carriers in Corneal Endothelial Tissue Engineering. *PloS one* **10**, e0136067 (2015). https://doi.org:10.1371/journal.pone.0136067

183 Lu, P. L., Lai, J. Y., Ma, D. H. & Hsiue, G. H. Carbodiimide cross-linked hyaluronic acid hydrogels as cell sheet delivery vehicles: characterization and interaction with corneal endothelial cells. *J Biomater Sci Polym Ed* **19**, 1-18 (2008). https://doi.org:10.1163/156856208783227695

184 Dorishetty, P. *et al.* Tunable Biomimetic Hydrogels from Silk Fibroin and Nanocellulose. *ACS Sustainable Chemistry & Engineering* **8**, 2375-2389 (2020). https://doi.org:10.1021/acssuschemeng.9b05317

185 Padol, A. R. *et al.* Safety evaluation of silk protein film (a novel wound healing agent) in terms of acute dermal toxicity, acute dermal irritation and skin sensitization. *Toxicol Int* **18**, 17-21 (2011). https://doi.org:10.4103/0971-6580.75847

186 Yucel, T., Lovett, M. L., Giangregorio, R., Coonahan, E. & Kaplan, D. L. Silk fibroin rods for sustained delivery of breast cancer therapeutics. *Biomaterials* **35**, 8613-8620 (2014). https://doi.org:10.1016/j.biomaterials.2014.06.030

187 Lawrence, B. D., Marchant, J. K., Pindrus, M. A., Omenetto, F. G. & Kaplan, D. L. Silk film biomaterials for cornea tissue engineering. *Biomaterials* **30**, 1299-1308 (2009). https://doi.org:10.1016/j.biomaterials.2008.11.018

188 Kim, E. Y. *et al.* Bioengineered neo-corneal endothelium using collagen type-I coated silk fibroin film. *Colloids Surf B Biointerfaces* **136**, 394-401 (2015). https://doi.org:10.1016/j.colsurfb.2015.09.041

189 Ramachandran, C., Gupta, P., Hazra, S. & Mandal, B. B. In Vitro Culture of Human Corneal Endothelium on Non-Mulberry Silk Fibroin Films for Tissue Regeneration. *Transl Vis Sci Technol* **9**, 12 (2020). https://doi.org:10.1167/tvst.9.4.12

190 Vazquez, N. *et al.* Silk Fibroin Films for Corneal Endothelial Regeneration: Transplant in a Rabbit Descemet Membrane Endothelial Keratoplasty. *Invest Ophthalmol Vis Sci* **58**, 3357-3365 (2017). https://doi.org:10.1167/iovs.17-21797

191 Elieh-Ali-Komi, D. & Hamblin, M. R. Chitin and Chitosan: Production and Application of Versatile Biomedical Nanomaterials. *Int J Adv Res (Indore)* **4**, 411-427 (2016).

192 Wang, T. J., Wang, I. J., Chen, S., Chen, Y. H. & Young, T. H. The phenotypic response of bovine corneal endothelial cells on chitosan/polycaprolactone blends. *Colloids Surf B Biointerfaces* **90**, 236-243 (2012). https://doi.org:10.1016/j.colsurfb.2011.10.043

193 Wang, Y. H., Young, T. H. & Wang, T. J. Investigating the effect of chitosan/ polycaprolactone blends in differentiation of corneal endothelial cells and extracellular matrix compositions. *Exp Eye Res* **185**, 107679 (2019). https://doi.org:10.1016/j.exer.2019.05.019

194 Gao, X., Liu, W., Han, B., Wei, X. & Yang, C. Preparation and properties of a chitosan-based carrier of corneal endothelial cells. *J Mater Sci Mater Med* **19**, 3611-3619 (2008). https://doi.org:10.1007/s10856-008-3508-0

195 Seyed, M. A. & Vijayaraghavan, K. Evaluation of an Improved Chitosan Scaffold Cross-Linked With Polyvinyl Alcohol and Amine Coupling Through 1-Ethyl-3-(3-Dimethyl Aminopropyl)-Carbodiimide (EDC) and 2 N-Hydroxysuccinimide (NHS) for Corneal Applications. *Open Access Maced J Med Sci* **6**, 1561-1570 (2018). https://doi.org:10.3889/oamjms.2018.322

196 Luo, X. *et al.* Research Progress of Polymer Biomaterials as Scaffolds for Corneal Endothelium Tissue Engineering. *Nanomaterials (Basel)* **13** (2023). https://doi.org:10.3390/nano13131976

197 Kim, E. Y., Tripathy, N., Cho, S. A., Lee, D. & Khang, G. Collagen type I–PLGA film as an efficient substratum for corneal endothelial cells regeneration. *Journal of tissue engineering and regenerative medicine* **11**, 2471-2478 (2017). https://doi.org:https://doi.org/10.1002/term.2145

198 Wang, T. J., Wang, I. J., Chen, Y. H., Lu, J. N. & Young, T. H. Polyvinylidene fluoride for proliferation and preservation of bovine corneal endothelial cells by enhancing type IV collagen production and deposition. *Journal of biomedical materials research. Part A* **100**, 252-260 (2012). https://doi.org:10.1002/jbm.a.33274

199 Ozcelik, B. *et al.* Ultrathin chitosan-poly(ethylene glycol) hydrogel films for corneal tissue engineering. *Acta biomaterialia* **9**, 6594-6605 (2013). https://doi.org:10.1016/j.actbio.2013.01.020

200 Ozcelik, B. *et al.* Biodegradable and biocompatible poly(ethylene glycol)-based hydrogel films for the regeneration of corneal endothelium. *Adv Healthc Mater* **3**, 1496-1507 (2014). https://doi.org:10.1002/adhm.201400045

201 Takahashi, H. & Okano, T. Thermally-triggered fabrication of cell sheets for tissue engineering and regenerative medicine. *Advanced drug delivery reviews* **138**, 276-292 (2019). https://doi.org:10.1016/j.addr.2019.01.004

202 Ide, T. *et al.* Structural characterization of bioengineered human corneal endothelial cell sheets fabricated on temperature-responsive culture dishes. *Biomaterials* **27**, 607-614 (2006). https://doi.org:https://doi.org/10.1016/j.biomaterials.2005.06.005

203 Hsiue, G. H., Lai, J. Y., Chen, K. H. & Hsu, W. M. A novel strategy for corneal endothelial reconstruction with a bioengineered cell sheet. *Transplantation* **81**, 473-476 (2006). https://doi.org:10.1097/01.tp.0000194864.13539.2c

204 Nitschke, M. *et al.* Thermo-responsive poly(NiPAAm-co-DEGMA) substrates for gentle harvest of human corneal endothelial cell sheets. *Journal of biomedical materials research. Part A* **80**, 1003-1010 (2007). https://doi.org:10.1002/jbm.a.31098

205 Madathil, B. K., Anil Kumar, P. R. & Kumary, T. V. N-Isopropylacrylamide-co-glycidylmethacrylate as a Thermoresponsive Substrate for Corneal Endothelial Cell Sheet Engineering. *BioMed Research International* **2014**, 450672 (2014). https://doi.org:10.1155/2014/450672

206 Soh, W. W. M. *et al.* Detachment of bovine corneal endothelial cell sheets by cooling-induced surface hydration of poly[(R)-3-hydroxybutyrate]-based thermoresponsive copolymer coating. *J Mater Chem B* **10**, 8407-8418 (2022). https://doi.org:10.1039/d2tb01926d

207 Hong, Y. *et al.* Light-induced cell detachment for cell sheet technology. *Biomaterials* **34**, 11-18 (2013). https://doi.org:10.1016/j.biomaterials.2012.09.043

208 Guillaume-Gentil, O. *et al.* pH-controlled recovery of placenta-derived mesenchymal stem cell sheets. *Biomaterials* **32**, 4376-4384 (2011). https://doi.org:10.1016/j.biomaterials.2011.02.058

209 Seto, Y. *et al.* Engineering of capillary-like structures in tissue constructs by electrochemical detachment of cells. *Biomaterials* **31**, 2209-2215 (2010). https://doi.org:10.1016/j.biomaterials.2009.11.104

210 Nakamura, A. *et al.* Cell sheet transplantation of cultured mesenchymal stem cells enhances bone formation in a rat nonunion model. *Bone* **46**, 418-424 (2010). https://doi.org:10.1016/j.bone.2009.08.048

211 Hitani, K. *et al.* Transplantation of a sheet of human corneal endothelial cell in a rabbit model. *Mol Vis* **14**, 1-9 (2008).

212 Bednarz, J., Teifel, M., Friedl, P. & Engelmann, K. Immortalization of human corneal endothelial cells using electroporation protocol optimized for human corneal endothelial and human retinal pigment epithelial cells. *Acta Ophthalmol Scand* **78**, 130-136 (2000). https://doi.org:10.1034/j.1600-0420.2000.078002130.x

213 Lopez, J. M., Imperial, S., Valderrama, R. & Navarro, S. An improved Bradford protein assay for collagen proteins. *Clin Chim Acta* **220**, 91-100 (1993). https://doi.org:10.1016/0009-8981(93)90009-s

214 Bradford, M. M. A rapid and sensitive method for the quantitation of microgram quantities of protein utilizing the principle of protein-dye binding. *Anal Biochem* **72**, 248-254 (1976). https://doi.org:10.1006/abio.1976.9999

215 Kapoor, R. *et al.* Type VIII collagen has a restricted distribution in specialized extracellular matrices. *J Cell Biol* **107**, 721-730 (1988). https://doi.org:10.1083/jcb.107.2.721

216 Sawada, H., Konomi, H. & Hirosawa, K. Characterization of the collagen in the hexagonal lattice of Descemet's membrane: its relation to type VIII collagen. *J Cell Biol* **110**, 219-227 (1990). https://doi.org:10.1083/jcb.110.1.219

217 Karsdal, M. A., Leeming, D. J., Henriksen, K. & Bay-Jensen, A.-C. *Biochemistry of collagens, laminins and elastin : structure, function and biomarkers*. (Elsevier/AP, Academic Press is an imprint of Elsevier, 2016).

218 Okumura, N. *et al.* Involvement of ZEB1 and Snail1 in excessive production of extracellular matrix in Fuchs endothelial corneal dystrophy. *Lab Invest* **95**, 1291-1304 (2015). https://doi.org:10.1038/labinvest.2015.111

219 Ko, M. K. & Kay, E. P. Regulatory role of FGF-2 on type I collagen expression during endothelial mesenchymal transformation. *Invest Ophthalmol Vis Sci* **46**, 4495-4503 (2005). https://doi.org:10.1167/iovs.05-0818

220 Gospodarowicz, D., Delgado, D. & Vlodavsky, I. Permissive effect of the extracellular matrix on cell proliferation in vitro. *Proceedings of the National Academy of Sciences of the United States of America* **77**, 4094-4098 (1980). https://doi.org:10.1073/pnas.77.7.4094

221 Ando, J., Albelda, S. M. & Levine, E. M. Culture of human adult endothelial cells on liquid-liquid interfaces: a new approach to the study of cell-matrix interactions. *In Vitro Cell Dev Biol* **27A**, 525-532 (1991). https://doi.org:10.1007/BF02631282

222 Lu, H., Hoshiba, T., Kawazoe, N. & Chen, G. Autologous extracellular matrix scaffolds for tissue engineering. *Biomaterials* **32**, 2489-2499 (2011). https://doi.org:10.1016/j.biomaterials.2010.12.016

223 Chen, X. D., Dusevich, V., Feng, J. Q., Manolagas, S. C. & Jilka, R. L. Extracellular matrix made by bone marrow cells facilitates expansion of marrow-derived mesenchymal progenitor cells and prevents their differentiation into osteoblasts. *J Bone Miner Res* **22**, 1943-1956 (2007). https://doi.org:10.1359/jbmr.070725

224 Kelliher, C. *et al.* A cellular model for the investigation of Fuchs' endothelial corneal dystrophy. *Exp Eye Res* **93**, 880-888 (2011). https://doi.org:10.1016/j.exer.2011.10.001

225 Tamura, Y., Konomi, H., Sawada, H., Takashima, S. & Nakajima, A. Tissue distribution of type VIII collagen in human adult and fetal eyes. *Invest Ophthalmol Vis Sci* **32**, 2636-2644 (1991).

226 Goyer, B. *et al.* Extracellular Matrix and Integrin Expression Profiles in Fuchs Endothelial Corneal Dystrophy Cells and Tissue Model. *Tissue engineering. Part A* **24**, 607-615 (2018). https://doi.org:10.1089/ten.TEA.2017.0128

227 Bandeira, F. *et al.* A Framework for Human Corneal Endothelial Cell Culture and Preliminary Wound Model Experiments with a New Cell Tracking Approach. *Int J Mol Sci* **24** (2023). https://doi.org:10.3390/ijms24032982

228 Cai, W. *et al.* Effect of bradykinin on TGF-beta1-induced retinal pigment epithelial cell proliferation and extracellular matrix secretion. *BMC Ophthalmol* **16**, 199 (2016). https://doi.org:10.1186/s12886-016-0373-3

229 Xing, H., Lee, H., Luo, L. & Kyriakides, T. R. Extracellular matrix-derived biomaterials in engineering cell function. *Biotechnology advances* **42**, 107421 (2020). https://doi.org:10.1016/j.biotechadv.2019.107421

230 Zhu, W. *et al.* Cell-derived decellularized extracellular matrix scaffolds for articular cartilage repair. *Int J Artif Organs* **44**, 269-281 (2021). https://doi.org:10.1177/0391398820953866

231 Yang, L., Ge, L. & van Rijn, P. Synergistic Effect of Cell-Derived Extracellular Matrices and Topography on Osteogenesis of Mesenchymal Stem Cells. *ACS Appl Mater Interfaces* **12**, 25591-25603 (2020). https://doi.org:10.1021/acsami.0c05012

232 Muncie, J. M. & Weaver, V. M. The Physical and Biochemical Properties of the Extracellular Matrix Regulate Cell Fate. *Curr Top Dev Biol* **130**, 1-37 (2018). https://doi.org:10.1016/bs.ctdb.2018.02.002

233 Piera-Velazquez, S. & Jimenez, S. A. Endothelial to Mesenchymal Transition: Role in Physiology and in the Pathogenesis of Human Diseases. *Physiol Rev* **99**, 1281-1324 (2019). https://doi.org:10.1152/physrev.00021.2018

234 Beaulieu Leclerc, V., Roy, O., Santerre, K. & Proulx, S. TGF-beta1 promotes cell barrier function upon maturation of corneal endothelial cells. *Sci Rep* **8**, 4438 (2018). https://doi.org:10.1038/s41598-018-22821-9

235 Sumioka, T. *et al.* Inhibitory effect of blocking TGF-beta/Smad signal on injury-induced fibrosis of corneal endothelium. *Mol Vis* **14**, 2272-2281 (2008).

236 Wrighton, K. H., Lin, X. & Feng, X. H. Phospho-control of TGF-beta superfamily signaling. *Cell Res* **19**, 8-20 (2009). https://doi.org:10.1038/cr.2008.327

237 De Craene, B. *et al.* The transcription factor snail induces tumor cell invasion through modulation of the epithelial cell differentiation program. *Cancer Res* **65**, 6237-6244 (2005). https://doi.org:10.1158/0008-5472.CAN-04-3545

238 Whiteman, E. L., Liu, C. J., Fearon, E. R. & Margolis, B. The transcription factor snail represses Crumbs3 expression and disrupts apico-basal polarity complexes. *Oncogene* **27**, 3875-3879 (2008). https://doi.org:10.1038/onc.2008.9

239 Xu, J., Lamouille, S. & Derynck, R. TGF-beta-induced epithelial to mesenchymal transition. *Cell Res* **19**, 156-172 (2009). https://doi.org:10.1038/cr.2009.5

240 Peh, G. S., Toh, K. P., Wu, F. Y., Tan, D. T. & Mehta, J. S. Cultivation of human corneal endothelial cells isolated from paired donor corneas. *PloS one* **6**, e28310 (2011). https://doi.org:10.1371/journal.pone.0028310

241 Wongvisavavit, R., Parekh, M., Ahmad, S. & Daniels, J. T. Challenges in corneal endothelial cell culture. *Regenerative medicine* **16**, 871-891 (2021). https://doi.org:10.2217/rme-2020-0202

242 Lamouille, S., Xu, J. & Derynck, R. Molecular mechanisms of epithelial–mesenchymal transition. *Nature Reviews Molecular Cell Biology* **15**, 178 (2014). https://doi.org:10.1038/nrm3758

243 Medici, D. & Kalluri, R. Endothelial–mesenchymal transition and its contribution to the emergence of stem cell phenotype. *Seminars in Cancer Biology* **22**, 379-384 (2012). https://doi.org:https://doi.org/10.1016/j.semcancer.2012.04.004

244 Gumbiner, B. M. Cell Adhesion: The Molecular Basis of Tissue Architecture and Morphogenesis. *Cell* **84**, 345-357 (1996). https://doi.org:10.1016/S0092-8674(00)81279-9

245 Huang, R. Y. J., Guilford, P. & Thiery, J. P. Early events in cell adhesion and polarity during epithelial-mesenchymal transition. *Journal of Cell Science* **125**, 4417-4422 (2012). https://doi.org:10.1242/jcs.099697

246 Hsieh, P. & Baum, J. Effects of fibroblastic and endothelial extracellular matrices on corneal endothelial cells. *Invest Ophthalmol Vis Sci* **26**, 457-463 (1985).

247 Underwood, P. A. & Bennett, F. A. The effect of extracellular matrix molecules on the in vitro behavior of bovine endothelial cells. *Exp Cell Res* **205**, 311-319 (1993). https://doi.org:10.1006/excr.1993.1091

248 Honda, N., Mimura, T., Usui, T. & Amano, S. Descemet stripping automated endothelial keratoplasty using cultured corneal endothelial cells in a rabbit model. *Arch Ophthalmol* **127**, 1321-1326 (2009). https://doi.org:10.1001/archophthalmol.2009.253

249 Hopfer, U. *et al.* Targeted disruption of Col8a1 and Col8a2 genes in mice leads to anterior segment abnormalities in the eye. *FASEB J* **19**, 1232-1244 (2005). https://doi.org:10.1096/fj.04-3019com

250 Bourne, W. M., Johnson, D. H. & Campbell, R. J. The ultrastructure of Descemet's membrane. III. Fuchs' dystrophy. *Arch Ophthalmol* **100**, 1952-1955 (1982). https://doi.org:10.1001/archopht.1982.01030040932013

251 Wei, Q. *et al.* Long-Term Clinical Outcomes of Small-Incision Femtosecond Laser-Assisted Intracorneal Concave Lenticule Implantation in Patients with Keratoconus. *J Ophthalmol* **2022**, 9774448 (2022). https://doi.org:10.1155/2022/9774448

252 Konomi, K. & Joyce, N. C. Age and topographical comparison of telomere lengths in human corneal endothelial cells. *Mol Vis* **13**, 1251-1258 (2007).

253 Liang, C. C., Park, A. Y. & Guan, J. L. In vitro scratch assay: a convenient and inexpensive method for analysis of cell migration in vitro. *Nat Protoc* **2**, 329-333 (2007). https://doi.org:10.1038/nprot.2007.30

254 Pinto, B. I., Cruz, N. D., Lujan, O. R., Propper, C. R. & Kellar, R. S. In Vitro Scratch Assay to Demonstrate Effects of Arsenic on Skin Cell Migration. *Journal of visualized experiments : JoVE* (2019). https://doi.org:10.3791/58838

255 Sibinga, N. E. *et al.* Collagen VIII is expressed by vascular smooth muscle cells in response to vascular injury. *Circ Res* **80**, 532-541 (1997). https://doi.org:10.1161/01.res.80.4.532

256 Gospodarowicz, D. & Ill, C. The extracellular matrix and the control of proliferation of corneal endothelial and lens epithelial cells. *Exp Eye Res* **31**, 181-199 (1980). https://doi.org:10.1016/0014-4835(80)90077-9

257 Stamov, D. R. & Pompe, T. Structure and function of ECM-inspired composite collagen type I scaffolds. *Soft Matter* **8**, 10200-10212 (2012). https://doi.org:10.1039/C2SM26134K

258 Somaiah, C. *et al.* Collagen Promotes Higher Adhesion, Survival and Proliferation of Mesenchymal Stem Cells. *PloS one* **10**, e0145068 (2015). https://doi.org:10.1371/journal.pone.0145068

259 Sivaraman, K., Muthukumar, K. & Shanthi, C. Adhesion and proliferation properties of type I collagen-derived peptide for possible use in skin tissue engineering application. *Cell Biol Int* **46**, 391-402 (2022). https://doi.org:10.1002/cbin.11737

260 Li, C. *et al.* Notch signal regulates corneal endothelial-to-mesenchymal transition. *Am J Pathol* **183**, 786-795 (2013). https://doi.org:10.1016/j.ajpath.2013.05.025

261 Mayor, R. & Carmona-Fontaine, C. Keeping in touch with contact inhibition of locomotion. *Trends Cell Biol* **20**, 319-328 (2010). https://doi.org:10.1016/j.tcb.2010.03.005

262 Yanoff, M. In vitro biology of corneal epithelium and endothelium. *Trans Am Ophthalmol Soc* **73**, 571-620 (1975).

263 Hernandez, J. A., Chifflet, S., Justet, C. & Torriglia, A. A mathematical model of wound healing in bovine corneal endothelium. *J Theor Biol* **559**, 111374 (2023). https://doi.org:10.1016/j.jtbi.2022.111374

264 de Oliveira, R. C. & Wilson, S. E. Descemet's membrane development, structure, function and regeneration. *Exp Eye Res* **197**, 108090 (2020). https://doi.org:10.1016/j.exer.2020.108090

265 Gruschwitz, R. *et al.* Alignment and cell-matrix interactions of human corneal endothelial cells on nanostructured collagen type I matrices. *Invest Ophthalmol Vis Sci* **51**, 6303-6310 (2010). https://doi.org:10.1167/iovs.10-5368

266 Zhu, Y. T. *et al.* Engineering of Human Corneal Endothelial Grafts. *Curr Ophthalmol Rep* **3**, 207-217 (2015). https://doi.org:10.1007/s40135-015-0077-5

Appendices

Appendix 1

List of Antibodies Used in the Experiments

Primary antibodies	Dilutions	
	Western blot	Immunofluorescence
ZO-1 (rabbit anti human)	1:1500	1:400
ATP1A1 (mouse anti human)	1:2000	1:20
α-SMA (mouse anti human)	1:300	1:150
β-actin (mouse anti human)	1:4000	N/A
COL1 (mouse anti human)	1:500	1:50
COL4 (mouse anti human)	1:2000	1:50
COL8A2 (rabbit anti human)	1:2000	1:50

Secondary antibodies	Dilutions	
	Western blot	Immunofluorescence
Mouse anti-rabbit IgG-HRP	1:3000	
m-IgGκ BP-HRP	1:3000	
Alexa Fluor 488 Goat anti-Rabbit		1:500
Alexa Fluor 568 Goat anti-Rabbit		1:1000
Alexa Fluor 647 Goat anti-Rabbit		1:1000
Alexa Fluor 488 Goat anti-Mouse		1:2000
Alexa Fluor 568 Goat anti-Rabbit		1:1000
Alexa Fluor 647 Goat anti-Rabbit		1:1000

Appendix 2

Comprehensive Immunofluorescence Micrographs of HCEC-12 Cultured on TCPS, 100µg/mL COL4 coating, dECM-TCPS, and dECM-COL4

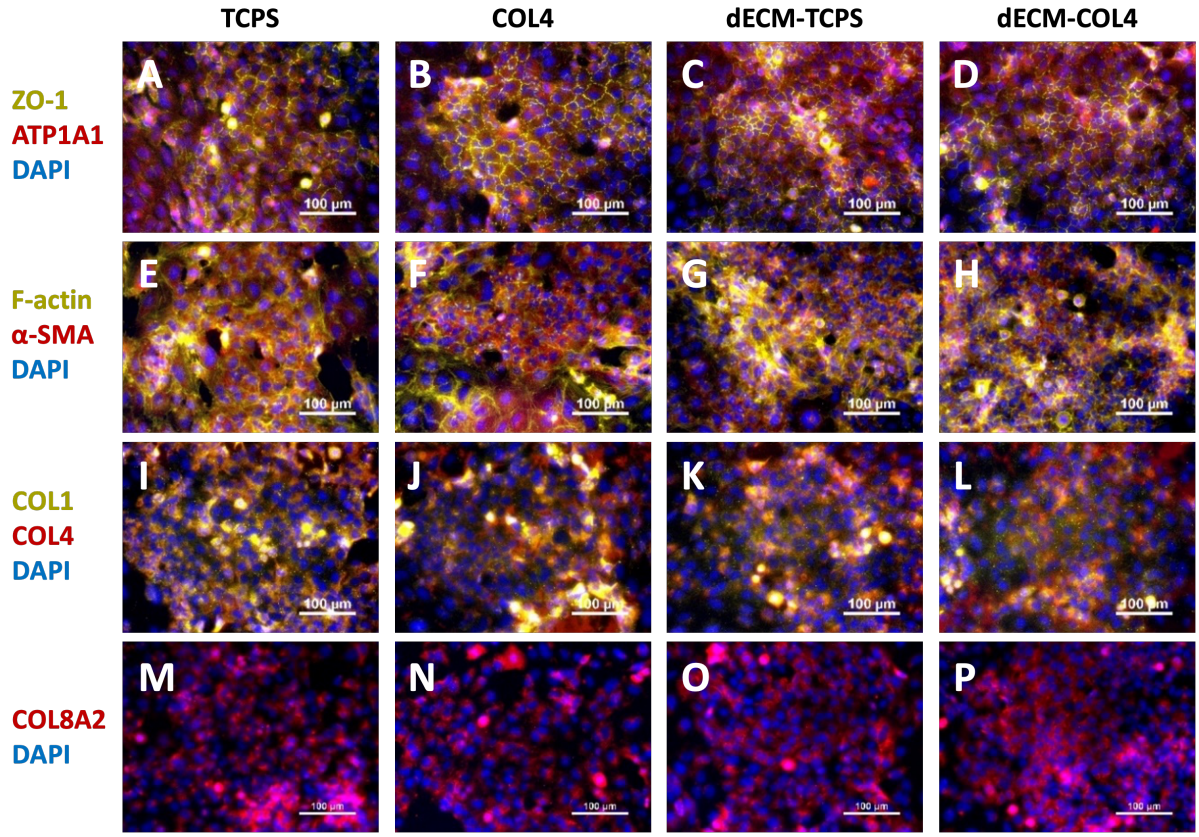

Figure 28. Supplementary Figure: Comprehensive immunofluorescence staining of HCEC-12 P4 on various substrates. Representative micrographs depicting HCEC-12 cells at passage 4 (P4) cultured on TCPS, 100µg/mL COL4 coating, dECM-TCPS, and dECM-COL4. Images display cells stained for (A-D) for ZO-1 (yellow), ATP1A1 (red), and nuclei (blue); (E-H) F-actin (yellow), α-SMA (red), and nuclei (blue); (I-L) collagen type I (yellow), collagen type IV (red), and nuclei (blue); (M-P) collagen type VIII (red) and nuclei (blue). All images are scaled with bars representing 100µm.

Appendix 3

Comprehensive Immunofluorescence Micrographs of HCEC-12 Cultured on TCPS, 100µg/mL COL4 coating, dECM-TCPS, and dECM-COL4, with TGF- β1 treatment

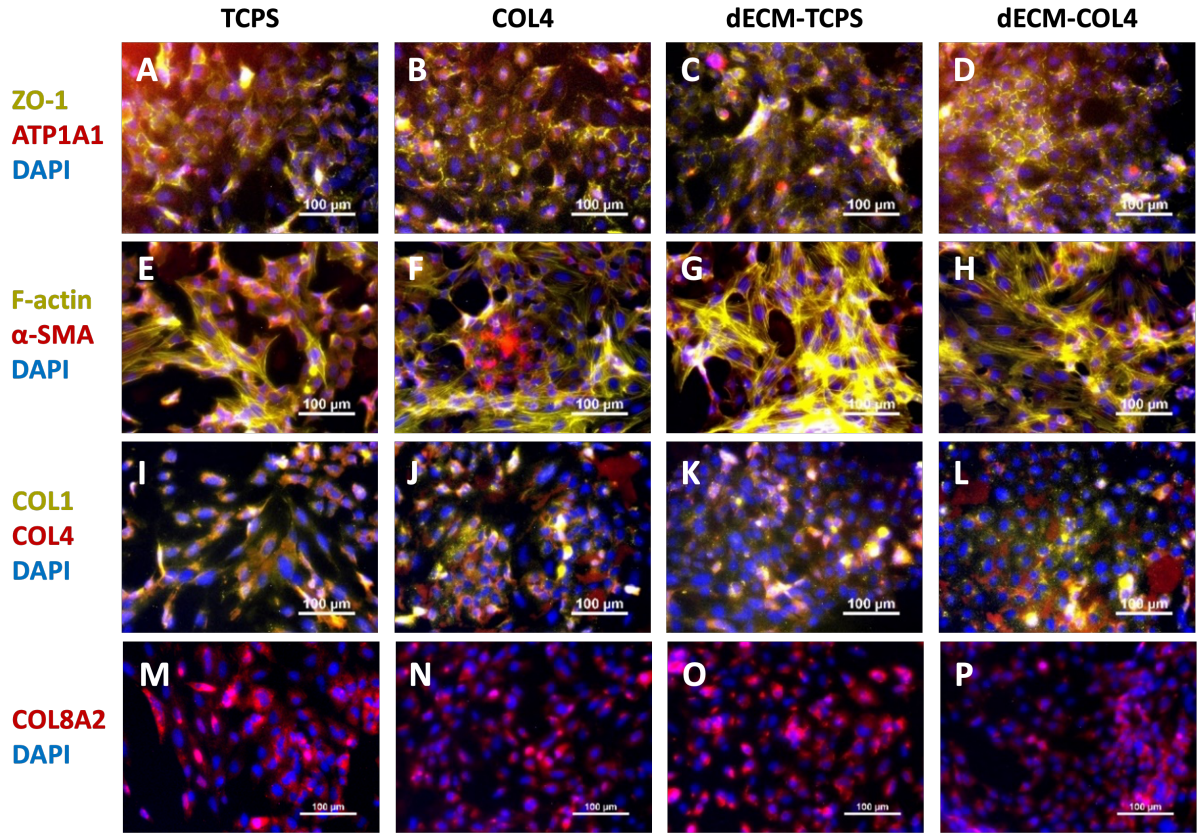

Figure 29. Supplementary Figure: Comprehensive immunofluorescence staining of HCEC-12 P4 on various substrates, with TGF-β1 treatment. Representative micrographs depicting HCEC-12 cells at passage 4 (P4) cultured on TCPS, 100µg/mL COL4 coating, dECM-TCPS, and dECM-COL4, with TGF-β1 treatment to induce EMT. Images display cells stained for (A-D) for ZO-1 (yellow), ATP1A1 (red), and nuclei (blue); (E-H) F-actin (yellow), α-SMA (red), and nuclei (blue); (I-L) collagen type I (yellow), collagen type IV (red), and nuclei (blue); (M-P) collagen type VIII (red) and nuclei (blue). All images are scaled with bars representing 100µm.